NASA TN D-692

TECHNICAL NOTE

D-692

A DESIGN STUDY OF THE INFLATED SPHERE LANDING VEHICLE, INCLUDING THE LANDING PERFORMANCE AND THE EFFECTS OF DEVIATIONS FROM DESIGN CONDITIONS

By E. Dale Martin

Ames Research Center
Moffett Field, Calif.

NATIONAL AERONAUTICS AND SPACE ADMINISTRATION
WASHINGTON

April 1961

NATIONAL AERONAUTICS AND SPACE ADMINISTRATION

TECHNICAL NOTE D-692

A DESIGN STUDY OF THE INFLATED SPHERE LANDING VEHICLE, INCLUDING THE LANDING PERFORMANCE AND THE EFFECTS OF DEVIATIONS FROM DESIGN CONDITIONS

By E. Dale Martin

SUMMARY

The impact motion of the inflated sphere landing vehicle with a payload centrally supported from the spherical skin by numerous cords has been determined on the assumption of uniform isentropic gas compression during impact. The landing capabilities are determined for a system containing suspension cords of constant cross section.

The effects of deviations in impact velocity and initial gas temperature from the design conditions are studied. Also discussed are the effects of errors in the time at which the skin is ruptured. These studies indicate how the design parameters should be chosen to insure reliability of the landing system.

Calculations have been made and results are presented for a sphere inflated with hydrogen, landing on the moon in the absence of an atmosphere. The results are presented for one value of the skin-strength parameter.

INTRODUCTION

Various devices and techniques are being considered as solutions to the problem of alleviating or minimizing the acceleration of a payload during impact with the surface of the moon or the planets. Among the simpler methods (in concept) which have been proposed is the gas-inflated impact bag. A possible configuration, the inflated sphere landing vehicle, was described and its motion and performance were analyzed in references 1 and 2.

The inflated sphere landing vehicle has a strong and flexible, but relatively nonstretchable skin. The inflating gas is light, but has high energy-absorbing properties. The best such gases are hydrogen and helium.

The payload package to be landed is suspended in the center of the sphere by numerous cords attached to the skin. Because of the nonstretchable skin and the internal gas pressure, the vehicle maintains a truncated spherical shape during the impact as the part of the skin in contact with the impact surface is collapsed, folded, and held on the surface by the gas pressure. The payload comes to rest on the surface when the kinetic energy of the system has been absorbed by the gas in the vehicle. The skin may be ruptured at the instant of zero velocity to prevent rebound.

The results obtained from the analysis of reference 1 showed that the maximum impact velocity was limited by the skin strength to values less than about 1000 feet per second. The vehicle could, however, be advantageously used in the terminal phase of a landing maneuver because it functions without the need for maneuverability, guidance, control, attitude stabilization, or complex landing gear.

In the analysis of reference 1 the approximation was made that the pressure throughout the inflating gas was uniform at a given time. It was shown that the condition under which this is a good approximation is that the square of the ratio of the impact velocity to the speed of sound in the gas be small compared to unity. Fortuitously, the limitation on impact velocity due to skin strength of practical materials automatically satisfies this condition if inflating gases with high speeds of sound, such as helium or hydrogen, are used.

The preliminary analysis of reference 1 has left some questions unanswered. In reference 1 the mass of the suspension cords was assumed either to be negligible or to be taken into account approximately by being included in the mass of the package at the center. The present report is a design study of the inflated sphere landing vehicle in which definite consideration is given to the mass of cords required. The required mass of cords depends, of course, on their mass density and strength; and this mass is found to be of very significant magnitude for constant-area cords constructed of practical materials.[1] There is also the question of how critical will be the effects of deviations from the design impact velocity and design initial gas temperature, and the effects of errors in the time at which the skin is ruptured. A knowledge of these effects would aid in the selection of the design parameters. A principal function of this report, therefore, is to consider these effects and present the results. The results of the analysis show essentially the behavior of the vehicle when deviations from design conditions occur at impact; hence indications are given as to how the design parameters should be chosen for reliability. The actual tolerances in the deviations from design conditions are, in fact, found.

---

[1]Further investigation has shown that if the suspension cords were tapered so that a constant stress were present over the length of one cord at a given time, the payload mass which could be landed, for some design conditions, would be significantly higher than for the case of constant-area cords. (See appendix.)

SYMBOLS

a	acceleration of the sphere center
$\bar{a}$	$\left(\frac{r}{u_1^2}\right) a$, dimensionless acceleration
A_c	cross-sectional area of one suspension cord
c_v	specific heat at constant volume
E	effective longitudinal modulus of elasticity of each cord
f	$\frac{\varphi}{\varphi_o}$, distribution of force in the cords
F_p	resultant vertical force due to the gas pressure
g_e	gravitational acceleration on the earth
h_m	drop altitude above the moon surface
m	total mass of the landing system, including payload
$m_{(\ )}$	mass of a particular part of the system, depending on the subscript
n	maximum acceleration in earth g's
N_c	total number of suspension cords
p	pressure of the inflating gas
p_a	pressure of the atmosphere outside the vehicle
$\bar{p}_a$	$\frac{p_a}{p_1}$
r	radius of the sphere
R	gas constant
t	time measured from first instant of impact
$\bar{t}$	$\left(\frac{\lvert u_1 \rvert}{r}\right) t$
T	temperature of the inflating gas
u	velocity of the sphere center, $\frac{dy}{dt}$
$\bar{u}$	$\frac{u}{\lvert u_1 \rvert}$

y	distance from the impact surface to the sphere center
$\overline{y}$	$\frac{y}{r}$
α	arc $\cos(-\overline{y})$ (see fig. 1)
$\beta_1 \ldots \beta_6$	given by equations (28) and (36)
$\beta_7 \ldots \beta_9$	given by equations (41) through (43)
γ	ratio of specific heats
δ_p	vertical distance the package deflects as a result of the elastic extension of all cords
ϵ_T	fractional error in initial temperature
ϵ_u	fractional error in the initial impact velocity
ϵ_ξ	fractional error in the initial energy ratio
$\epsilon_\xi{}^*$	critical value of ϵ_ξ; the value for which $\overline{y}_{2A} = 0$
η	radial coordinate (see fig. 1)
θ	angle indicated in figure 1
μ	defined by equation (20); may vary from 1/3 to 1/2
ξ	initial energy ratio, $\frac{m_g c_v T_1}{\left(\frac{1}{2}\right) m u_1^2}$
ρ	mass density
σ	stress
φ	tensile force at $\eta = r$ in each cord at angle θ
Φ	total vertical force on the skin from the cords

Subscripts

o	value at $\theta = 0$
1	condition at first instant of impact
2	condition at maximum compression, when the velocity is zero

A	value of a parameter in the actual case
c	suspension cords
D	design value of a parameter
f	condition at final impact; that is either at $y = 0$ or at end of rebound
g	inflating gas
p	payload package
r	condition at the time skin is ruptured
s	skin
v	portion in motion with velocity u

ANALYSIS

Properties of the Sphere During Impact

As in the analysis in reference 1, it is assumed that the skin material is flexible, but nonstretchable, and thus that the part of the sphere skin not in contact with the impact surface retains its spherical shape, because it is supported by the internal gas pressure (see fig. 1). Then each particle of that part of the skin moves with velocity u, which is also the velocity of the center of the sphere. If it is also assumed that the suspension cords are flexible but nonstretchable, then the suspended payload package remains coincident with the sphere center and moves with velocity u, and the parts of the cords not in contact with the stationary part of the skin which is held on the surface may also be assumed to be moving with velocity u. Thus, all particles of the system which have struck the impact surface are assumed to have velocity zero, and all others, except for gas particles, are assumed to have velocity u. At the first instant of impact, $t = t_1$, all particles of the system have velocity u_1. At the instant of maximum compression, $t = t_2$, all particles have velocity zero. Also at $t = t_2$, if the sphere has compressed nearly to a hemisphere, the payload has just reached the surface at the instant its velocity is zero, and the maximum permissible amount of energy has been absorbed by the inflating gas.

Equation of Motion

The total mass of the system, m, is considered to consist of four parts:

$$m = m_p + m_s + m_c + m_g \tag{1}$$

where m_p is the mass of the payload package suspended in the center, m_s is the mass of the skin, m_c is the mass of the cords, and m_g is the mass of the inflating gas. One may follow a procedure similar to that used in reference 1 and define that portion of the mass which remains in motion, m_v, by

$$m_v = m_{sv} + m_{cv} + m_p \tag{2}$$

where m_{sv} and m_{cv} are, respectively, the parts of the mass of skin and mass of cords which are in motion with velocity u.

It was shown in reference 1 that, if the gravitational force and flexural stresses at the impact surface are neglected and if the uniform gas approximation is used for the internal gas pressure, application of Newton's second law of motion to the mass m_v leads to the differential equation of motion:

$$\bar{a} = \frac{1}{2}\frac{d(\bar{u}^2)}{d\bar{y}} = \frac{3(\gamma - 1)\xi}{8}\frac{m}{m_v}(1 - \bar{y}^2)\left[\left(\frac{4}{2 + 3\bar{y} - \bar{y}^3}\right)^{\gamma} - \bar{p}_a\right] \tag{3}$$

where $\bar{p}_a$ is the outside aerodynamic pressure (taken to be essentially constant at the value of the local atmospheric pressure), ξ is the initial energy ratio defined as in reference 1 by

$$\xi = \frac{m_g c_v T_1}{(1/2)m u_1^2} \tag{4}$$

and $y = r\bar{y}$ is the distance from the impact surface to the sphere center. Equation (3) applies to the present analysis if the relation for m_v given by equation (2) replaces that used in reference 1.

The differential equation, (3), can be solved if m_v/m is written as a function of $\bar{y}$. As shown in reference 1, m_{sv} is given by

$$m_{sv} = \frac{1}{2} m_s(1 + \bar{y}) \tag{5}$$

The portion of the mass of cords which has not struck the surface, m_{cv}, may be found as follows: let η be the radial coordinate and θ be the cone angle as indicated in figure 1. The mass density and cross-sectional area of one cord are ρ_c and A_c, respectively; both are constants. The

mass of an element of length of one cord, $d\eta$, is then $\rho_c A_c d\eta$. If the total number of suspension-cords is N_c, then the number of cords in the angle $d\theta$ is

$$dN_c = \frac{1}{2} N_c \sin\theta \, d\theta \tag{6}$$

Equation (6) is, of course, approximate if N_c is finite. Therefore the mass in a radial element, $d\eta$, and an element of θ, $d\theta$, is

$$dm_c = \frac{1}{2} N_c \rho_c A_c \sin\theta \, d\theta \, d\eta \tag{7}$$

but the total mass of the cords, if A_c is constant, is

$$m_c = N_c \rho_c A_c r \tag{8}$$

Equation (7) may thus be written

$$dm_c = \frac{m_c}{2r} \sin\theta \, d\theta \, d\eta \tag{9}$$

Then m_{cv} is

$$m_{cv} = \int_{\theta=0}^{\theta=\alpha} \int_{\eta=0}^{\eta=r} dm_c + \int_{\theta=\alpha}^{\theta=\pi} \int_{\eta=0}^{\eta=-y/\cos\theta} dm_c \tag{10}$$

where

$$\alpha = \arccos(-\bar{y}) \tag{11}$$

Substitution of equation (9) into (10) and use of the result, along with equation (5), in equation (2) give the following relation for m_v/m as a function of $\bar{y}$:

$$\frac{m_v}{m} = \frac{m_p}{m} + \frac{m_s}{m}\left(\frac{1+\bar{y}}{2}\right) + \frac{m_c}{m}\left(\frac{1+\bar{y}-\bar{y}\ln\bar{y}}{2}\right) \tag{12}$$

For specified values for the masses of components of the system, the differential equation, (3), may now be integrated to obtain $\bar{u}$ as a function of $\bar{y}$. Simultaneously, the equation

$$d\bar{t}/d\bar{y} = 1/\bar{u} \tag{13}$$

may be integrated to obtain $\bar{y}$ as a function of $\bar{t}$. The initial conditions for equations (3) and (13) are:

$$\bar{t} = 0 , \quad \bar{y} = 1 , \quad \bar{u} = -1 \tag{14}$$

The value of ξ to be used in equation (3) may either be specified or be found, for a desired value of $\bar{y}_2$ (the value of $\bar{y}$ when $\bar{u} = 0$ and $\bar{t} = \bar{t}_2$, the instant of maximum compression of the gas), by the procedure discussed in reference 1. Thus the motion of the sphere during impact is determined if m_p/m, m_c/m, m_s/m, and either ξ (defined by eq. (4)) or $\bar{y}_2$ are specified.

Performance Requirements and Capabilities

In addition to determining the motion, that is, acceleration, velocity, and location histories of the sphere center, equation (3) can also be used in conjunction with certain other relationships among the various parameters to determine the performance requirements and capabilities of the landing system. The performance includes mass of skin required, mass of gas required, mass of suspension cords required, mass of payload package allowed, and the required radius of the sphere. It was seen in reference 1 that these characteristics depend on initial gas temperature, gas constant and ratio of specific heats in the gas, a stress to mass ratio in the skin, impact velocity, final volume ratio, and outside atmospheric pressure. The radius required was also seen to be inversely proportional to the allowable maximum acceleration of the payload. Because the mass of suspension cords is included in the present analysis, the performance characteristics will also be a function of the strength to mass ratio of the cords.

The procedure to be used in evaluating the performance is as follows: Specify values for the parameters σ_{s1}/ρ_s, σ_{c2}/ρ_c, γ, R, T_1, $\bar{p}_a$, $\bar{y}_2$, and m_p/m. Then develop four equations for determining the proper values of m_c/m, m_s/m, m_g/m, and nr in relation to each other and to the specified parameters. Integrate the differential equation, (3), to determine ξ, from which can be found the corresponding impact velocity u_1.

One of the four required relationships is the same as equation (33) of reference 1, an expression relating the mass of skin to the mass of gas

$$\frac{m_s}{m} = \frac{3RT_1(1-\bar{p}_a)}{2(\sigma_{s1}/\rho_s)} \frac{m_g}{m} \tag{15}$$

where σ_{s1} is the stress in the skin before impact. Another relation, from equation (1), is

$$\frac{m_g}{m} = 1 - \frac{m_p}{m} - \frac{m_s}{m} - \frac{m_c}{m} \tag{16}$$

The mass of suspension cords required can be found in terms of the maximum stress in the top cord (which can be chosen to be less than the ultimate strength of the cord material).

The cords can support only radial tensile forces. Let the distribution of force in the cords be given by

$$\varphi = \varphi_o f \tag{17}$$

where φ_o, the force in the vertical cord ($\theta = 0$), is a function of $\bar{y}$ and f is a function of $\bar{y}$ and θ. The vertical force from the cords on the skin in the angle $d\theta$ is

$$\begin{aligned} d\Phi &= \varphi \cos\theta \, dN_c \\ &= \frac{1}{2} N_c \varphi_o f \cos\theta \sin\theta \, d\theta \end{aligned} \tag{18}$$

where use has been made of equations (6) and (17). Only the cords from $\theta = 0$ to $\theta = \pi/2$ are in tension during the impact. Therefore, the total vertical force transmitted by the cords to the skin is

$$\Phi = \int_{\theta=0}^{\theta=\pi/2} d\Phi = \frac{1}{2} N_c \varphi_o \mu \tag{19}$$

where

$$\mu = \int_0^{\pi/2} f \sin\theta \cos\theta \, d\theta \tag{20}$$

The total vertical force exerted by the gas pressure in decelerating m_v is, from equation (8) in reference 1,

$$F_p = m_v(du/dt) \tag{21}$$

Because it is assumed that all parts of m_v, that is, m_{sv}, m_{cv}, and m_p, have the same velocity, u, the rate of change of momentum to m_{sv} is $m_{sv}(du/dt)$. The remainder of F_p is transmitted to the mass $(m_p + m_{cv})$. Therefore, the rate of change of momentum transmitted to $(m_p + m_{cv})$ is $(m_p + m_{cv})(du/dt)$ and is equal to the force transmitted through the cords:

$$\Phi = (m_p + m_{cv})(du/dt) \tag{22}$$

Thus, from equations (17), (19), and (22), the force at $\eta = r$ in one cord at angle θ is

$$\varphi = \frac{2}{N_c \mu} (m_p + m_{cv}) \frac{du}{dt} f \tag{23}$$

The maximum force at a given time during the impact, as will be seen, is in the vertical cord at $\theta = 0$, $\eta = r$, and the maximum occurs at the instant of maximum compression ($t = t_2$). (When $y_2 = 0$, the maximum occurs a very short time before t_2 but is always nearly identical to the value at $t = t_2$.) Therefore,

$$\varphi_{max} = \frac{2}{N_c \mu_2} (m_p + m_{cv2}) \left(\frac{du}{dt}\right)_2 \tag{24}$$

The maximum acceleration is

$$(du/dt)_2 = n g_e \tag{25}$$

that is, n is the number of earth g's maximum acceleration. The left side of equation (24) may be written as

$$\varphi_{max} = \sigma_{c2} A_c \tag{26}$$

where σ_{c2} is the maximum stress in the vertical cord. Substitution of equations (25) and (26) along with equation (8) into equation (24) then gives

$$\frac{m_c}{m} = \frac{m_p}{m} \left[\frac{\mu_2 (\sigma_{c2}/\rho_c)}{2 g_e (nr)} - \beta_2 \right]^{-1} \tag{27}$$

where, from equations (9) and (10),

$$\beta_2 = \frac{m_{cv2}}{m_c} = \frac{1}{2} (1 + \bar{y}_2 - \bar{y}_2 \ln \bar{y}_2) \tag{28}$$

Equation (27) supplies the third of the four required equations relating the various parameters.

It is now seen that the required m_c/m depends on the strength to mass ratio of the cords, σ_{c2}/ρ_c. It also depends on the value of μ_2, given by equation (20) when $f = f(\bar{y}_2, \theta)$. It is noted that exact knowledge of f, the distribution of force in the cords, is not of critical importance in this study because only μ_2, the integral of the product of f times a function of θ over θ from zero to $\pi/2$ at $\bar{y} = \bar{y}_2$, is involved in the final results. The final results can be given in terms of $[\mu_2(\sigma_{c2}/\rho_c)]$. Then μ_2 can be estimated, and the effect of the choice of μ_2 can be considered to be equivalent to a change in the allowable value of σ_{c2}/ρ_c. Limits to the variation of $f(y_2, \theta)$, and thus to the choice of μ_2, can be shown. In those cases for which the tensile stress at all points in the upper hemisphere remains greater than zero, the shape of the skin will necessarily remain exactly spherical, regardless of the forces acting normal to the skin, because of the assumption of high modulus of elasticity in the skin. The skin above a horizontal diameter will then act as a rigid shell as long as $\sigma_s > 0$ at all points in the upper hemisphere. Then, if the mass of one cord is negligible in comparison to m_p and if $(\delta_p/r) \ll 1$, φ is given by

$$\Delta L = \delta_p \cos \theta = \varphi L / A_c E , \qquad (0 \leq \theta \leq \pi/2) \tag{29}$$

(where ΔL is the small change in length of each cord whose original length is $L = r$, the sphere radius), as long as $\sigma_s > 0$ at all points in $(0 \leq \theta \leq \pi/2)$. Thus if $\sigma_s > 0$

$$f = \varphi/\varphi_0 = \cos\theta\ , \qquad (0 \le \theta \le \pi/2) \tag{30}$$

and, from equation (20), if $\sigma_s > 0$ at all points in $0 \le \theta \le \pi/2$,

$$\mu = 1/3 \tag{31}$$

For all cases the skin stress is everywhere greater than zero in the upper hemisphere at least for a time at the beginning of the impact. In some cases this condition will exist until $t = t_2$, and thus μ_2 will have the value 1/3. For other cases, because the maximum force per unit area on the skin is at $\theta = 0$ (eq. (30)), the skin stress at $\theta = 0$ may be reduced to zero at some time during the impact (as the acceleration increases, and thus as the forces in the cords increase). After that time, the cosine cord-force distribution given by equation (30) is no longer valid because the upper hemisphere can no longer be considered entirely a rigid shell. If f were required to maintain the cosine distribution as the acceleration increased further, $(\sigma_s)_0$ would tend to become negative and thus a small part of the skin at $\theta = 0$ would tend to collapse because it is flexible. However, if this happened, the force in the vertical cord would tend toward zero while the cords at higher θ carried the increased load. But, if the force in any of the cords became reduced because of skin collapse, the cause of the reduction in the skin stress would be removed. Therefore the skin should tend not to collapse, and the cord force distribution would simply accommodate accordingly; that is, f becomes nearly constant in the region of zero skin stress. It is seen that, for those cases in which m_p/m and m_c/m are sufficiently large, large cord forces are present during the impact, and a region of zero stress may occur; hence the function f becomes implicitly involved with the stresses in the sphere skin. A detailed analysis of the skin stress distribution would be required to determine $f(\bar{y}_2, \theta)$, and thus μ_2, exactly.

As noted above, for purposes of obtaining results in the present study, it is sufficient to determine limits to the estimated values of μ_2. It is therefore noted that, after $(\sigma_s)_0$ becomes zero, the cord force distribution accommodates so that the cord force is nearly constant in the region of zero skin stress. The limiting case is therefore a constant value of φ over θ, that is, f = 1, for which $\mu = 1/2$. Thus μ_2 will be as low as 1/3 in some cases, but, for those cases where m_p/m and m_c/m are high, it may be nearly 1/2, and the effect of varying μ_2 is simply a change in the value of the allowable σ_{c2}/ρ_c.

The final expression of the four required (as discussed above) may be obtained from equation (3) by noting that the maximum acceleration is given by

$$\bar{a}_{max} = \bar{a}_2 = (r/u_1^{\,2})ng_e \tag{32}$$

and by making use also of equation (4) and the equation of state of the gas at $t = t_1$:

$$p_1\left(\frac{4}{3}\pi r^3\right) = m_g R T_1 = m_g(\gamma - 1)c_v T_1 \tag{33}$$

The result, which can be used as the fourth required equation relating the parameters, is

$$nr = \frac{3RT_1}{4g_e}\frac{m_g}{m}\frac{m}{m_{v2}}(1 - \bar{y}_2^2)\left[\left(\frac{4}{2 + 3\bar{y}_2 - \bar{y}_2^3}\right)^{\gamma} - \bar{p}_a\right] \tag{34}$$

where, from equations (12) and (28):

$$\frac{m_{v2}}{m} = \frac{m_p}{m} + \frac{m_s}{m}\left(\frac{1 + \bar{y}_2}{2}\right) + \beta_2\frac{m_c}{m} \tag{35}$$

Equation (34) may now be combined with equations (15), (16), and (27) to obtain independent explicit relations for m_s/m, m_g/m, m_c/m, and nr in terms of m_p/m and the various other parameters involved. For convenience in the ensuing manipulations, the following parameters are defined:

$$\beta_1 = \mu_2(\sigma_{c2}/\rho_c)/2g_e \tag{36a}$$

β_2 given by equation (28)

$$\beta_3 = (3/2)RT_1 \tag{36b}$$

$$\beta_4 = \sigma_{s1}/\rho_s \tag{36c}$$

$$\beta_5 = \frac{1 - \bar{y}_2^2}{2g_e}\left[\left(\frac{4}{2 + 3\bar{y}_2 - \bar{y}_2^3}\right)^{\gamma} - \bar{p}_a\right] \tag{36d}$$

$$\beta_6 = \frac{1}{2}(1 + \bar{y}_2) \tag{36e}$$

Substitution of equations (16) and (35) into (34) gives

$$nr = \frac{\beta_3\beta_5(1 - \bar{m}_p - \bar{m}_s - \bar{m}_c)}{\bar{m}_p + \beta_6\bar{m}_s + \beta_2\bar{m}_c} \tag{37}$$

where $\bar{m}_{(\ )}$ indicates $m_{(\ )}/m$. Equations (15) and (16) can be combined to eliminate m_g/m and to obtain

$$\bar{m}_s = \frac{\beta_3(1 - \bar{p}_a)(1 - \bar{m}_p - \bar{m}_c)}{\beta_4 + \beta_3(1 - \bar{p}_a)} \tag{38}$$

Substitution of equation (38) into (37) then gives an expression for the product nr in which the only mass ratios involved are $\bar{m}_p$ and $\bar{m}_c$:

$$nr = \frac{\beta_3\beta_4\beta_5(1 - \bar{m}_p - \bar{m}_c)}{[\beta_4 + \beta_3(1 - \bar{p}_a)](\bar{m}_p + \beta_2\bar{m}_c) + \beta_3\beta_6(1 - \bar{p}_a)(1 - \bar{m}_p - \bar{m}_c)} \tag{39}$$

Equation (39) may then be substituted back into equation (27), from which a quadratic expression for $\bar{m}_c$ is obtained. The result is

$$\frac{m_c}{m} = \frac{-\beta_8}{2\beta_7} \pm \sqrt{\left(\frac{\beta_8}{2\beta_7}\right)^2 + \frac{\beta_9}{\beta_7}} \tag{40}$$

where

$$\beta_7 = \beta_1\beta_2[\beta_4 + \beta_3(1 - \bar{p}_a)] - \beta_1\beta_3\beta_6(1 - \bar{p}_a) + \beta_2\beta_3\beta_4\beta_5 \tag{41}$$

$$\beta_8 = \beta_1[\beta_4 + \beta_3(1 - \bar{p}_a)]\bar{m}_p + \beta_1\beta_3\beta_6(1 - \bar{p}_a)(1 - \bar{m}_p) - \beta_2\beta_3\beta_4\beta_5(1 - \bar{m}_p) + \beta_3\beta_4\beta_5\bar{m}_p \tag{42}$$

$$\beta_9 = \beta_3\beta_4\beta_5\bar{m}_p(1 - \bar{m}_p) \tag{43}$$

The positive sign on the square root must be used to give positive values of m_c/m. As $\bar{m}_p$ approaches zero, $\bar{m}_c$ approaches a positive finite value. Thus, if there are cords in the vehicle and if $\bar{m}_p = 0$, the plus sign must be used, and a certain mass of cords is required. However, if there are no cords in the vehicle, $\bar{m}_p = 0$ and the minus sign may be used to give $\bar{m}_c = 0$ (since β_8 is negative).

If m_p/m is given, the corresponding required m_c/m can be found directly from equation (40). Then the required value of m_s/m is found from equation (38), and the required m_g/m, from equation (16). Finally, the product nr is found from equation (37). Each of these results, however, corresponds to a certain impact velocity, u_1. The impact velocity can only be found by integrating the differential equation, (3), and using the procedure outlined in reference 1 to obtain the correct value of ξ corresponding to the desired $\bar{y}_2$ and the other input conditions. The correct value of u_1 is then found from equation (4), which can be rearranged in the form

$$u_1 = -\sqrt{\frac{4\beta_3\bar{m}_g}{3(\gamma - 1)\xi}} \tag{44}$$

The drop altitude above the moon surface corresponding to a given impact

velocity is

$$h_m = u_1^2/2g_m = u_1^2/(10.94 \text{ ft/sec}^2) \tag{45}$$

where g_m is the gravitational acceleration on the moon. For convenience this correspondence is shown in figure 2.

Effects of Deviations in Gas Temperature and Impact Velocity From Design Conditions

In the design of the inflated sphere landing vehicle a certain initial gas temperature, T_1, and a certain impact velocity, u_1, would be assumed. The appropriate design mass ratios and sphere radius would then be calculated from the equations in the preceding section. In the actual landing, however, the gas temperature and impact velocity may differ slightly from the design conditions. The effects of these deviations may be inconsequential or very critical, depending on whether a certain condition was overestimated or underestimated. The choice of the design parameters will thus be influenced by the effects of deviations from design conditions.

For example, suppose the landing vehicle is designed for a given u_1 and T_1 so that it compresses to a hemisphere, that is, $\overline{y}_{2D} = 0$. Then, if the actual impact velocity is slightly higher than the design u_1, the payload will strike the surface with some residual velocity because it has not been completely decelerated to zero velocity at $\overline{y}_2 = 0$. However, if the actual velocity is slightly less than the design u_1, then the maximum compression will occur at $\overline{y}_2$ slightly greater than zero; that is, the payload package will come to rest a short distance above the surface, then drop to the surface when the skin is ruptured. The effect of the error in u_1 in this case would be much more tolerable than in the former case. The design $\overline{y}_2$ should therefore be chosen so that there is a high probability that the latter case will occur rather than the former.

Errors in the initial gas temperature will have similar effects. A negative error (value below design) in T_1 will cause $\overline{y}_{2A}$ to be less than $\overline{y}_{2D}$, or the payload will strike the surface with some residual velocity, whereas a positive error in T_1 will have the effect of decelerating the payload to zero velocity at $\overline{y}_{2A}$ greater than $\overline{y}_{2D}$ because of the higher gas pressure. In the case of positive error in T_1, the effect may not necessarily be inconsequential because the final acceleration will be higher than the design value.

It is the purpose here to estimate the magnitudes of the effects of deviations from design conditions and hence to show how the design parameters should be chosen for reliability.

The landing vehicle is designed for the conditions T_{1D} and u_{1D}, as well as the desired $\overline{y}_{2D}$, n_D, and other parameters involved. The

corresponding design values of m_s/m, m_g/m, m_c/m, m_p/m, r, and ξ are found by application of the theory in the previous section so that $\bar{u} = 0$ when $\bar{y} = \bar{y}_{2D}$, where $\bar{u} = u/|u_{1D}|$. In the actual case, in order for the initial condition, equation (14), to apply in the integration of equation (3), $\bar{u}$ must be considered to be $u/|u_{1A}|$, but this difference does not affect the integrated results of equation (3). The only parameter in equation (3) which can differ from the design condition is the initial energy ratio, ξ; that is, ξ_A may not be equal to ξ_D and hence $\bar{y}_{2A}$ will not equal $\bar{y}_{2D}$. An error in ξ may occur because of an error in T_1, u_1, or both.

Denote a fractional error in ξ by ϵ_ξ; that is,

$$\xi_A = (1 + \epsilon_\xi)\xi_D \tag{46}$$

Also denote errors in T_1 and u_1 by ϵ_T and ϵ_u, respectively. Thus

$$T_{1A} = (1 + \epsilon_T)T_{1D} \tag{47}$$

$$u_{1A} = (1 + \epsilon_u)u_{1D} \tag{48}$$

Therefore, since

$$\xi = 2(m_g/m)c_v(T_1/u_1^2) \tag{49}$$

the result from equations (46), (47), (48) and (49) is

$$1 + \epsilon_\xi = \frac{1 + \epsilon_T}{(1 + \epsilon_u)^2} \tag{50}$$

For no error in velocity, then, the error in ξ due to an error in temperature is simply

$$(\epsilon_\xi)_{\epsilon_u=0} = \epsilon_T \tag{51}$$

and for the case of no error in temperature, the error in ξ due to an error in velocity is

$$(\epsilon_\xi)_{\epsilon_T=0} = \frac{-\epsilon_u(2 + \epsilon_u)}{(1 + \epsilon_u)^2} \tag{52}$$

In the cases where ϵ_u is small,

$$(\epsilon_\xi)_{\epsilon_T=0} \approx -2\epsilon_u , \qquad |\epsilon_u| \ll 1 \tag{53}$$

For the cases where ϵ_ξ is positive (e.g., $\epsilon_T > 0$ and $\epsilon_u = 0$, or $\epsilon_u < 0$ and $\epsilon_T = 0$) the actual value of $\bar{y}_2$ is greater than the design value, that is, for $\epsilon_\xi > 0$,

$$\bar{y}_{2A} > \bar{y}_{2D} \tag{54}$$

For the cases in which ϵ_ξ is negative (e.g., $\epsilon_T < 0$ and $\epsilon_u = 0$, or $\epsilon_u > 0$ and $\epsilon_T = 0$) either the payload strikes the surface with final residual velocity u_f or the payload does not reach the surface, but the actual value of $\bar{y}_2$ is less than the design value; that is, for $\epsilon_\xi < 0$: either

$$\bar{u} = \bar{u}_f \quad \text{when} \quad \bar{y} = 0 \tag{55a}$$

or

$$0 \leq \bar{y}_{2A} < \bar{y}_{2D} \tag{55b}$$

The effects of deviations from the design conditions for a given case (given T_{1D}, $\bar{y}_{2D}$, m_p/m, and other input parameters and the calculated values of ξ_D, u_{1D}, m_s/m, m_g/m, and m_c/m) are thus found by integrating equation (3) again, using the same values for the mass ratios, but using ξ_A in place of ξ_D. The results of the integration ($\bar{y}$ vs. $\bar{a}$, $\bar{u}$, and $\bar{t}$) show either the value of $\bar{y}_{2A}$ when $\bar{u} = 0$ (and the corresponding value of $\bar{a}_{2A}$) or the value of $\bar{u}_f$ when $\bar{y} = 0$. It should be noted that $\bar{u}_f = u_f/|u_{1A}|$ and therefore that

$$u_f = (1 + \epsilon_u)|u_{1D}|\bar{u}_f \tag{56}$$

The ratio of actual maximum acceleration to design maximum acceleration, for those cases in which the payload does not strike the surface, can be found as follows:

From equation (25),

$$(u_1^2/r)\bar{a}_2 = ng_e \tag{57}$$

Therefore,

$$\bar{a}_{2D} = g_e n_D r/u_{1D}^2 \tag{58}$$

$$\bar{a}_{2A} = g_e n_A r/u_{1A}^2 \tag{59}$$

and thus,

$$n_A/n_D = (\bar{a}_{2A}/\bar{a}_{2D})(1 + \epsilon_u)^2 \tag{60}$$

Effect of Error In the Time at Which Skin Is Ruptured

It is desired to have the skin rupture at time t_{2A} when the actual velocity is zero. It is assumed that some method is used to rupture the skin instantaneously around a great circle of the sphere. Each half of the sphere skin will remain attached by half the suspension cords to the payload. The gas will escape simultaneously in all directions outward from the center in the plane of the rupture. The vehicle will tend, therefore, not to be propelled by the escaping gas.

Let t_r denote the actual time of skin rupture, which may not be the same as the most desirable time of skin rupture, t_{2A}. If Δt is the time error, then

$$t_r = t_{2A} + \Delta t \tag{61}$$

where Δt may be positive or negative and where, it must be noted,

$$\Delta t = \frac{r}{|u_{1A}|}\Delta\bar{t} = \left[\frac{r}{(1 + \epsilon_u)|u_{1D}|}\right]\Delta\bar{t} \tag{62}$$

to satisfy condition (14) on equations (3) and (13).

If the error Δt is negative, the inflating gas will be released from the vehicle before the payload has been decelerated to zero velocity. The decelerating pressure force will therefore be eliminated, and, if this occurs instantaneously, the payload package will strike the surface with the velocity it had at the time of skin rupture; that is, $u_f = u_r$. The velocity u_r can be found directly from the integrated results of $\bar{y}$ versus $\bar{a}$, $\bar{u}$, and $\bar{t}$, provided the velocity u_{1A} is used in the conversion from dimensionless to dimensional parameters.

If the error Δt is positive, the sphere will reach its maximum compression and begin to rebound before the skin is ruptured. The magnitude of the velocity will be essentially the same at $t_r = t_{2A} + \Delta t$ as at time $t_{2A} - \Delta t$, but the motion is in the opposite direction. This velocity, u_r, however, is not the same as the final impact velocity of the payload after it falls back to the surface. The reason for this is that, at $t = t_r$, nearly half of the mass of the skin and cords is at rest; therefore, some of the rebound momentum is taken up in putting this stationary material back into motion. The velocity of the payload at final impact, u_f, is therefore nearly the same (in magnitude) as the velocity after the entire system has just left the surface. It is assumed here, of course, that u_r is great enough that the sphere rebounds completely and with a final velocity great enough that the increment in velocity on the final impact due to the difference in height (equal to the sphere radius) is negligible. Equating the momentum at $t = t_r$ to the momentum at the instant the entire mass has left the surface during the

rebound, assuming the gas is moving at the same velocity as the rest of the system prior to t_r and is dispersed simultaneously in all directions at $t = t_r$, one finds

$$(m_{vr} + m_g)u_r = (m_p + m_s + m_c)(-u_f)$$

Thus

$$u_f = -u_{1A}\left(\frac{u_r}{u_{1A}}\right)\left[\frac{(m_{vr}/m) + (m_g/m)}{(m_p/m) + (m_s/m) + (m_c/m)}\right] \tag{63}$$

where m_{vr}/m is the value of m_v/m given by equation (12) when $\bar{y}$ has the value corresponding to $\bar{t} = \bar{t}_r$. Of course, $\bar{t}_r$ is given by

$$\bar{t}_r = \frac{|u_{1A}|}{r}\left(t_{2A} + \Delta t\right) \tag{64}$$

where Δt is positive in this case.

DISCUSSION OF RESULTS

Performance Requirements and Capabilities

In the analysis of the performance of the inflated sphere landing vehicle, the mass of the suspension cords has been considered. The results are shown in figures 3 through 7. The design parameters, including the distribution of the component masses of the system and the radius required, are shown plotted versus impact velocity (the corresponding drop altitude above the moon is shown by fig. 2). The results are given for the case of no outside atmospheric pressure and for hydrogen as the inflating gas with $\gamma = 1.41$ and $R = 766.5$ ft-lb/lb$_m$°R. The skin strength parameter for all results shown is $\sigma_{s1}/\rho_s = 10^6$ ft^2/sec^2, a reasonably attainable value, as is discussed in reference 1. Several values of $\bar{y}_{2D}$ and various combinations of the values of initial gas temperature of 200° and 500° R and the values of the product of μ_2 and the strength-mass ratio of the cords of 1.2×10^6 and 1.6×10^6 ft^2/sec^2 are employed. These values were computed assuming $\mu_2 = 0.4$ and using for (σ_{c2}/ρ_c) typical values of yield strength to mass density ratio of either nylon cords or steel wires: 3×10^6 ft^2/sec^2 and 4×10^6 ft^2/sec^2. Therefore, if actually $\mu_2 = 1/2$, then the results computed for $[\mu_2(\sigma_{c2}/\rho_c)] = 1.6\times10^6$ ft^2/sec^2 would correspond to $\sigma_{c2}/\rho_c = 3.2\times10^6$ ft^2/sec^2, or if μ_2 actually is 1/3, then the results computed for $[\mu_2(\sigma_{c2}/\rho_c)] = 1.6\times10^6$ ft^2/sec^2 would correspond to $\sigma_{c2}/\rho_c = 4.8\times10^6$ ft^2/sec^2. The value of μ may remain at 1/3 during the impact in some cases, whereas in others it may vary to a number between 1/3 and 1/2. In those cases where m_p/m and m_c/m are large, μ_2 may be nearly 1/2. It should be noted that, in the

calculations for figures 3 through 7, there has been no consideration of mass of any devices for attaching the cords to the sphere skin. It is presumed that a method of attachment could be developed which would not require a significant extra mass at the cord ends, but which would nevertheless minimize stress concentrations in the sphere skin at points of attachment by distributing the force from a cord over a circle or an area rather than applying it at a single point.

The performance results given by figures 3 to 7 can be used as follows: For a given desired impact velocity, the ratio of the mass of the payload package to the total mass of the system is found from figure 3. (Note that these results depend strongly on the impact velocity. Their dependence on the allowable strength-mass ratio of the cords is also significant, just as it was found in reference 1 that the results depend strongly on the skin strength parameter, σ_{s1}/ρ_s.) The required mass of skin, mass of suspension cords, mass of gas, and value of the product nr are found from figures 4 through 7. For a given allowable acceleration, then, the radius required is known. For the desired total mass, m, the required skin thickness may be calculated from

$$m_s = 4\pi r^2 \rho_s \delta$$

using the value of m_s/m from figure 4. The quantity $N_c \rho_c A_c$ can then be found from equation (8) using the value of m_c/m obtained from figure 5. Therefore, if a given cross-sectional area for the cords and the cord material are chosen, the number of cords required is determined. (As a check to insure that the volume of cords is not a significant percentage of the sphere volume so as to affect the results, one can calculate the ratio

$$\frac{m_c/\rho_c}{(4/3)\pi r^3} = \frac{3}{4\pi}\left(\frac{m}{\rho_c r^3}\right)\left(\frac{m_c}{m}\right)$$

For practical cases, this ratio is very small. In a numerical example given later in the discussion, if the total mass is less than 1300 pounds and if steel wires are used as the cords, this ratio is less than 10^{-3}.) Finally, the ratio of mass of gas to total mass is found from figure 6. The internal gas pressure may then be determined by the equation of state, (33).

Figure 8 has been plotted to illustrate the comparison with respect to temperature for the ratio of the payload package mass to the total mass of the system. It is seen that m_p/m varies little with varying initial temperature of the inflating gas.

In figure 9 is given a comparison of the present results with those of reference 1. It is seen that the results for m_p/m differ significantly, because the required mass of cords has been considered separately

from the payload mass in the present report, but that they very nearly agree if the value of m_p/m in reference 1 is assumed to include both payload and required cord mass. (The reason that $(m_p + m_c)/m \neq (m_p/m)_{ref.\ 1}$ is that the center of mass of m_{cv} does not remain coincident with that of m_p.) Note that at the higher velocities the mass of cords required in the present analysis would exceed the value of m_p given by the analysis of reference 1. Also note that the mass of cords required (for constant-area cords) does not approach zero as m_p/m approaches zero. (See also fig. 5.)

Effects of Deviations in Impact Velocity and Initial Temperature

As indicated in the Analysis, ϵ_ξ is a convenient parameter for relating the deviations in initial temperature and impact velocity to the resulting effects of such deviations. The effects are therefore shown in subsequent figures only as effects corresponding to deviations in ξ. For convenience, figure 10 shows a graphic representation of the relationship between the deviation in ξ and the corresponding deviations in u_1 and T_1 plotted directly from equation (50). It can be observed from these curves that the largest errors in ξ occur for positive errors in T_1 and negative errors in u_1. However, this condition gives a positive error in ξ, and, as mentioned in the Analysis, this is not the critical case.

The effects of deviations in u_1 and T_1, through the relationship of ϵ_u and ϵ_T, with ϵ_ξ given in figure 10, are presented in figures 11, 12, and 13. In those cases where ϵ_ξ is negative and where the payload has not been decelerated to zero velocity at $\overline{y} = 0$, the residual velocity, u_f, is given by figure 11. The values of u_{1D} correspond with the design parameters given by figures 3 through 7. Curves are shown for various values of ϵ_ξ and various $\overline{y}_{2D}$. The results are left in terms of ϵ_u so that only ϵ_ξ need be specified. In part (a) of figure 11 the results are for $T_{1D} = 500^\circ$ R, whereas those of part (b) are for $T_{1D} = 200^\circ$ R. One may note that the results shown are very nearly identical for this temperature range except for the upper end of the curve for $\epsilon_\xi = -0.40$ and $\overline{y}_{2D} = 0$. It is seen that, when negative deviations in ξ occur, the payload may strike the surface with a high velocity if the design value of $\overline{y}_2$ is too low. As $\overline{y}_{2D}$ is increased, this is much less likely to occur. In fact, for $\overline{y}_{2D} = 0.2$, the payload does not strike the surface even for $\epsilon_\xi = -0.40$ under the design conditions indicated in figures 11(a) and 11(b).

In the cases where the payload does not strike the surface before the vehicle rebounds, the velocity will be zero at $\overline{y} = \overline{y}_{2A}$ and the maximum acceleration will be n_A earth g's. This occurs whenever ϵ_ξ is positive and in some cases when ϵ_ξ is negative. Curves of $\overline{y}_{2A}$ versus $-u_{1D}$ are given in figure 12.

A result of greater interest than the value of $\bar{y}_{2A}$ for these cases is the ratio of actual to design maximum acceleration, shown in figure 13. Each point in figure 13 corresponds to a point in figure 12. It is noted that, for many cases, the actual maximum acceleration exceeds the design value. However, n_A/n_D is, in general, not much greater than unity. This ratio tends to be near or less than unity especially at the higher velocities, which are of greater practical interest. The higher values of $(n_A/n_D)/(1 + \epsilon_u)^2$ occur for positive values of ϵ_ξ and for low design impact velocities. It is seen from figure 10 that large positive values of ϵ_ξ occur only for negative values of ϵ_u. Thus the actual value of n_A/n_D will be less than $(n_A/n_D)/(1 + \epsilon_u)^2$ plotted on figure 13 when ϵ_ξ has a large positive value. Figures 13(a) through 13(d) show that n_A/n_D is slightly greater for higher $\bar{y}_{2D}$ when ϵ_ξ is positive, but that n_A/n_D is lower for higher $\bar{y}_{2D}$ when ϵ_ξ is negative. The results for n_A/n_D are useful not only in determining the actual maximum acceleration of the payload but also in finding the actual maximum stress in the cords. For this purpose, it can be shown from equations (24), (25), and (26) that

$$\frac{\sigma_{c2A}}{\sigma_{c2D}} = \frac{n_A}{n_D}\left[\frac{(m_p/m_c) + \beta_{2A}}{(m_p/m_c) + \beta_{2D}}\right] \tag{65}$$

where β_{2A} is the function of $\bar{y}_{2A}$ given by equation (28) and β_{2D} is the same function of $\bar{y}_{2D}$.

The critical deviation in ξ, ϵ_ξ^*, may be defined as the fractional error, for a given design case, which causes the sphere to just compress to a hemisphere; that is, the deviation in ξ has a value such that $\bar{y}_{2A} = 0$. If $\bar{y}_{2D} = 0$, then, of course, $\epsilon_\xi^* = 0$. Plotted in figure 14 are the values of $-\epsilon_\xi^*$ corresponding to design impact velocity. It will again be noted that all cases considered here are calculated for a vehicle designed according to figures 3 through 7. It is seen that if the vehicle is designed with $\bar{y}_{2D}$ only slightly greater than zero the critical value of ϵ_ξ is fairly large. For example, a vehicle designed for $\bar{y}_{2D} = 0.10$, an impact velocity of 500 ft/sec, and the other conditions as indicated in figure 14(a), can experience a negative deviation in ξ as large as 25 percent and not have the payload strike the surface. If, instead, $\bar{y}_{2D}$ is 0.20, then the negative deviation in ξ can be as large as 45 percent. It may be noted that these results depend very little on T_{1D} in the range shown here.

As an example of the use of the above results, suppose a moon-landing vehicle is designed for an impact velocity of 500 ft/sec (which corresponds to a drop from an altitude of 23,000 ft above the moon's surface), an initial hydrogen gas temperature of 500° R, an allowable skin strength parameter $\sigma_{s1}/\rho_s = 10^6$ ft^2/sec^2, allowable strength-mass ratio of the cords of 4×10^6 ft^2/sec^2 (assuming $\mu_2 = 0.4$), and $\bar{y}_{2D} = 0.10$. Suppose also that the maximum acceleration allowed is 2000 earth g's. From the (a) parts of figures 3 through 7, the results are: $m_p/m = 0.441$, $m_s/m = 0.258$, $m_c/m = 0.287$, $m_g/m = 0.014$, and $nr = 11{,}200$ feet. The radius required is

therefore 5.6 feet. Because the vehicle is designed for $\bar{y}_{2D} = 0.10$, there can be some error in ξ and the payload will still not strike the surface (if the size of the payload itself is not considered). The critical error, from figure 14(a), is $\epsilon_\xi^* = -0.25$. This might correspond, for example, from figure 10(b), to $\epsilon_u = 0.20$ and $\epsilon_T = 0.08$; that is, the actual impact velocity can be 20 percent higher than design, or 600 ft/sec, if the temperature is 8 percent higher than design, or 540° R, before the payload will strike the surface with any residual final velocity. Suppose, however, that the deviation in ξ exceeds the critical value (negatively). For example, suppose that the initial gas temperature is 13 percent lower than the design temperature, or only 435° R, and that the impact velocity is 20 percent high; then $\epsilon_\xi = -0.40$. One can see then, from figure 11(a), that $-u_f/(1 + \epsilon_u) = 222$ ft/sec and therefore that the payload will strike the surface with a final velocity of 266 ft/sec. Consider now the opposite case in which the deviation in ξ from the design condition is less than the critical value. Take, for example, $\epsilon_\xi = -0.10$. This deviation in ξ would occur if there were no error in impact velocity, but a -10 percent deviation in temperature, that is, $T_{1A} = 450°$ R. It is found from figures 12(b) and 13(b) that the payload then reaches zero velocity at $\bar{y}_{2A} = 0.064$ and that the maximum acceleration, in earth g's, is $n_A = 0.992(2000) = 1980$.

Considering the above results, one can now evolve a "design philosophy" for the inflated sphere landing vehicle; that is, one can determine how the design parameters should be chosen for reliability. From figure 3 it is seen that the payload is somewhat decreased when $\bar{y}_{2D}$ is increased above zero. For small increases in $\bar{y}_{2D}$, the decrease in payload is small. Figures 7(a) through (d) show that the radius required is not significantly affected by increasing $\bar{y}_{2D}$. Figures 14(a) through (d) then show that the critical (allowable) deviation in ξ is greatly increased (in magnitude) by increasing $\bar{y}_{2D}$ slightly. If the critical deviation in ξ is only slightly exceeded negatively, figure 11 shows that the final impact velocity of the payload is very high, and therefore critical. Figure 13 shows that the consequences of negative deviations in ξ less in magnitude than the critical value and of positive deviations in ξ are insignificant.

It is now apparent that a value of $\bar{y}_{2D}$ should be used which is as high as possible but which allows a sufficient payload-landing capability. The actual $\bar{y}_{2D}$ used will, of course, be dictated to some extent by the expected deviations from design conditions. It should be noted that the choice of design $\bar{y}_2$ should also take into account allowances for the size of the payload, for slight elastic elongation of the suspension cords, and for the probable unevenness of the impact surface.

Effect of Error In the Time at Which Skin Is Ruptured

Shown in figure 15 is the final impact velocity versus $-u_{1D}$, to which correspond the design parameters given in figures 3 through 7, for various errors in the time of skin rupture. Note that results are given only for $\epsilon_\xi = 0$ and would be different if ξ deviated from the design value. These results may, however, be used when there is a deviation from the design impact velocity, provided

$$\epsilon_T = \epsilon_u(2 + \epsilon_u) , \qquad (\epsilon_\xi = 0)$$

The reader will note that the results are given for dimensionless time errors. One will recall from the analysis that, when $\Delta\bar{t}$ is negative, $\bar{u}_f$ is just the value of $\bar{u}$ when $\bar{t} = \bar{t}_r = \bar{t}_{2A} + \Delta\bar{t}$, but that when $\Delta\bar{t}$ is positive, $\bar{u}_f$ must be calculated from equation (63). The results for negative $\Delta\bar{t}$ are indicated by solid lines and those for positive $\Delta\bar{t}$, by dashed lines. Evidently negative errors in the time of skin rupture (i.e., early rupture) cause the payload to experience a higher final impact velocity than do positive errors. As an example of the results, consider the case discussed above in which $u_{1D} = -500$ ft/sec, $y_{2D} = 0.10$ and $T_1 = 500^\circ$ R, but in which there is no deviation from the design temperature or velocity. The radius for that case is 5.6 feet. Therefore

$$\Delta\bar{t} = \frac{500 \text{ ft/sec}}{5.6 \text{ ft}} \Delta t = \frac{\Delta t}{0.0112 \text{ sec}}$$

It can thus be found directly from figure 15(b) that the final impact velocity of the payload for this particular case would have the values in the following list for the given examples of time errors.

$\bar{t}$	t, sec	$-u_f$, ft/sec
-0.15	-0.00168	107
-.10	-.00112	72
-.05	-.000560	36
-.01	-.000112	7.5
0	0	0
.01	.000112	6
.05	.000560	29.5
.10	.00112	58
.15	.00168	86.5

It is seen that the time error must be very small if the final impact velocity is to be small. One may note, however, that Δt in these results is proportional to the sphere radius, so that if a larger radius is used (and, consequently, a lower maximum acceleration) the values of Δt in the above list will be larger.

Demonstrated by the results of figure 15 is the fact that, if the sphere skin is to be ruptured to prevent rebound, it is essential to develop a method for rupturing the skin at the precise moment the velocity is zero with respect to the impact surface.

CONCLUDING REMARKS

The performance of the inflated sphere landing vehicle, wherein a payload to be landed is centrally suspended by numerous cords, has been evaluated with regard to allowable mass of payload package, mass of skin required, mass of suspension cords required, mass of gas required, and radius of sphere required. The analysis suggests that the inflated sphere landing technique is a feasible method to use, for example, in the terminal phase of a moon landing which is initiated at an altitude as great as 25,000 to 50,000 feet from the surface.

From the results of the analysis in this report, in which the required mass of suspension cords has been approximately calculated, it has become evident that the fraction of the total mass of the system taken up by the mass of cords is, in general, of significant magnitude. It is seen upon comparing the results with those in a previous study, in which the mass of cords was assumed to be negligible, that the payload mass given in that study closely agrees with the sum of payload and required cord mass as given in the present study. The results of the present report allow determination, however, of the actual portion of the mass available for payload.

It is indicated that the skin-strength parameter and the strength-mass ratio of the suspension-cord material are important in determining the performance requirements and capabilities of the system, that is, the performance results depend critically on the allowable values of these parameters. Therefore, although the landing vehicle is shown to be feasible with the use of presently available materials, large gains in performance are to be expected as stronger, light-weight, filament-type materials for use in construction of flexible fabrics and cords become available.

The effects of deviations from design initial temperature and impact velocity have been studied. The conditions have been found for which, if the vehicle is designed to compress to a volume somewhat greater than a hemisphere, a successful landing can be accomplished even if the design impact velocity is exceeded and/or the design initial temperature is not achieved. Critical deviations are found which, if exceeded, will result in the payload striking the surface with high velocity.

It has been found that, if the sphere skin is to be ruptured to prevent rebound, the effects of errors in the time at which the skin is ruptured may be very critical unless these time errors are exceedingly small, in the order of 0.1 millisecond for a 10-foot diameter sphere.

Ames Research Center
National Aeronautics and Space Administration
Moffett Field, Calif., Nov. 22, 1960

APPENDIX

INFLATED SPHERE LANDING VEHICLE WITH TAPERED PAYLOAD SUSPENSION CORDS

In the Analysis, the payload suspension cords were assumed to be of constant cross-sectional area. Because the cords themselves have mass, then, the stress is not constant over the length of one cord at a given instant during the impact acceleration. The maximum allowable stress then occurs at only the top end of the vertical cord, and the stress in the remainder of the vertical cord is less than the maximum allowable at the instant of maximum acceleration. Hence the entire mass of cords is not being used to maximum advantage. The optimum use of the mass of cords can be realized if the stress in the entire length of the cords reaches the maximum allowable value during the impact. If this condition is imposed, the cords will be tapered, and the appropriate cord cross-sectional area distribution can be calculated. While possibly not as practical nor as easily fabricated as the system using constant-area cords, the system with tapered cords is studied in this appendix to show the advantages in payload-landing capability.

In addition to the symbols used in the text of the report, the following are applicable to the analysis in this appendix:

A_c' local area of suspension cord cross section

A^* value of A_c' at $\eta = 0$

b parameter defined by equation (A13)

f φ'/φ_o', distribution of force in the cords

β_2' given by equation (A20)

φ' tensile force in one cord (function of θ, η, and y (or t))

Φ' total vertical force in the cords at a radial distance η in $0 \leq \theta \leq \pi/2$

The conditions and assumptions used in the text for the case of constant-area cords will be retained and equations will be developed for the case of cords of cross-sectional area which varies so that the stress in the entire vertical cord has a constant value at the instant of maximum acceleration. Equations (1) through (5), (13), and (14) in the text determine the motion during impact for specified values of m_p/m, m_s/m,

m_c/m, and ξ, provided an expression for m_{cv}/m_c is known. (The procedure discussed in ref. 1 for finding the required value of ξ to realize a specified $\bar{y}_2$ may also be used.)

Calculation of the Cord Cross-Sectional Area and Effects of the Cord Mass and Cord Forces

For the purpose of determining an expression for m_{cv}, in place of equation (7) one must now write for the cord mass in a radial element, $d\eta$, and an element of θ, $d\theta$

$$dm_c = \frac{1}{2} N_c \rho_c A_c' \sin \theta \, d\theta \, d\eta \tag{A1}$$

where $A_c' = A_c'(\eta)$. The total mass of cords is

$$m_c = N_c \rho_c \int_o^r A_c' d\eta \tag{A2}$$

An expression for the portion of the mass of cords in motion, m_{cv}, is then determined by combining equations (A1) and (A2) and substituting the result for dm_c into equation (10). The expression is found, at this point, only in terms of the area distribution of the cord cross section:

$$\frac{m_{cv}}{m_c} = \frac{1 + \bar{y}}{2} + \frac{\int_\alpha^\pi \int_o^{-y/\cos\theta} A_c' d\eta \sin\theta \, d\theta}{2 \int_o^r A_c' d\eta} \tag{A3}$$

The development which follows will lead to a determination of $A_c'(\eta)$. In this analysis the function φ' will be defined as the tensile force at the radial distance η in the cord at angle θ. (Note the difference between φ' and the function φ used in the text for cords of constant cross section.) Then the distribution of force in the cords, f, is defined by

$$\varphi' = \varphi'(y, \theta, \eta) = \varphi_o'(y, \eta) f(y, \theta) \tag{A4}$$

The total vertical force in the cords at a radial distance η over θ from zero to $\pi/2$ is found by substituting equations (6) and (A4) into the following expression:

$$\Phi'(\eta) = \int_{\theta=o}^{\theta=\pi/2} \varphi' \cos\theta \, dN_c \tag{A5}$$

Thus

$$\Phi' = \frac{1}{2} N_c \varphi_o'(y, \eta) \mu \tag{A6}$$

where μ is defined by equation (20). The force $\Phi'(\eta)$ is being used to decelerate the mass of payload, the moving mass of cords below the horizontal diameter, and the mass of cords above a horizontal diameter within a radial distance η from the center. Therefore the mass being decelerated by $\Phi'(\eta)$ is

$$m_p + \left(m_{cv} - \frac{m_c}{2}\right) + \frac{1}{2} N_c \rho_c \int_o^\eta A_c' d\eta$$

Because all parts of the moving portion of the system have the same velocity and acceleration, Φ' may be written

$$\Phi' = \frac{du}{dt}\left(m_p + m_{cv} - \frac{m_c}{2} + \frac{1}{2} N_c \rho_c \int_o^\eta A_c' d\eta\right) \tag{A7}$$

From equations (A6) and (A7)

$$\varphi_o' = \frac{2}{N_c \mu}\left(\frac{du}{dt}\right)\left(m_p + m_{cv} - \frac{m_c}{2} + \frac{1}{2} N_c \rho_c \int_o^\eta A_c' d\eta\right) \tag{A8}$$

Because the cord cross-sectional area is made to vary so that the stress in a cord is constant throughout the length of the cord at a given time, one may write

$$\varphi' = \sigma_c(y, \theta) A_c'(\eta) \tag{A9}$$

The maximum stress occurs in the vertical cord ($\theta = 0$) at the instant of maximum acceleration ($du/dt = n g_e$) and is denoted by σ_{c2}. From equation (A8), then,

$$\left(\frac{N_c \sigma_{c2} \mu_2}{2}\right) A_c'(\eta) = n g_e \left(m_p + m_{cv2} - \frac{m_c}{2} + \frac{1}{2} N_c \rho_c \int_o^\eta A_c' d\eta\right) \tag{A10}$$

where m_{cv2} is the value of m_{cv} given by equation (A3) when $y = y_2$. The solution of the integral equation, (A10), is

$$A_c'(\eta) = A^* e^{b\bar{\eta}} \tag{A11}$$

where

$$\bar{\eta} = \eta / r \tag{A12}$$

and

$$b = \frac{g_e (nr)}{\mu_2 (\sigma_{c2}/\rho_c)} \tag{A13}$$

and where A^*, the value of A_c' at $\eta = 0$, is found from equation (A10) to be

$$A^* = \frac{2b}{N_c \rho_c r}\left[m_p + m_c\left(\frac{m_{cv2}}{m_c} - \frac{1}{2}\right)\right] \tag{A14}$$

Equation (A11) shows that the cord cross-sectional area distribution should be exponential with radial distance in order to have constant stress in a cord. The quantity m_{cv2}/m_c in equation (A14) is determined by the condition $y = y_2$ when the relationship for m_{cv}/m_c is known. Substitution of equation (A11) into equation (A3) gives the required relationship:

$$\frac{m_{cv}}{m_c} = \frac{1 + \bar{y}}{2} + \frac{1}{2}\left[\frac{I(\bar{y}) - 1 + \bar{y}}{e^b - 1}\right] \tag{A15}$$

where

$$I(\bar{y}) = \int_{\alpha}^{\pi} e^{-b\bar{y}/\cos\theta} \sin\theta \, d\theta \tag{A16}$$

The transformation

$$\cos\theta = \frac{-1}{w} \tag{A17}$$

then leads to

$$I = -\int_{1/\bar{y}}^{1} \frac{e^{(b\bar{y})w} dw}{w^2} \tag{A18}$$

which has the solution

$$I(\bar{y}) = e^{b\bar{y}} - \bar{y}e^b - b\bar{y}\log_e\bar{y} - b\bar{y}\sum_{n=1}^{\infty}\left[\frac{(b\bar{y})^n - b^n}{n \cdot n!}\right] \tag{A19}$$

The quantity m_{cv}/m_c as a function of $\bar{y}$ is now completely determined, by equations (A15) and (A19), in terms of the parameter b. Thus, by use of equations (2), (5), and (A15), the quantity m_v/m is completely determined for use in equation (3) when m_p/m, m_s/m, m_c/m, and b are specified. The cord cross-sectional area distribution is given by equation (A11) where A^* is given by equation (A14) and where m_{cv2}/m_c may now be found from equation (A15) to be

$$\beta_2' = \frac{m_{cv2}}{m_c} = \frac{1 + \bar{y}_2}{2} + \frac{1}{2}\left[\frac{I(\bar{y}_2) - 1 + \bar{y}_2}{e^b - 1}\right] \tag{A20}$$

The parameter b in the above development involves μ_2. As discussed on page 10 of this report, the final results can be given in terms of $[\mu_2(\sigma_{c2}/\rho_c)]$ and μ_2 can be estimated. Also as discussed, as long as the skin tensile stress remains greater than zero at all points in the upper hemisphere, the skin above a horizontal diameter can be assumed to act as a rigid shell. Then the total elongation of each cord in $0 \leq \theta \leq \pi/2$ due to a small vertical deflection δ_p of the payload

package is

$$\delta_p \cos\theta = \int_0^r \frac{\varphi'}{A_c' E}\, d\eta \quad ; \qquad \left(\sigma_s > 0 \quad \text{in} \quad 0 \le \theta \le \frac{\pi}{2}\right) \tag{A21}$$

Because σ_c is invariant with η, substitution of equation (A9) into (A21) gives the result

$$\delta_p \cos\theta = \frac{\sigma_c r}{E} \quad , \qquad \left(\sigma_s > 0 \quad , \quad 0 \le \theta < \frac{\pi}{2}\right) \tag{A22}$$

and further use of equation (A9) with (A22) gives

$$\varphi' = A_c' \left(\frac{E\delta_p}{r}\right) \cos\theta \tag{A23}$$

from which equation (A4) gives

$$f = \cos\theta \, , \qquad (\sigma_s > 0 \, , \qquad 0 \le \theta < \pi/2) \tag{A24}$$

Then, from equation (20), if $\sigma_s > 0$ at all θ in $0 \le \theta < \pi/2$,

$$\mu = \frac{1}{3} \tag{A25}$$

As explained on page 11, for those cases in which $(\sigma_s)_o$ is reduced to zero at some time during the impact, the value of μ_2 will lie between 1/3 and 1/2.

Landing Performance

In order to calculate the design payload-landing performance, the required relationships among the masses of the various components of the system and the sphere radius are found by a procedure similar to that used in the text for constant-area cords. Two of the required relationships are supplied by equations (16) and (38) in the text. A third expression is found by substituting equation (A11) into (A2) to obtain

$$m_c = \frac{N_c \rho_c r A^*}{b} (e^b - 1) \tag{A26}$$

which may be combined with equation (A14) to yield

$$\bar{m}_c = \frac{2(e^b - 1)\bar{m}_p}{1 + (e^b - 1)(1 - 2\beta_2')} \tag{A27}$$

where $\bar{m}(\ )$ indicates $m(\ )/m$. A fourth relationship, obtained from equation (34), may be written as

$$nr = \frac{\beta_3 \beta_5 \bar{m}_g}{\bar{m}_p + \beta_6 \bar{m}_s + \beta_2' \bar{m}_c} \tag{A28}$$

The four equations, (16), (38), (A27), and (A28), may be used to find the four quantities $\bar{m}_s$, $\bar{m}_c$, $\bar{m}_g$, and nr in terms of $\bar{m}_p$ and the various other input parameters involved. The product nr is implicitly involved in these equations since, from equation (A13),

$$b = \frac{nr}{2\beta_1} \tag{A29}$$

The explicit relationships can therefore be most easily found by a simple "trial and error" or iteration procedure. For a given value of $\bar{m}_p$ and given values of the various input parameters involved, an arbitrary value for the product nr can be used for the first trial in the iteration. The corresponding $\bar{m}_c$ can then be calculated from equation (A27), and $\bar{m}_s$ and $\bar{m}_g$ can be calculated from equations (38) and (16), respectively. Then, when the correct value of nr has been tried, equation (A28) will be satisfied, and the corresponding correct values of $\bar{m}_c$, $\bar{m}_s$, and $\bar{m}_g$ will be found. The design quantities (i.e., the mass ratios and the sphere radius) then correspond to a certain impact velocity u_1, which can be found only by integrating the differential equation of motion, (3), to obtain the required ξ (by the procedure outlined in ref. 1) and by making use of equation (44).

The equations in this analysis were programmed for solution on an IBM type 704 electronic data-processing machine. The differential equations involved were integrated by the Adams-Moulton predictor-corrector method. A comparison of the payload-landing capability of a sphere with exponentially tapered payload-suspension cords with that of a sphere employing constant-area cords is shown in figure 16. The results are shown only for $y_2 = 0$, $\sigma_{s1}/\rho_s = 10^6$ ft^2/sec^2, and $T_1 = 500^\circ$ R, and correspond to values of $[\mu_2(\sigma_{c2}/\rho_c)]$ as indicated. It is seen that the use of the exponentially tapered cords affords a somewhat greater payload-landing capability at a given impact velocity. The principal advantage is realized when low values of m_p/m are used, in which cases the impact velocity allowed is significantly higher. Specifically, for $\mu_2(\sigma_{c2}/\rho_c) = 1.6\times10^6$ ft^2/sec^2 (which corresponds to $\sigma_{c2}/\rho_c = 4\times10^6$ ft^2/sec^2 if $\mu_2 = 0.4$). a sphere with m_p/m of one-fifth can land at 11 percent higher velocity, and if m_p/m is 1/10, the increase in impact velocity afforded is 17 percent.

REFERENCES

1. Martin, E. Dale, and Howe, John T.: An Analysis of the Impact Motion of an Inflated Sphere Landing Vehicle. NASA TN D-314, 1960.

2. Howe, John T., and Martin, E. Dale: Gas Dynamics of an Inflated Sphere Striking a Surface. NASA TN D-315, 1960.

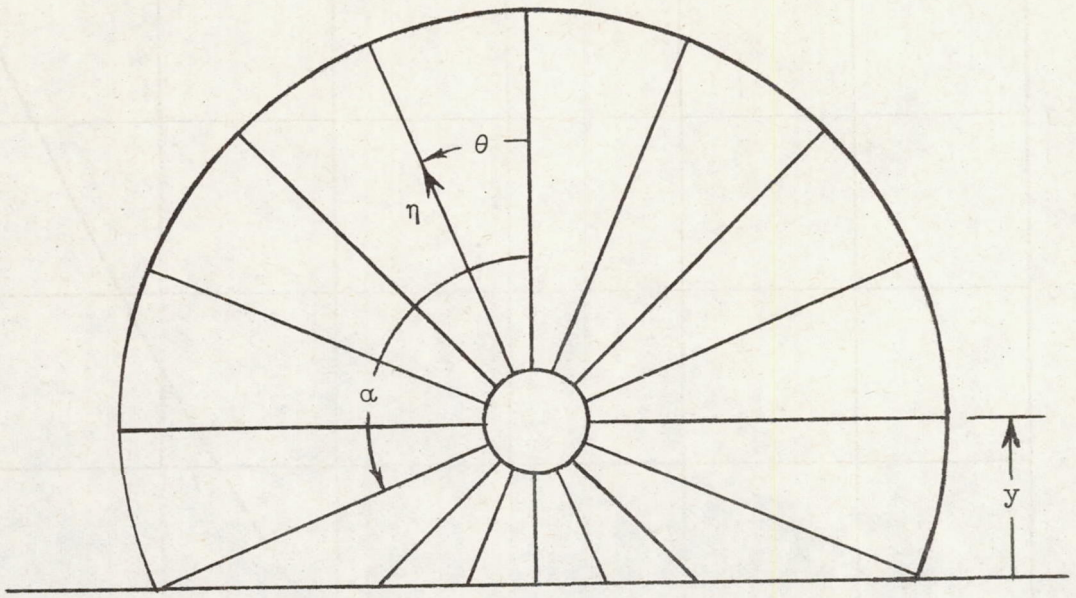

Figure 1.- Inflated sphere during impact.

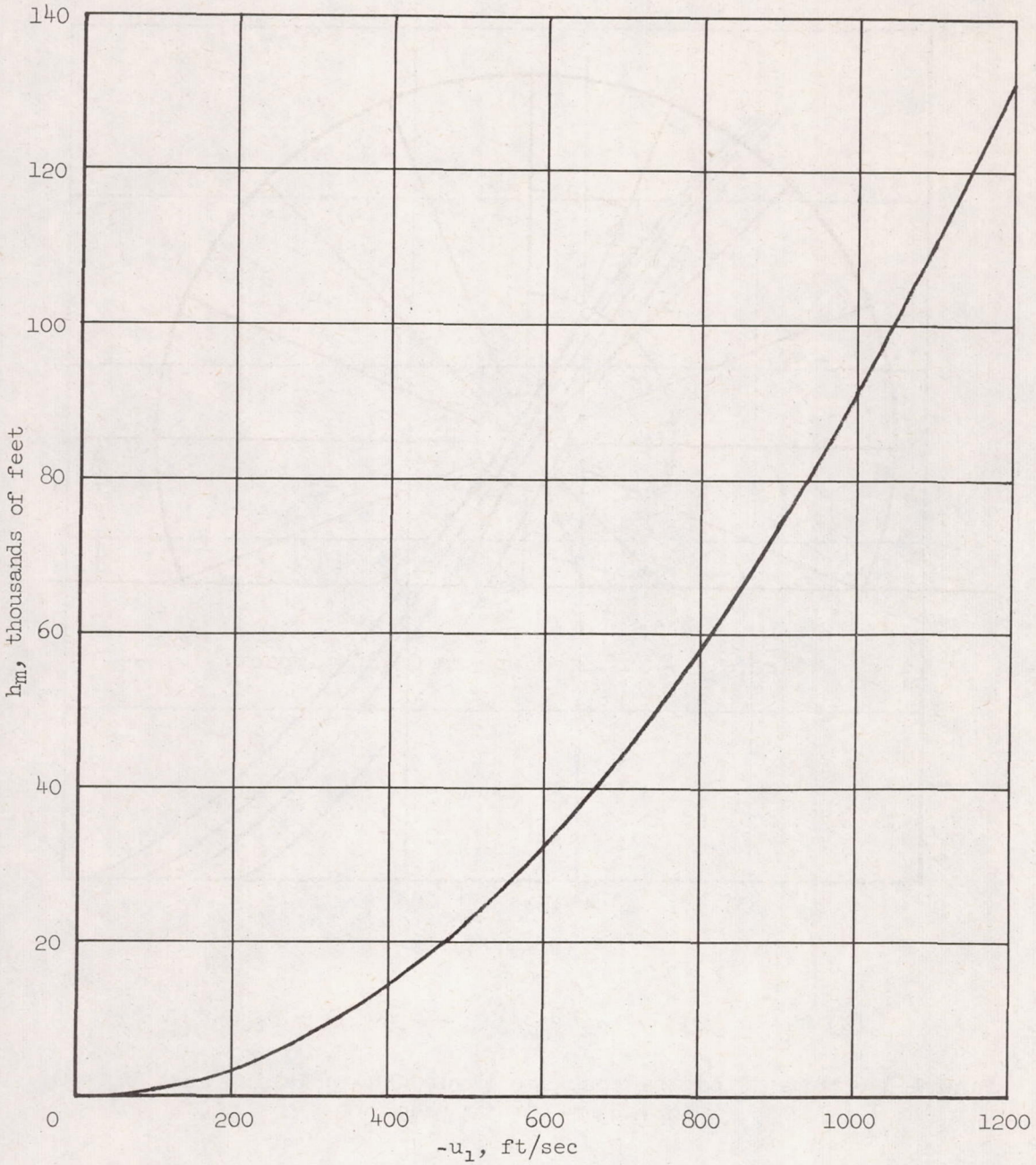

Figure 2.- Drop altitude above moon and corresponding impact velocity.

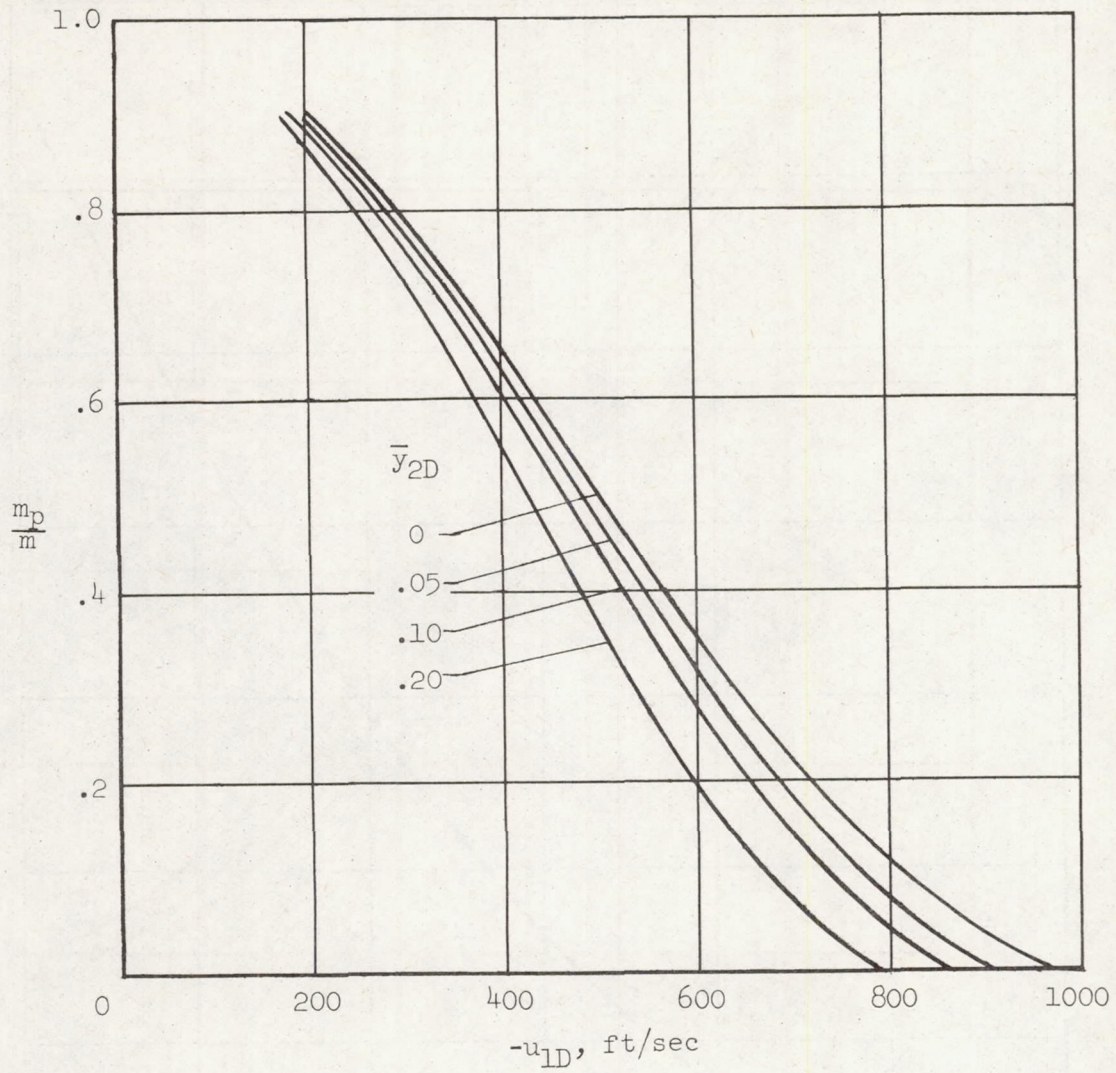

(a) $T_{1D} = 500^{\circ}$ R; $\mu_2(\sigma_{c2}/\rho_c) = 1.6 \times 10^6$ ft^2/sec^2

Figure 3.- Mass of payload package (hydrogen inflating gas; $\bar{p}_a = 0$; $\sigma_{s1}/\rho_s = 10^6$ ft^2/sec^2).

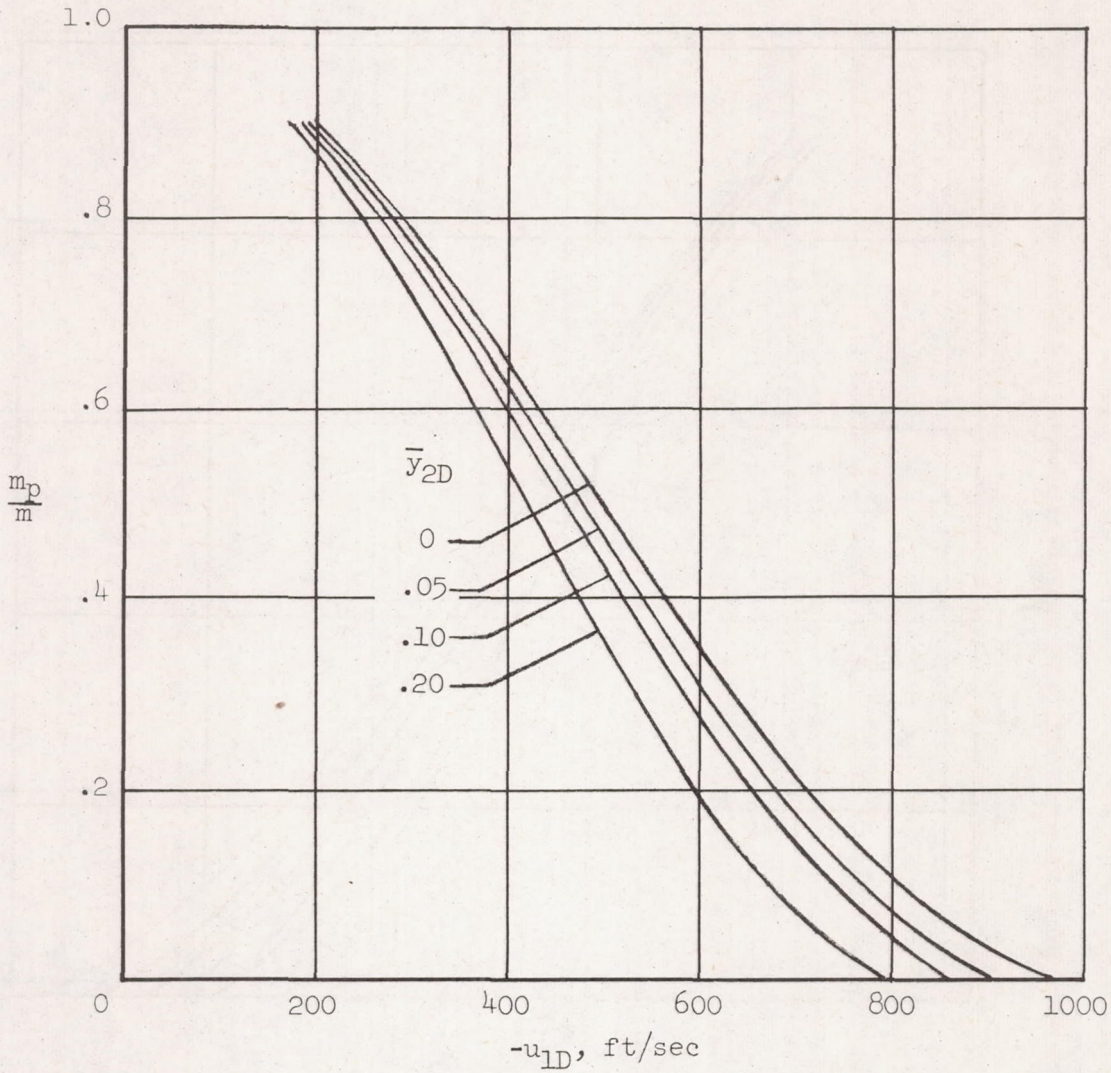

(b) T_{1D} = 200° R; $\mu_2(\sigma_{c2}/\rho_c)$ = 1.6×10^6 ft^2/sec^2

Figure 3.- Continued.

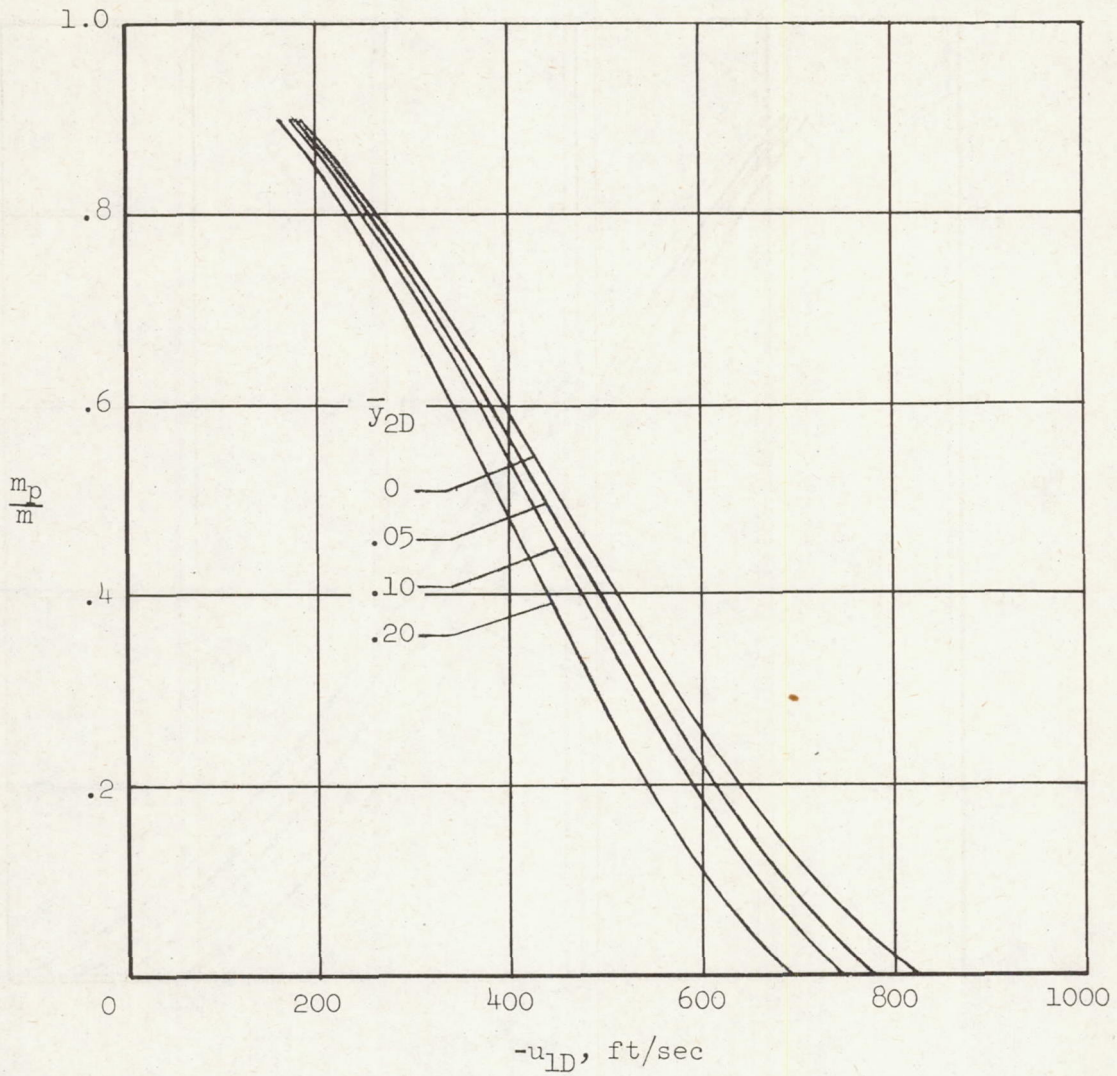

(c) $T_{1D} = 500^{\circ}$ R; $\mu_2(\sigma_{c2}/\rho_c) = 1.2 \times 10^6$ ft^2/sec^2

Figure 3.- Continued.

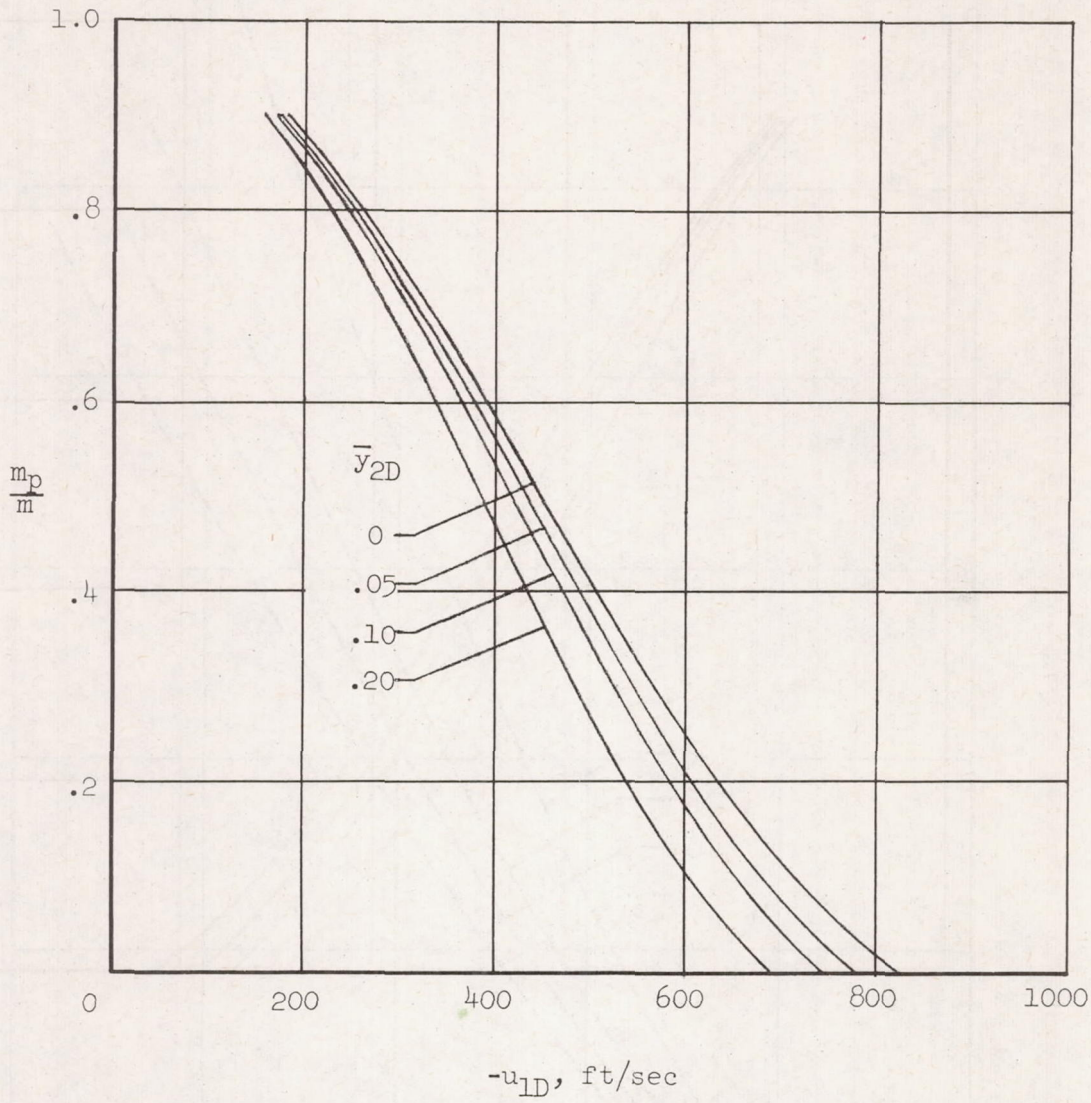

(d) $T_{1D} = 200^{\circ}$ R; $\mu_2(\sigma_{c2}/\rho_c) = 1.2 \times 10^6$ ft^2/sec^2

Figure 3.- Concluded.

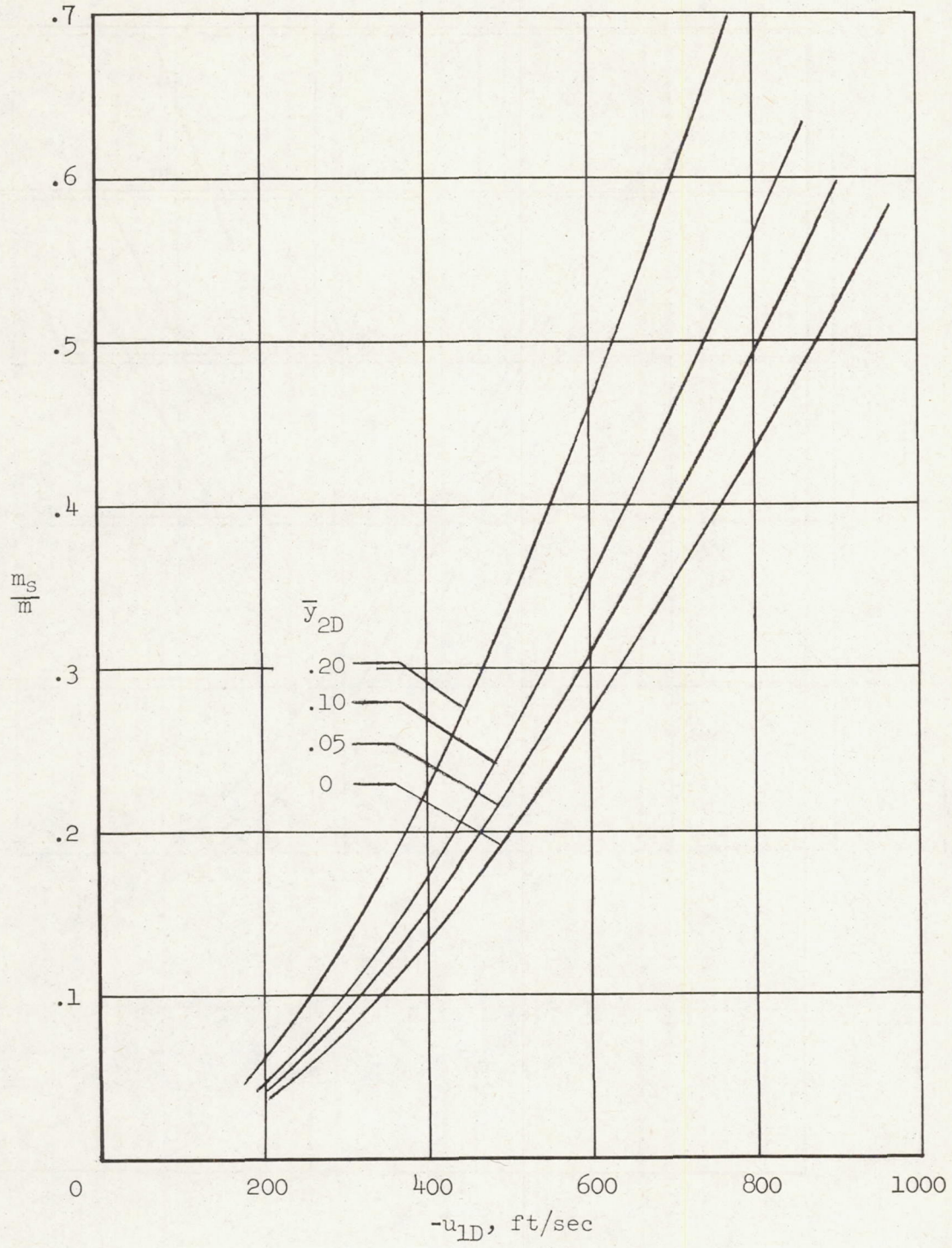

(a) $T_{1D} = 500^{\circ}$ R; $\mu_2(\sigma_{c2}/\rho_c) = 1.6 \times 10^6$ ft^2/sec^2

Figure 4.- Mass of skin required (hydrogen inflating gas; $\bar{p}_a = 0$; $\sigma_{s1}/\rho_s = 10^6$ ft^2/sec^2).

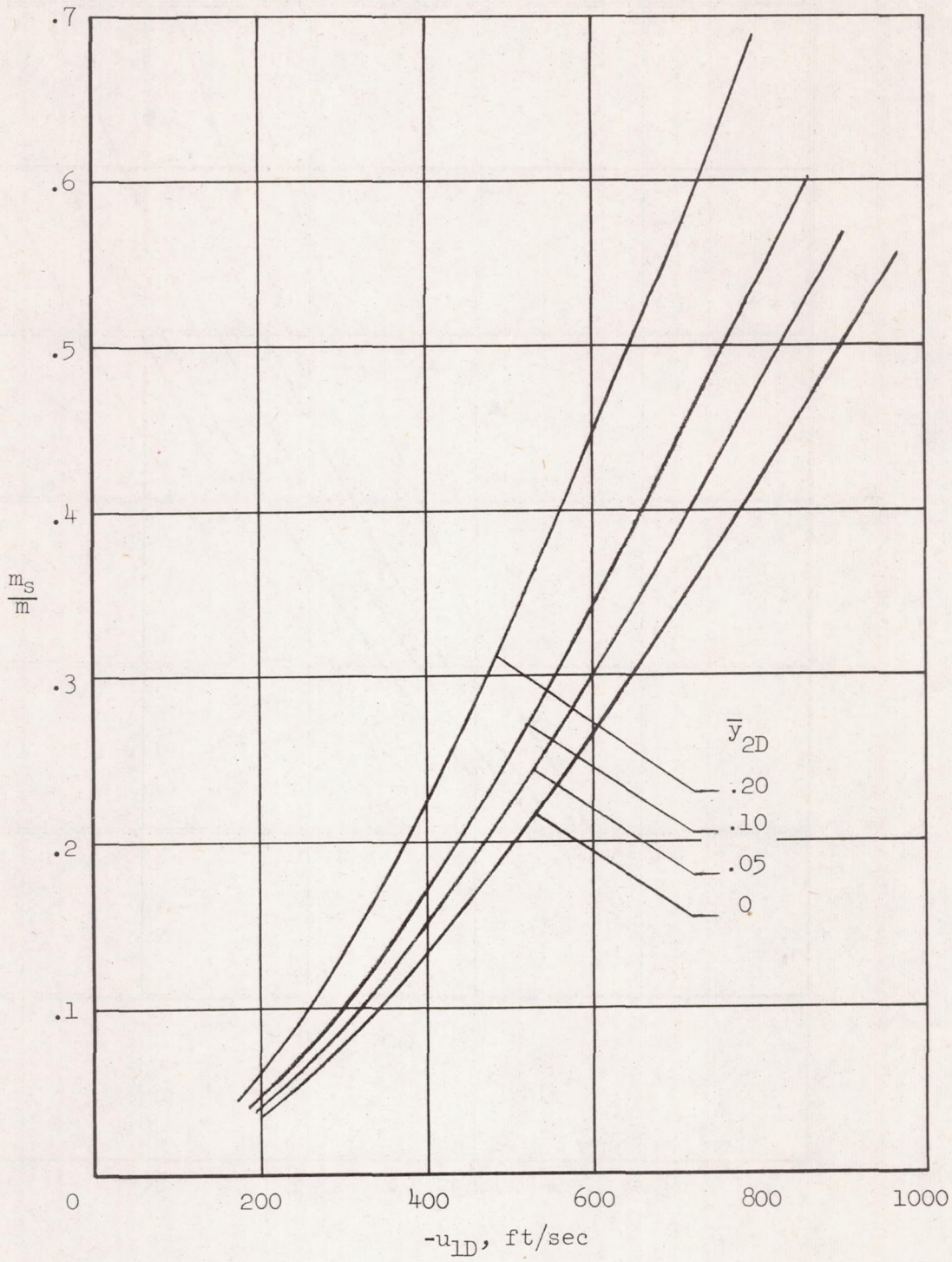

(b) $T_{1D} = 200^{\circ}$ R; $\mu_2(\sigma_{c2}/\rho_c) = 1.6 \times 10^6$ ft^2/sec^2

Figure 4.- Continued.

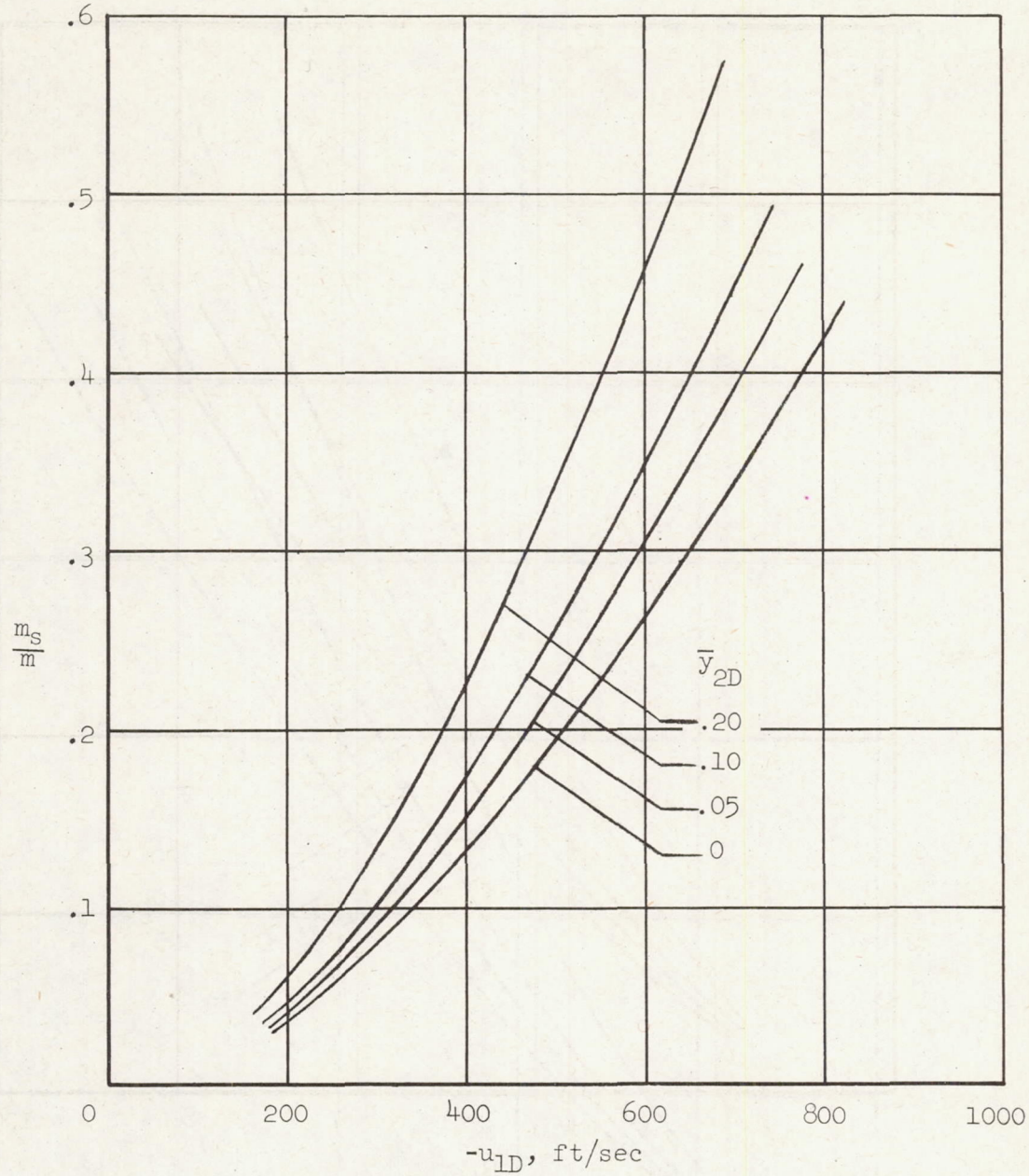

(c) $T_{1D} = 500^{\circ}$ R; $\mu_2(\sigma_{c2}/\rho_c) = 1.2 \times 10^6$ ft^2/sec^2

Figure 4.- Continued.

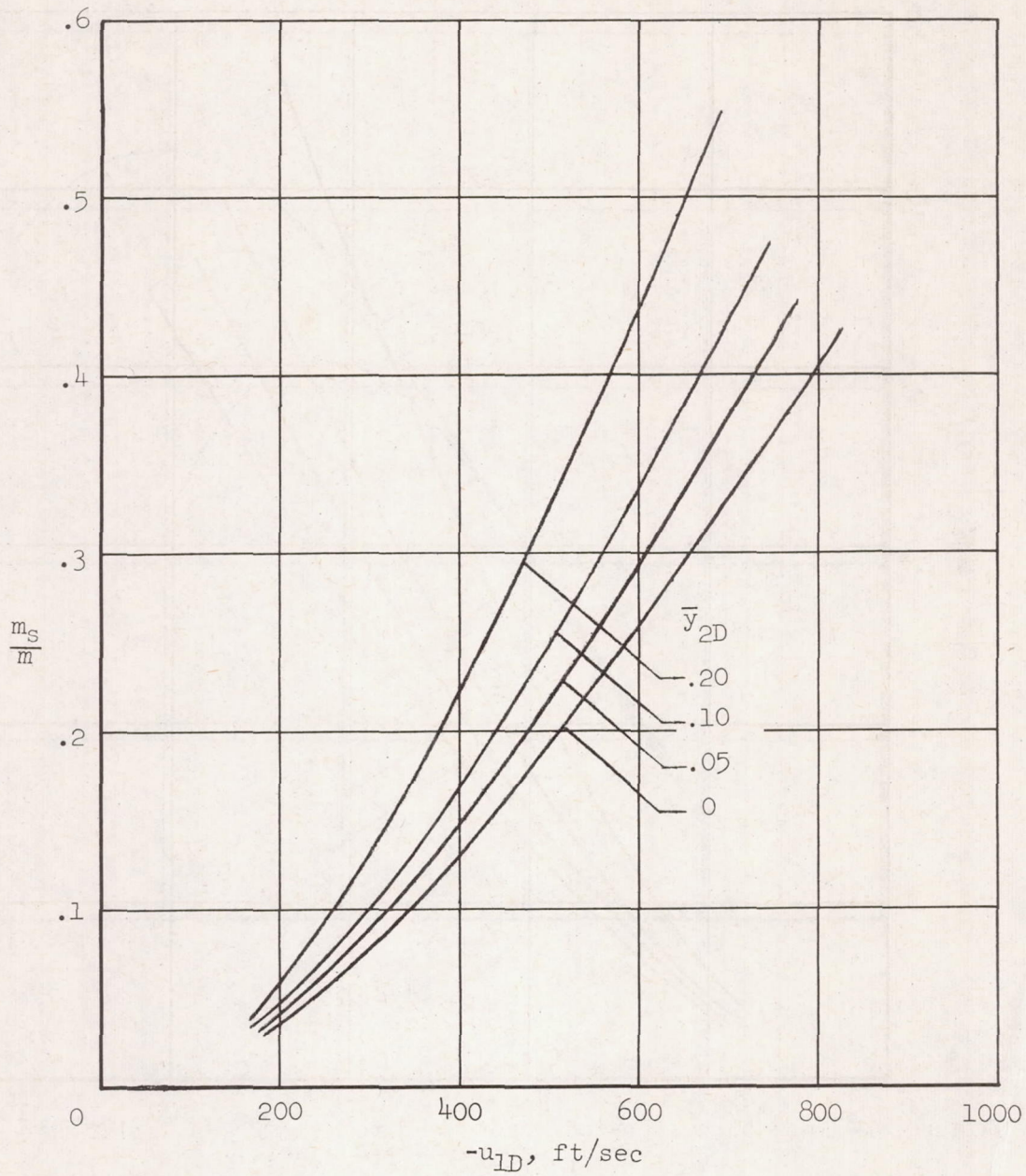

(d) $T_{1D} = 200^{\circ}$ R; $\mu_2(\sigma_{c2}/\rho_c) = 1.2 \times 10^6$ ft^2/sec^2

Figure 4.- Concluded.

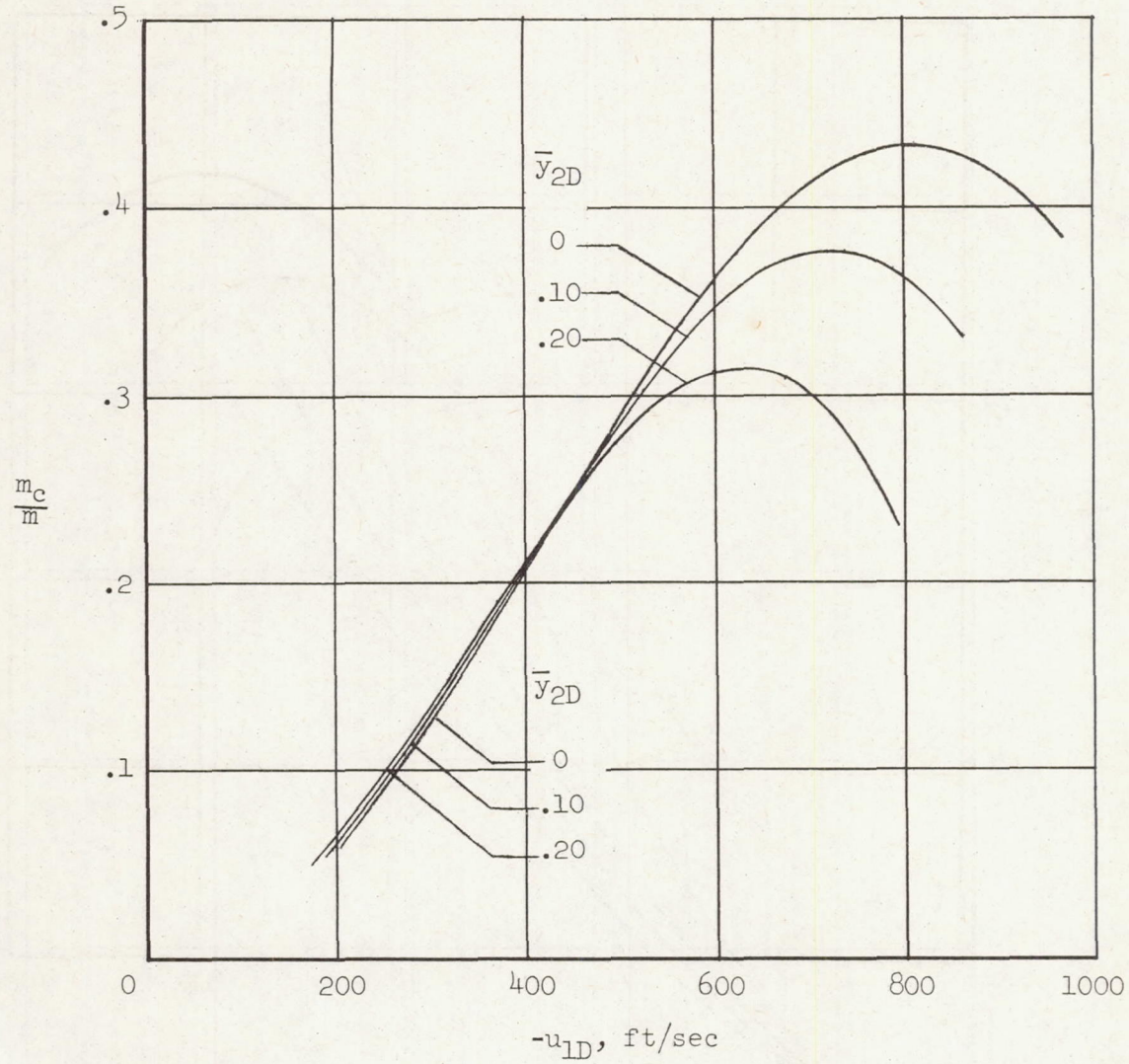

(a) $T_{1D} = 500^{\circ}$ R; $\mu_2(\sigma_{c2}/\rho_c) = 1.6 \times 10^6$ ft^2/sec^2

Figure 5.- Mass of suspension cords required (hydrogen inflating gas; $\bar{p}_a = 0$; $\sigma_{s1}/\rho_s = 10^6$ ft^2/sec^2).

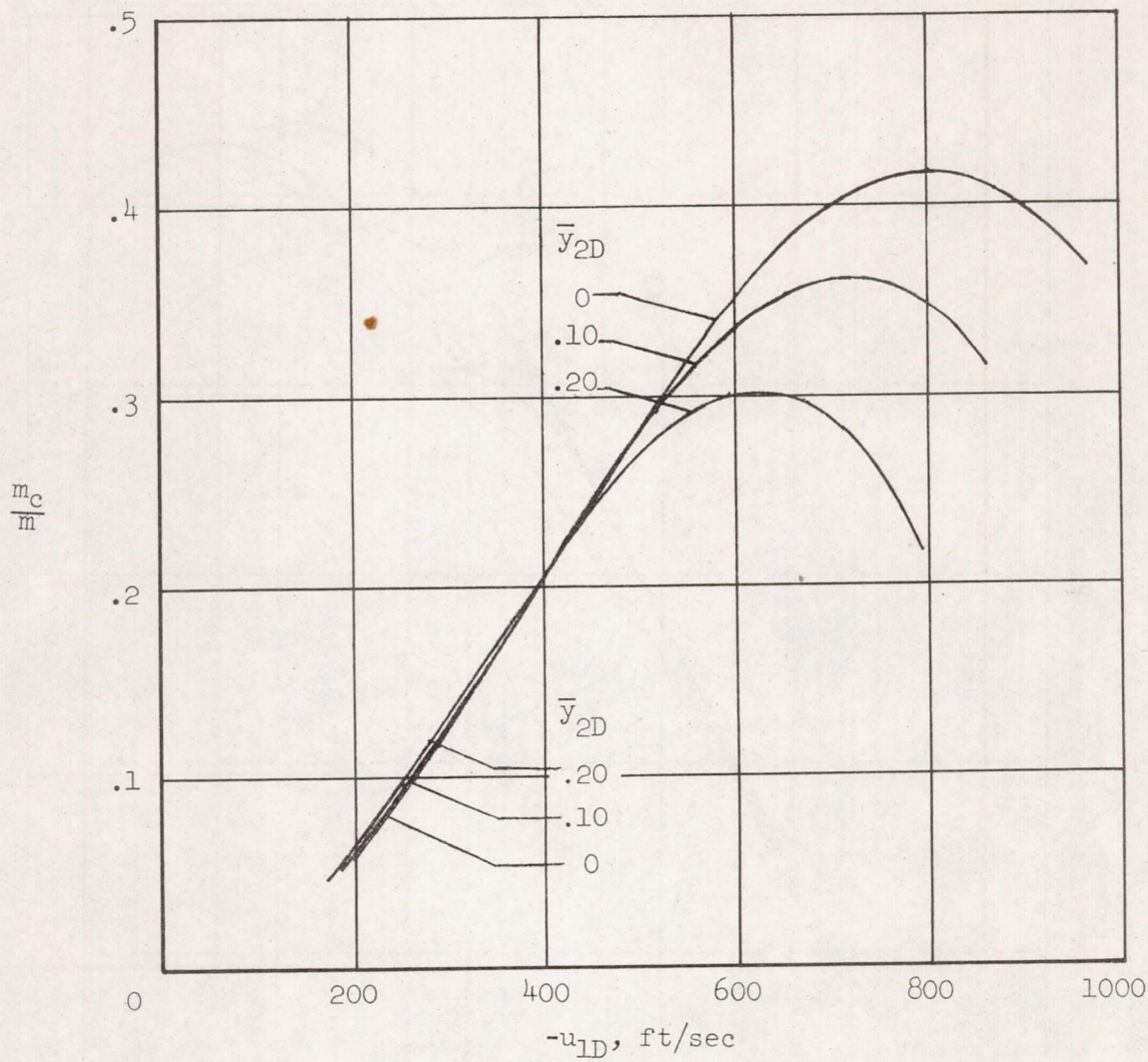

(b) $T_{1D} = 200^{\circ}$ R; $\mu_2(\sigma_{c2}/\rho_c) = 1.6 \times 10^6$ ft^2/sec^2

Figure 5.- Continued.

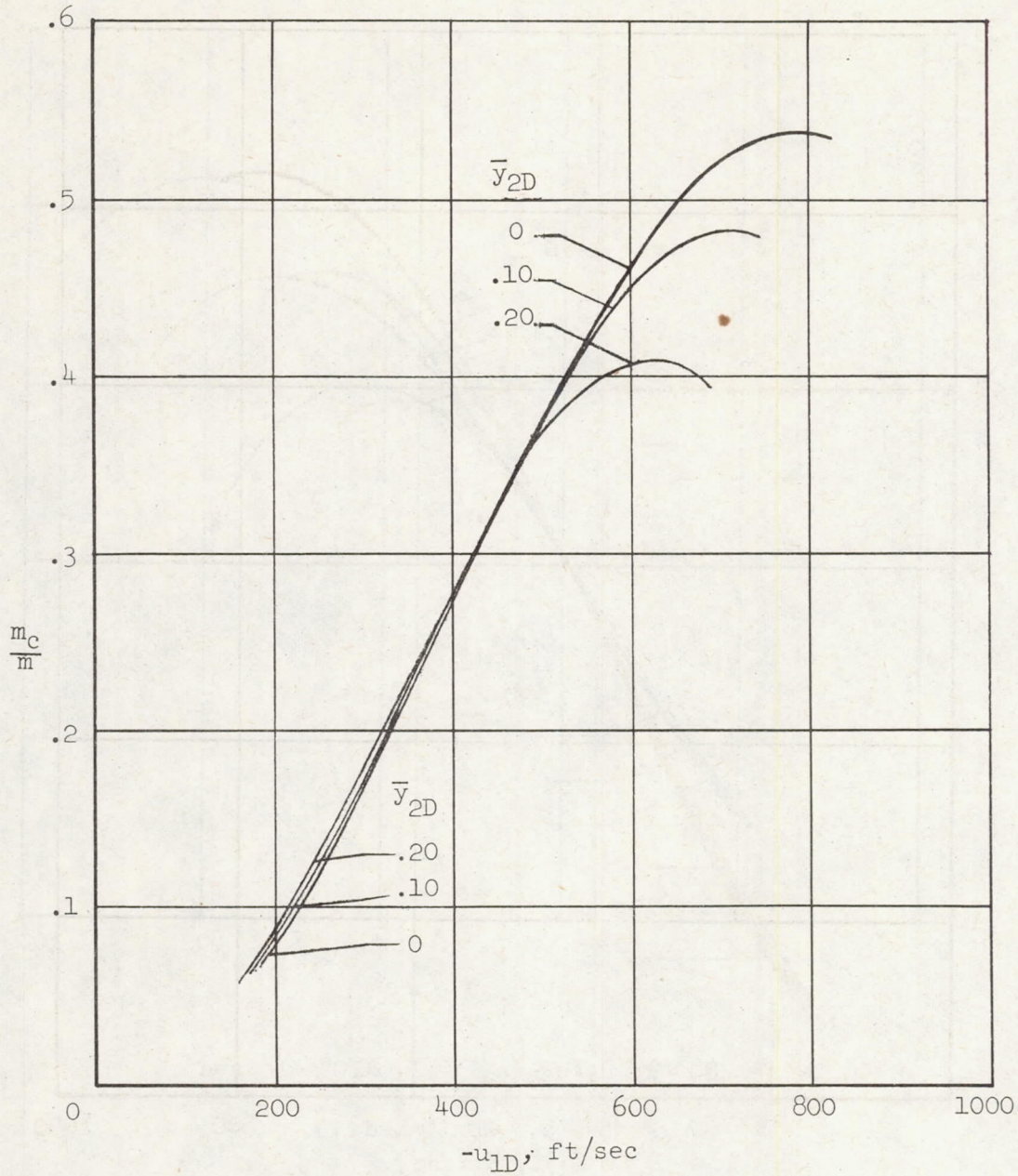

(c) $T_{1D} = 500^{\circ}$ R; $\mu_2(\sigma_{c2}/\rho_c) = 1.2 \times 10^6$ ft^2/sec^2

Figure 5.- Continued.

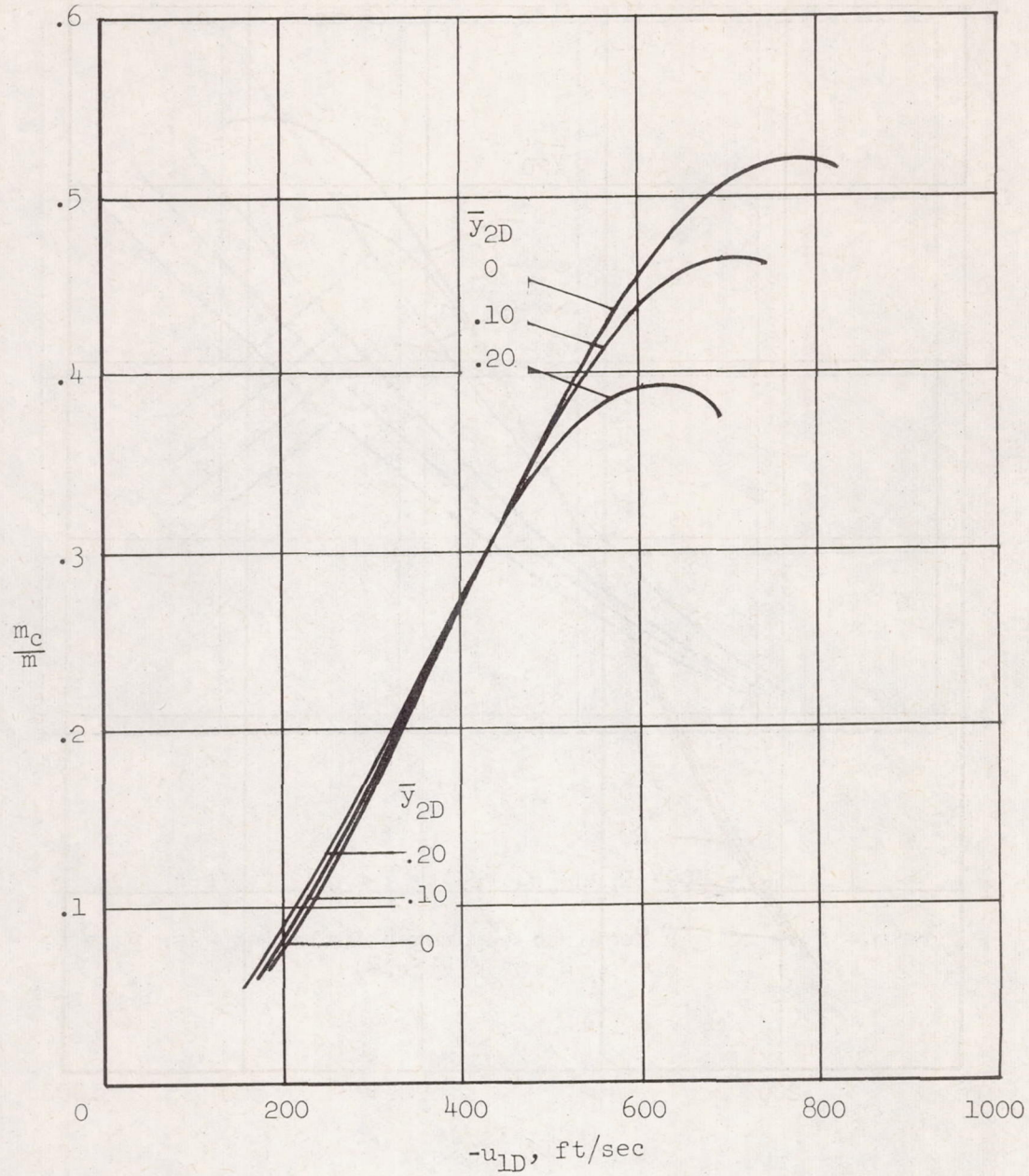

(d) $T_{1D} = 200^{\circ}$ R; $\mu_2(\sigma_{c2}/\rho_c) = 1.2 \times 10^6$ ft^2/sec^2

Figure 5.- Concluded.

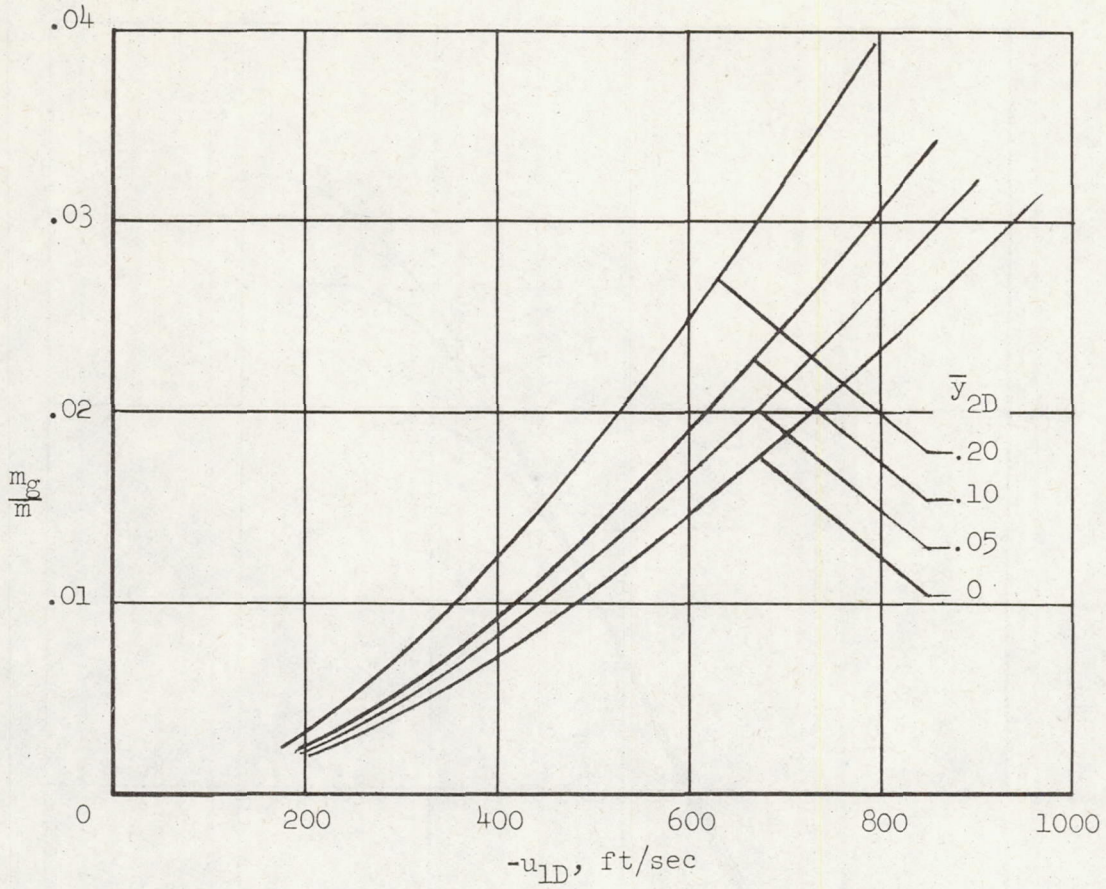

(a) $T_{1D} = 500^{\circ}$ R; $\mu_2(\sigma_{c2}/\rho_c) = 1.6 \times 10^6$ ft^2/sec^2

Figure 6.- Mass of gas required (hydrogen inflating gas; $\bar{p}_a = 0$; $\sigma_{s1}/\rho_s = 10^6$ ft^2/sec^2).

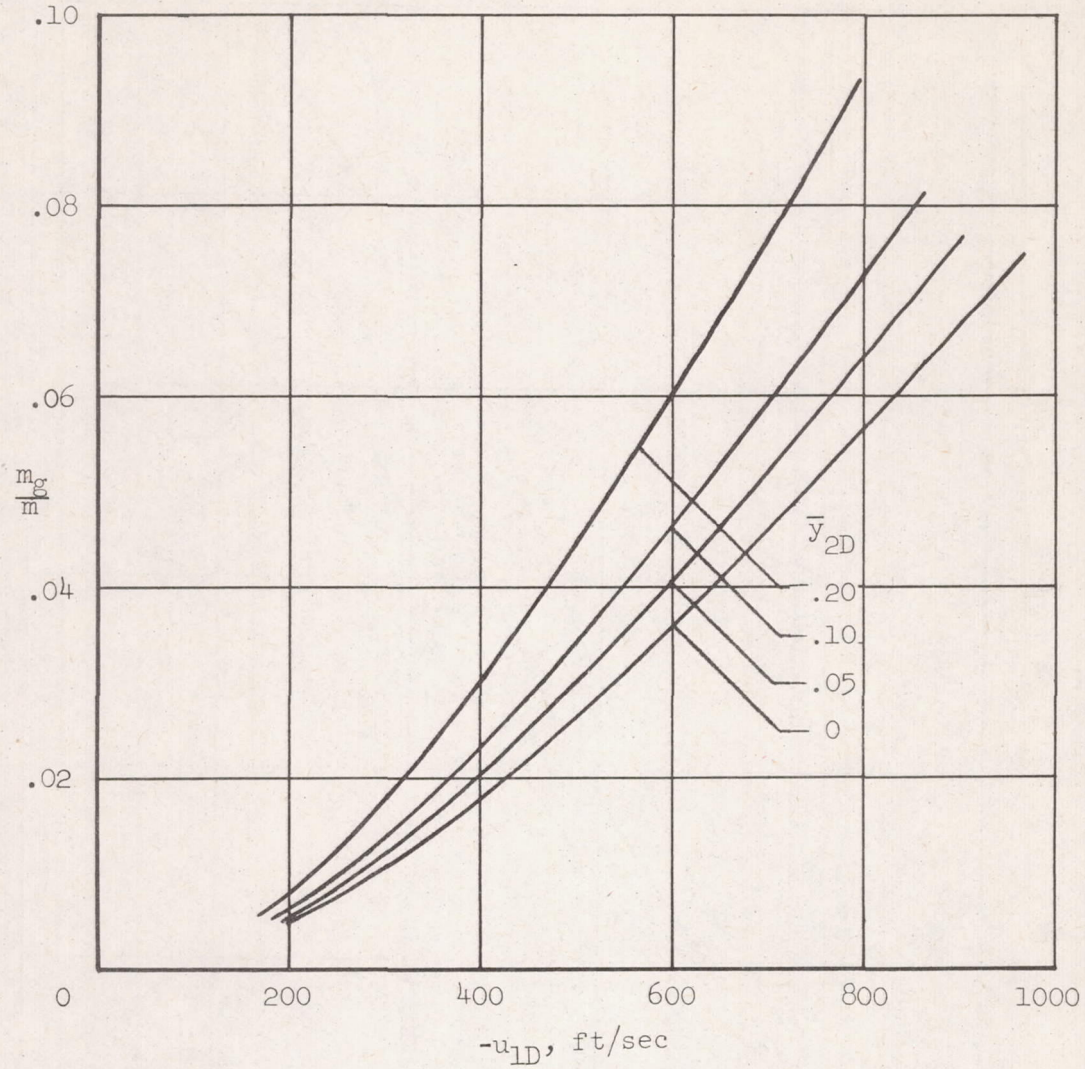

(b) $T_{1D} = 200^{\circ}$ R; $\mu_2(\sigma_{c2}/\rho_c) = 1.6 \times 10^6$ ft^2/sec^2

Figure 6.- Continued.

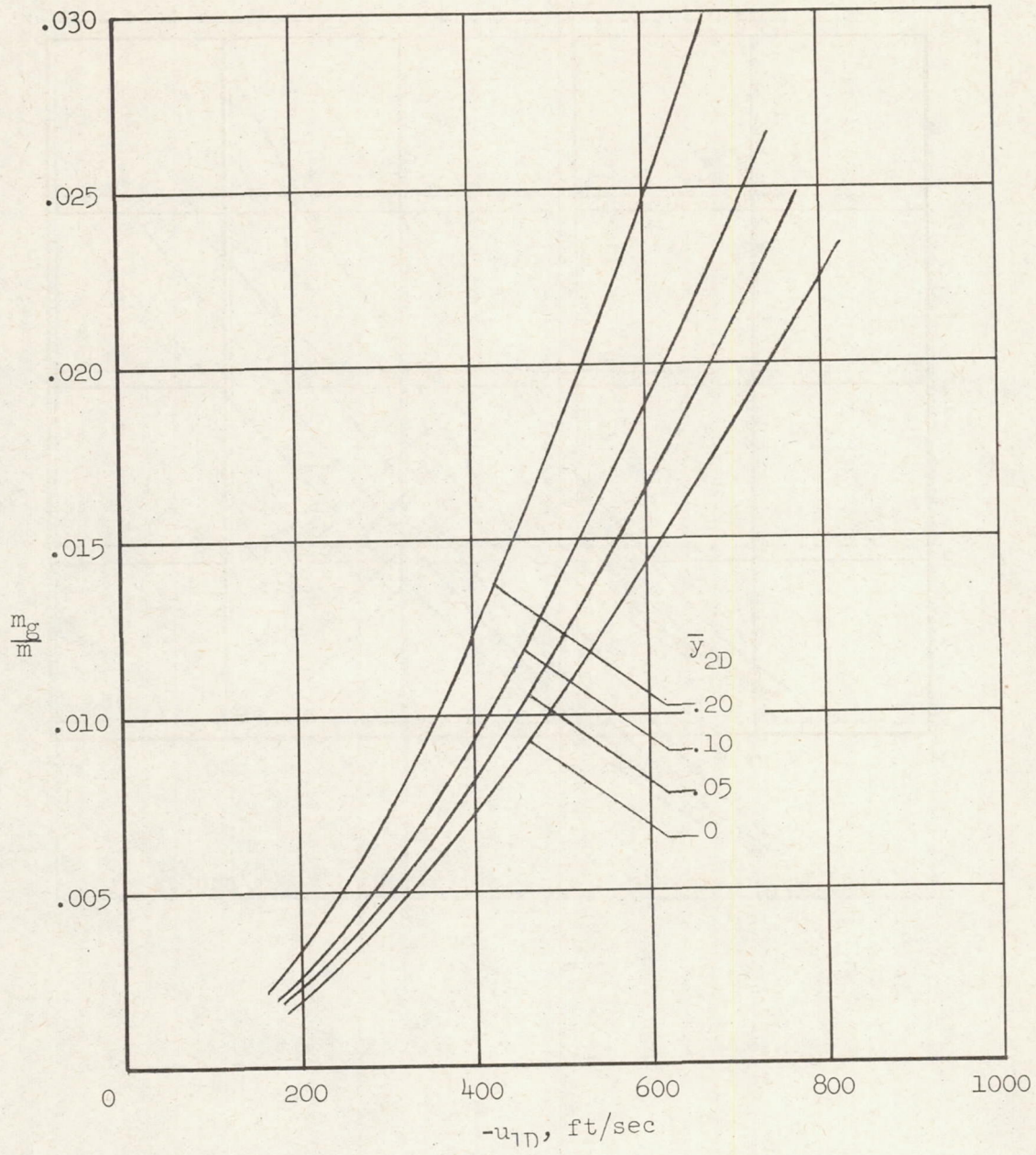

(c) $T_{1D} = 500^{\circ}$ R; $\mu_2(\sigma_{c2}/\rho_c) = 1.2 \times 10^8$ ft^2/sec^2

Figure 6.- Continued.

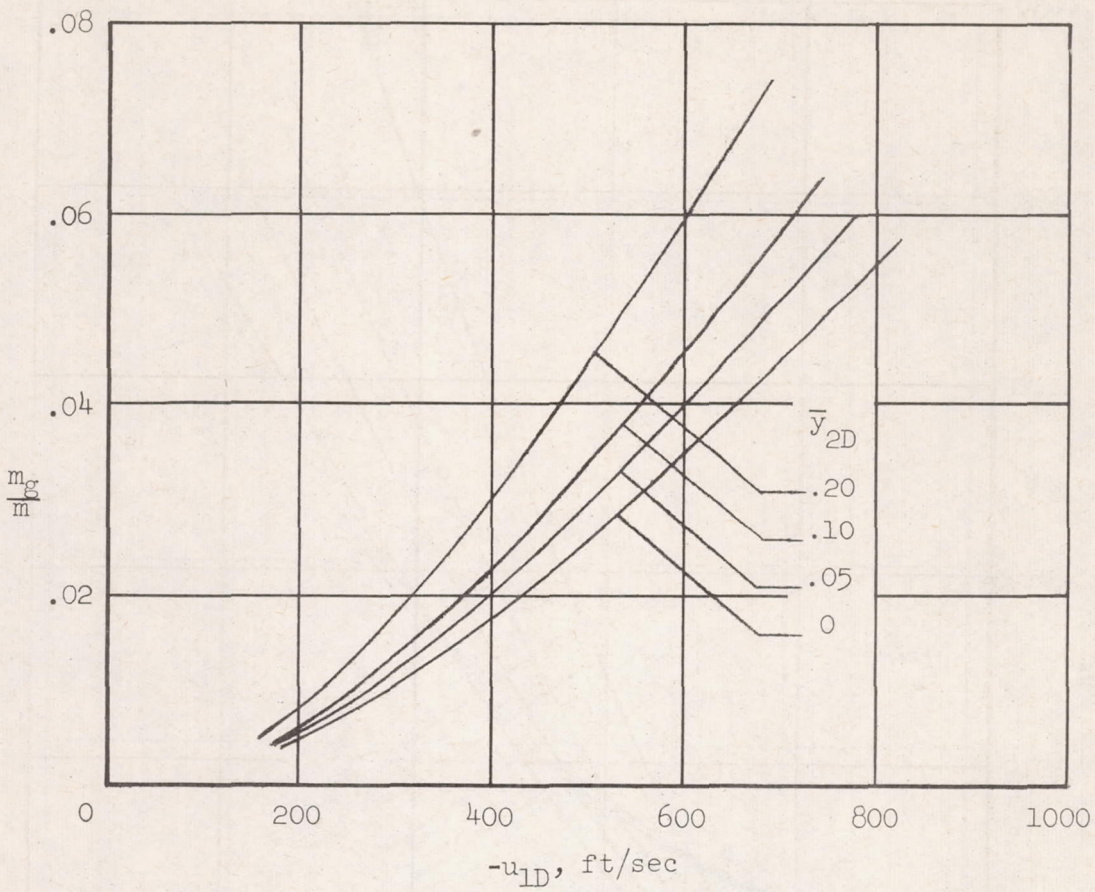

(d) $T_{1D} = 200^{\circ}$ R; $\mu_2(\sigma_{c2}/\rho_c) = 1.2 \times 10^6$ ft^2/sec^2

Figure 6.- Concluded.

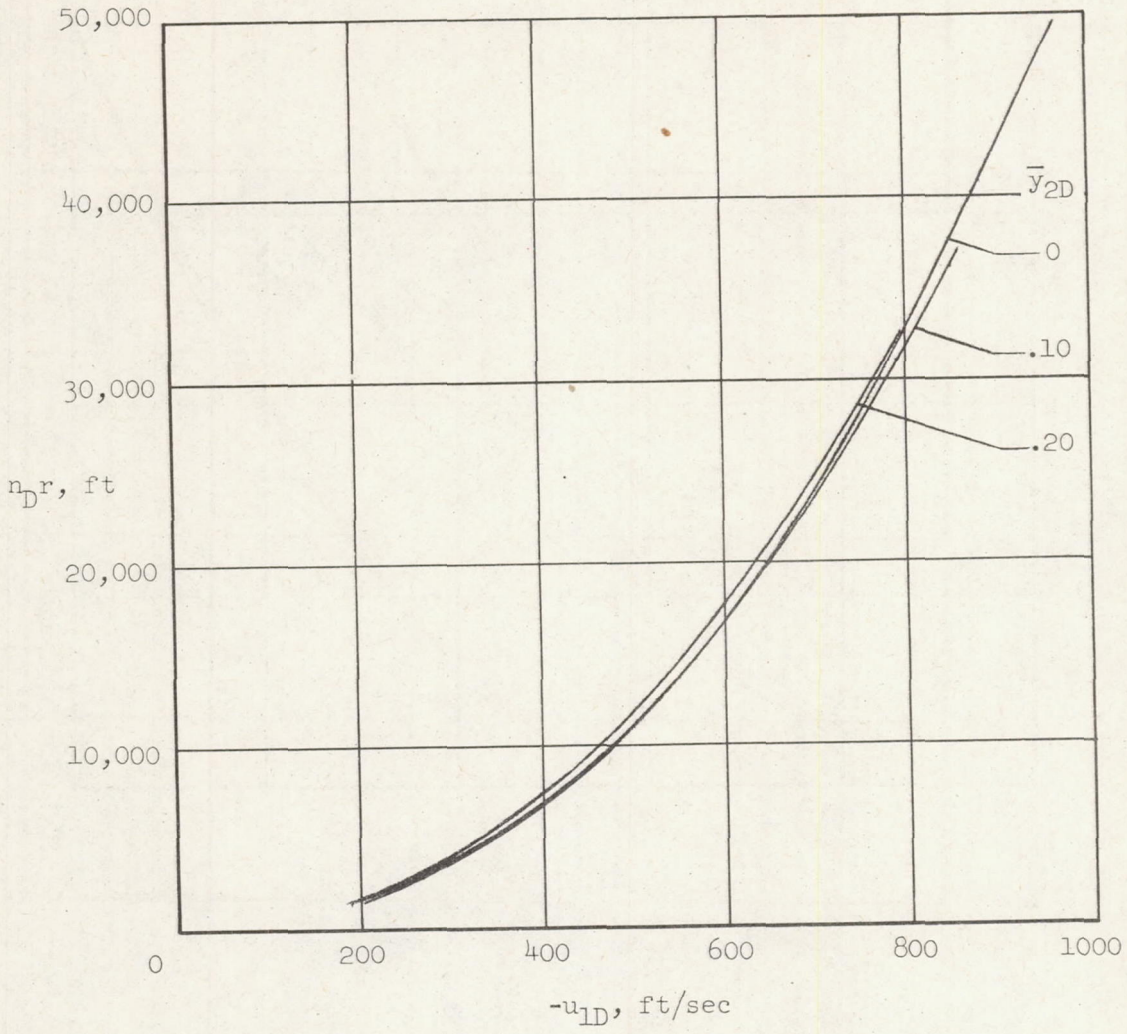

(a) $T_{1D} = 500^{\circ}$ R; $\mu_2(\sigma_{c2}/\rho_c) = 1.6 \times 10^6$ ft^2/sec^2

Figure 7.- Radius of sphere required (hydrogen inflating gas; $\bar{p}_a = 0$; $\sigma_{s1}/\rho_s = 10^6$ ft^2/sec^2).

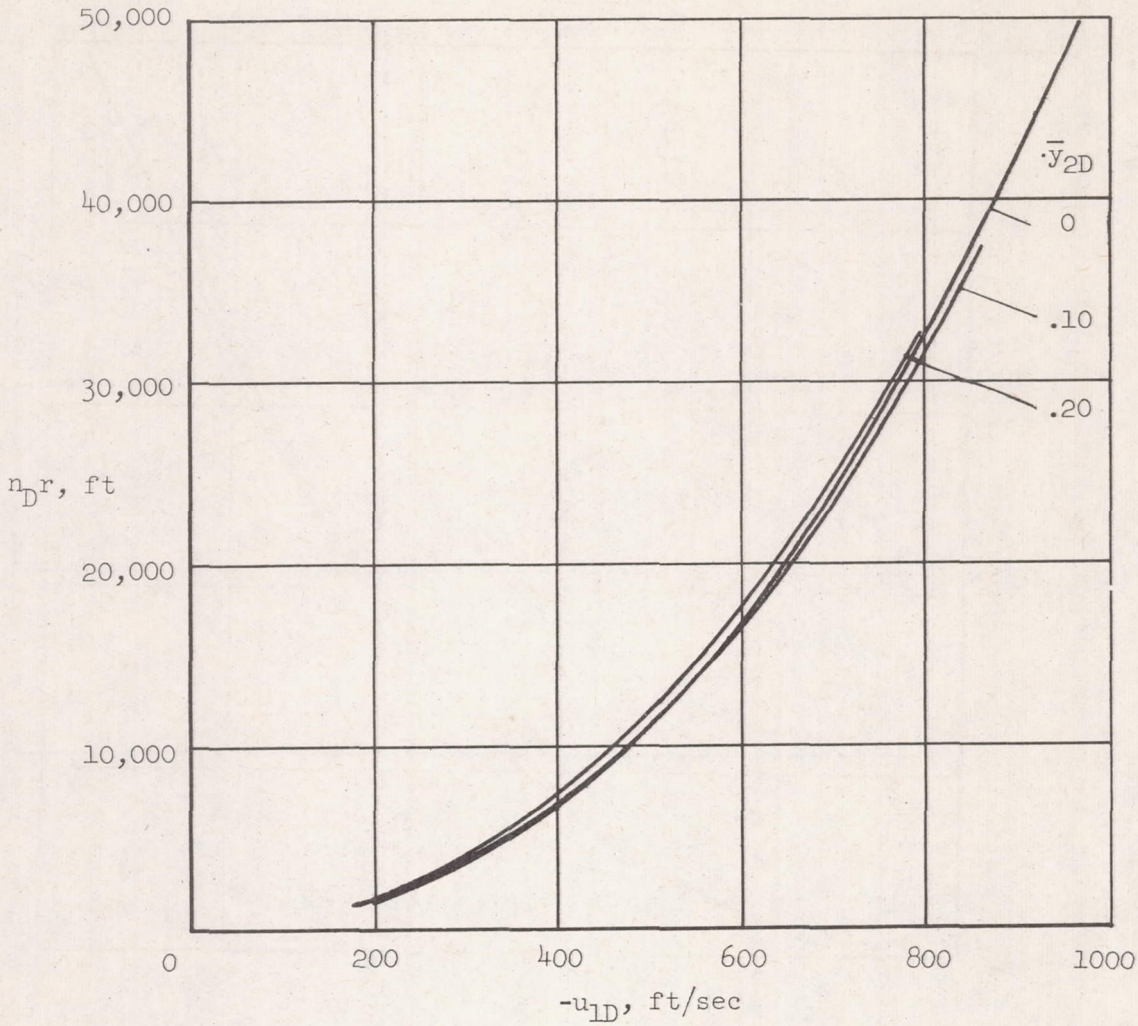

(b) $T_{1D} = 200^{\circ}$ R; $\mu_2(\sigma_{c2}/\rho_c) = 1.6 \times 10^6$ ft^2/sec^2

Figure 7.- Continued.

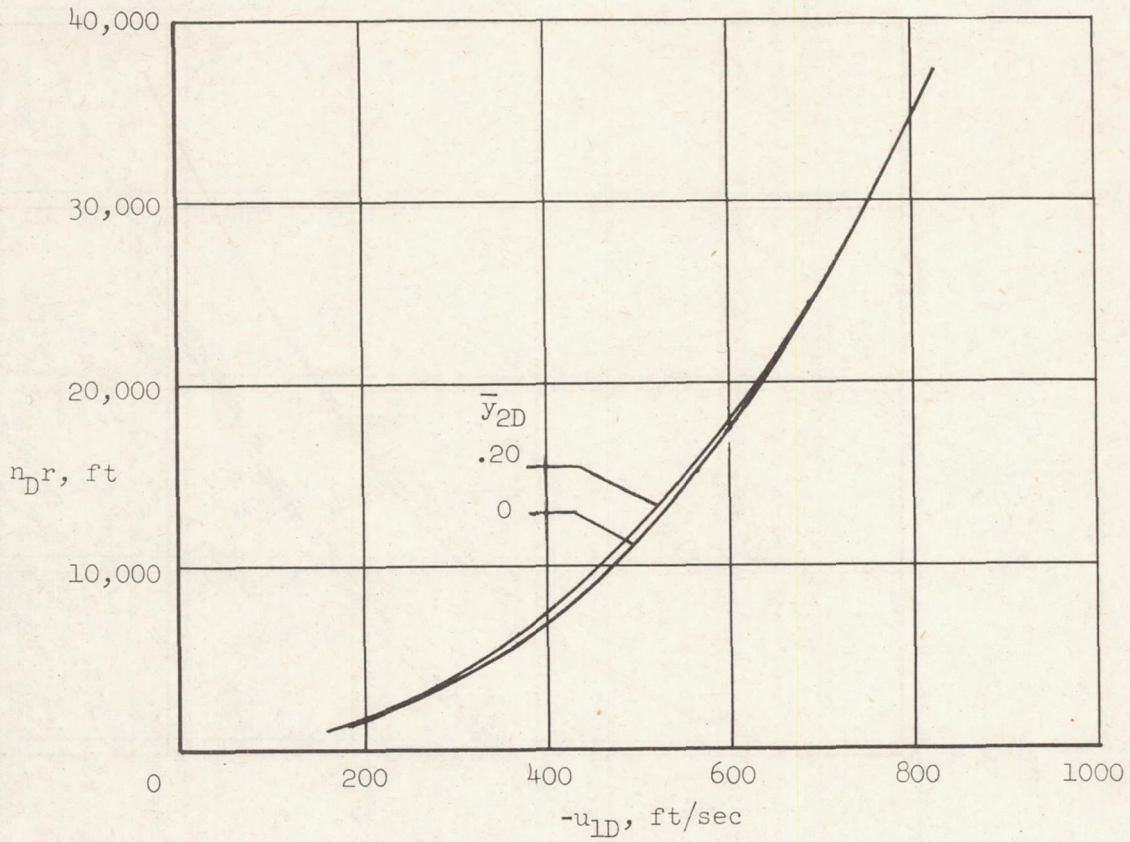

(c) $T_{1D} = 500^{\circ}$ R; $\mu_2(\sigma_{c2}/\rho_c) = 1.2 \times 10^6$ ft^2/sec^2

Figure 7.- Continued.

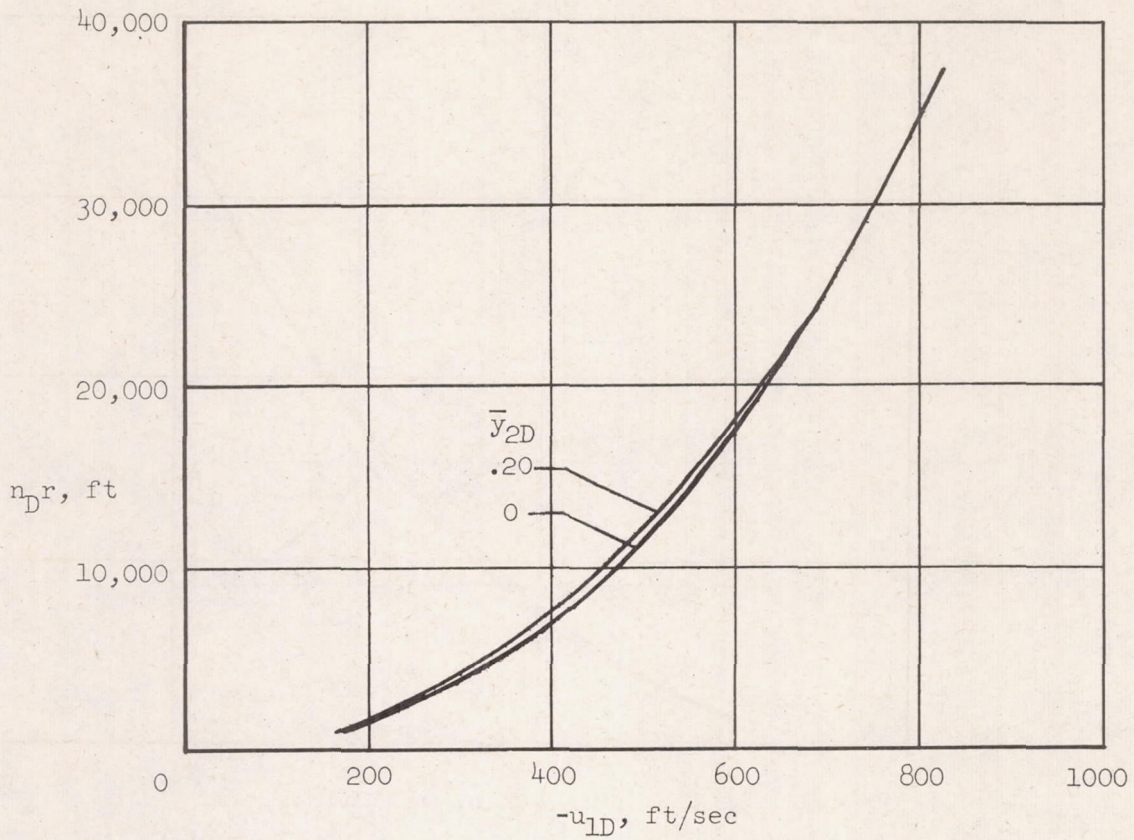

(d) $T_{1D} = 200^{\circ}$ R; $\mu_2(\sigma_{c2}/\rho_c) = 1.2 \times 10^6$ ft^2/sec^2

Figure 7.- Concluded.

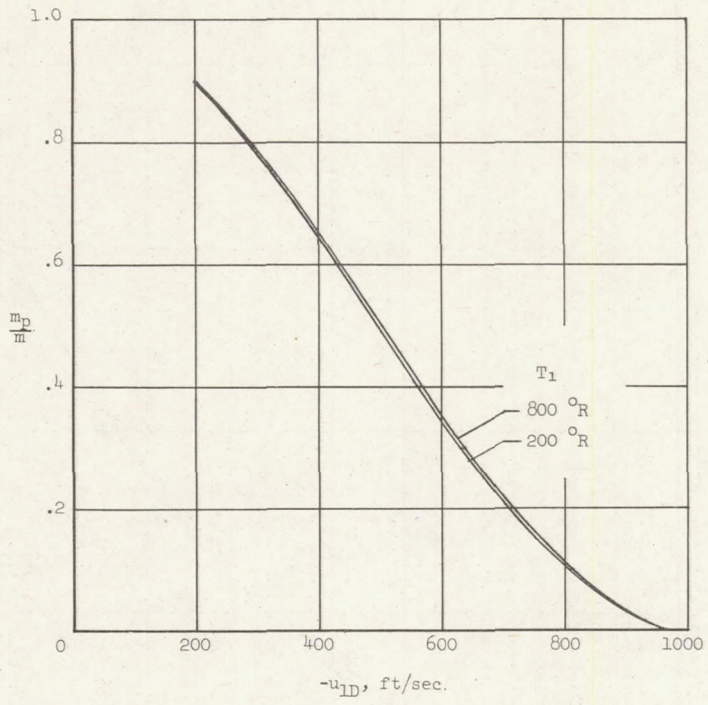

Figure 8.- Payload at two initial temperatures (hydrogen inflating gas; $\overline{p}_a = 0$; $\mu_2(\sigma_{c2}/\rho_c) = 1.6\times10^6$ ft^2/sec^2; $\sigma_{s1}/\rho_s = 10^6$ ft^2/sec^2; $\overline{y}_{2D} = 0$).

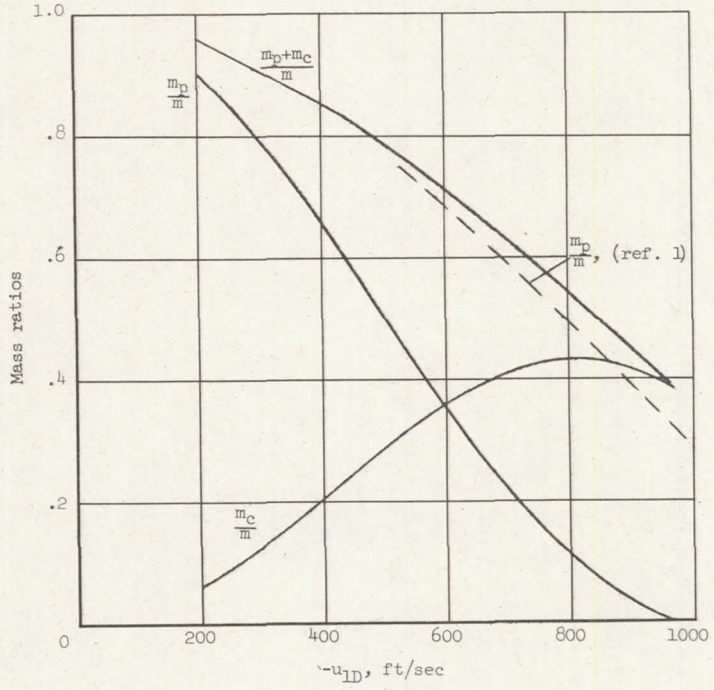

Figure 9.- Comparison of present analysis with preliminary analysis (hydrogen inflating gas; $\overline{p}_a = 0$; $\mu_2(\sigma_{c2}/\rho_c) = 1.6\times10^6$ ft^2/sec^2; $\sigma_{s1}/\rho_s = 10^6$ ft^2/sec^2; $T_1 = 500^\circ$ R; $\overline{y}_2 = 0$).

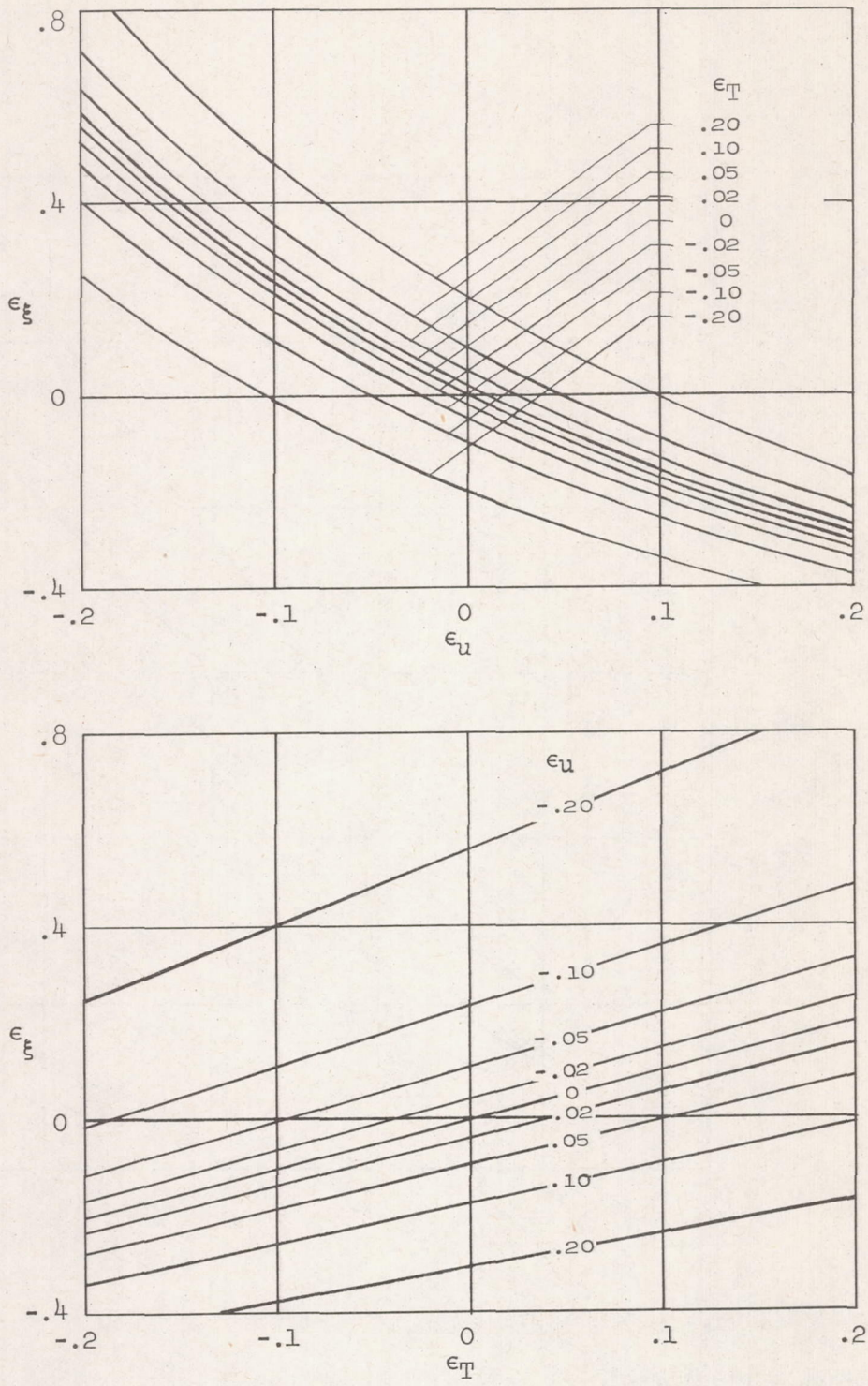

Figure 10.- Fractional errors in ξ corresponding to fractional errors in u_1 and T_1.

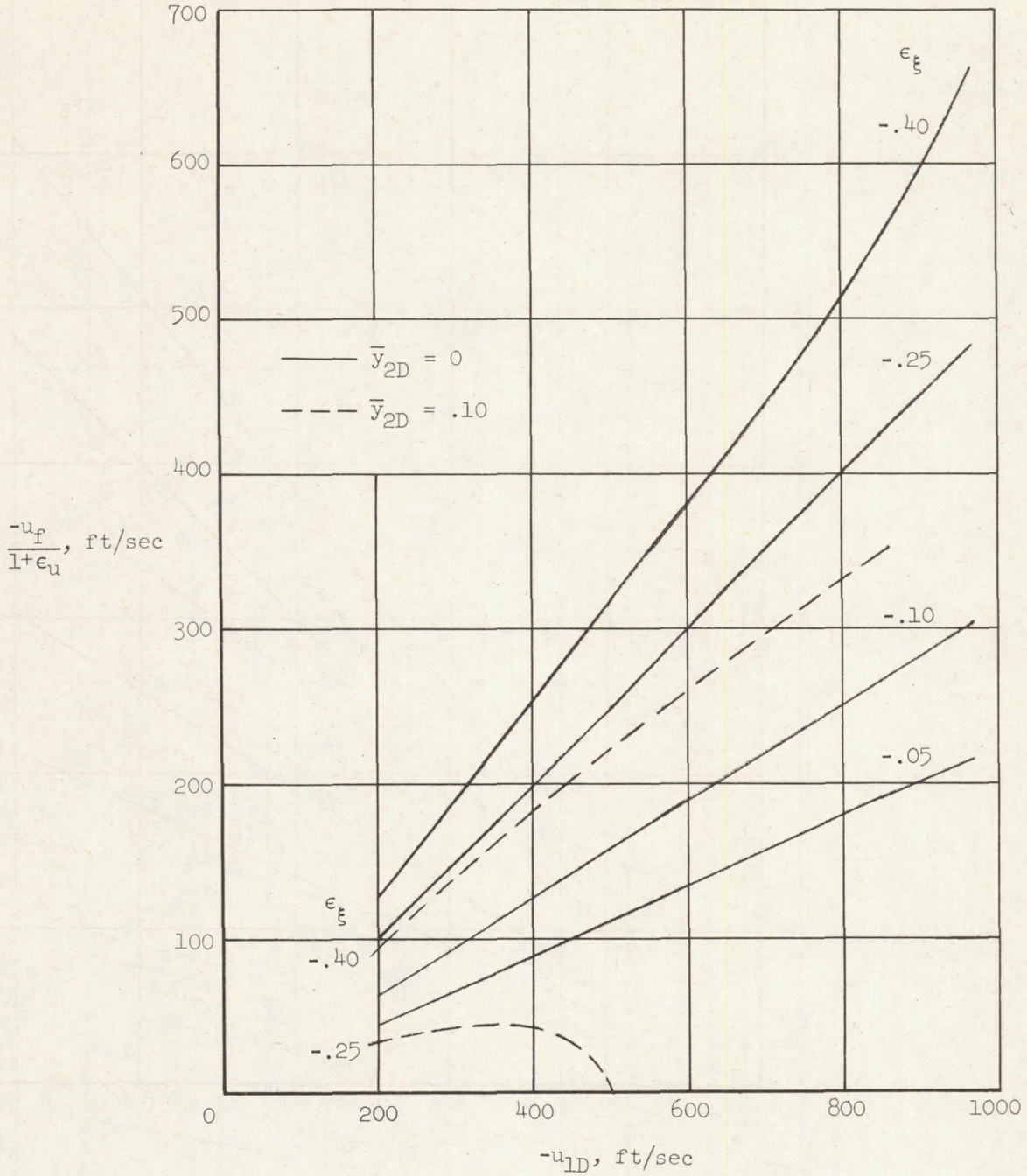

(a) $T_{1D} = 500^\circ$ R; $\mu_2(\sigma_{c2}/\rho_c) = 1.6\times10^6$ ft^2/sec^2

Figure 11.- Final residual velocity for errors in temperature or velocity (hydrogen inflating gas; $\bar{p}_a = 0$; $\sigma_{s1}/\rho_s = 10^6$ ft^2/sec^2).

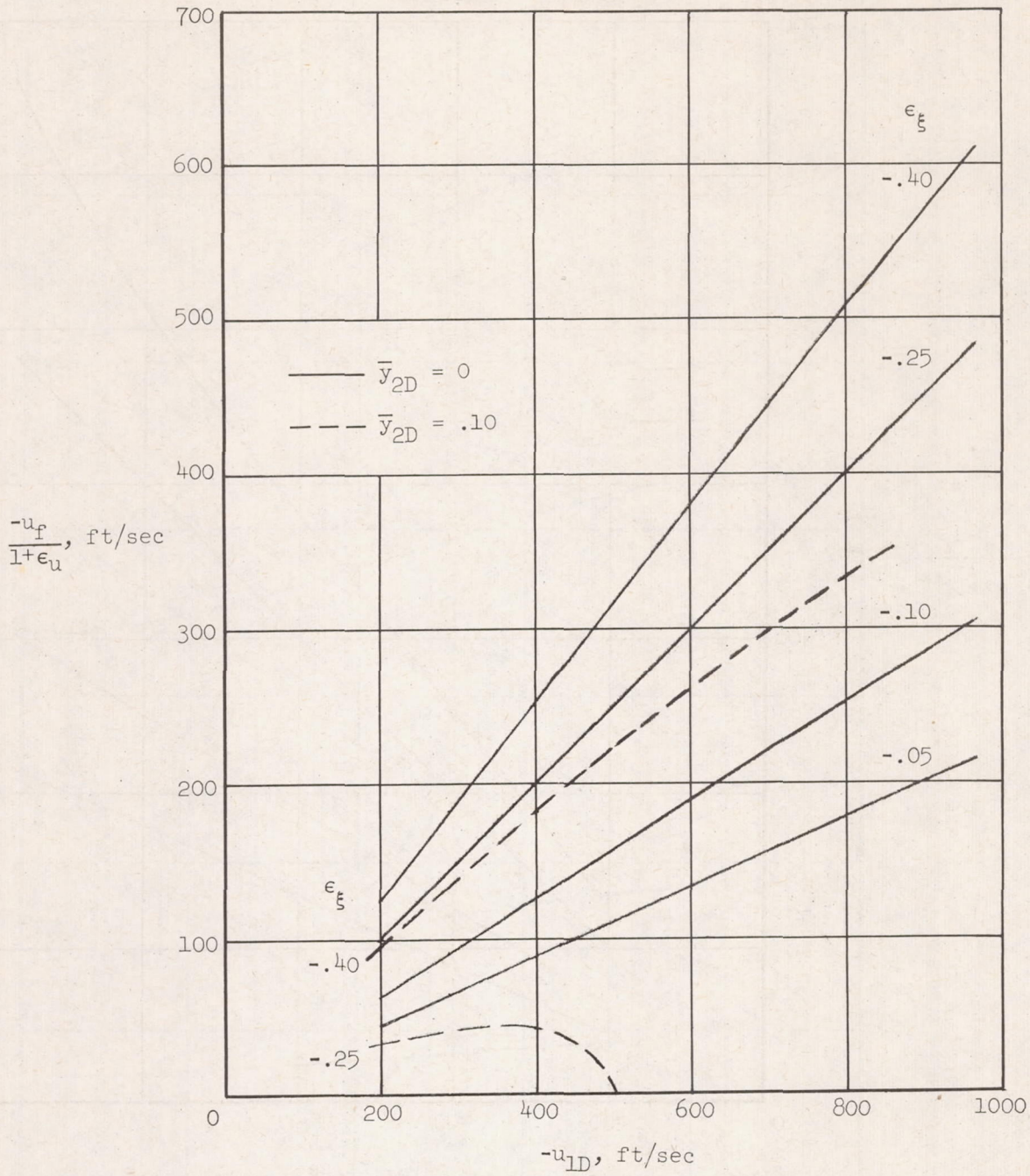

(b) $T_{1D} = 200^\circ$ R; $\mu_2(\sigma_{c2}/\rho_c) = 1.6\times10^6$ ft^2/sec^2

Figure 11.- Concluded.

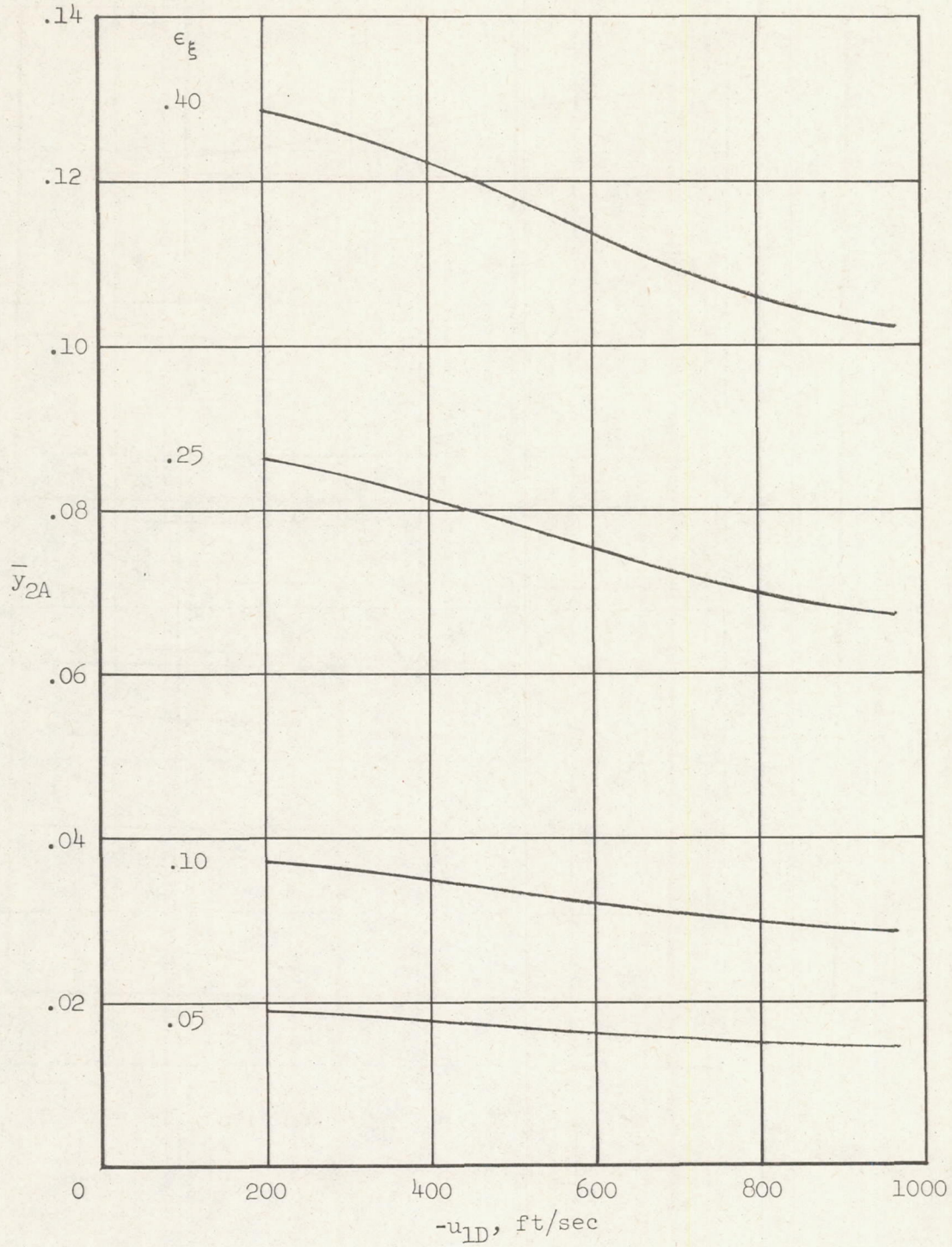

(a) $T_{1D} = 500^\circ$ R; $\mu_2(\sigma_{c2}/\rho_c) = 1.6\times10^6$ ft^2/sec^2; $\bar{y}_{2D} = 0$

Figure 12.- Final location of payload package for errors in temperature or velocity (hydrogen inflating gas; $\bar{p}_a = 0$; $\sigma_{s1}/\rho_s = 10^6$ ft^2/sec^2).

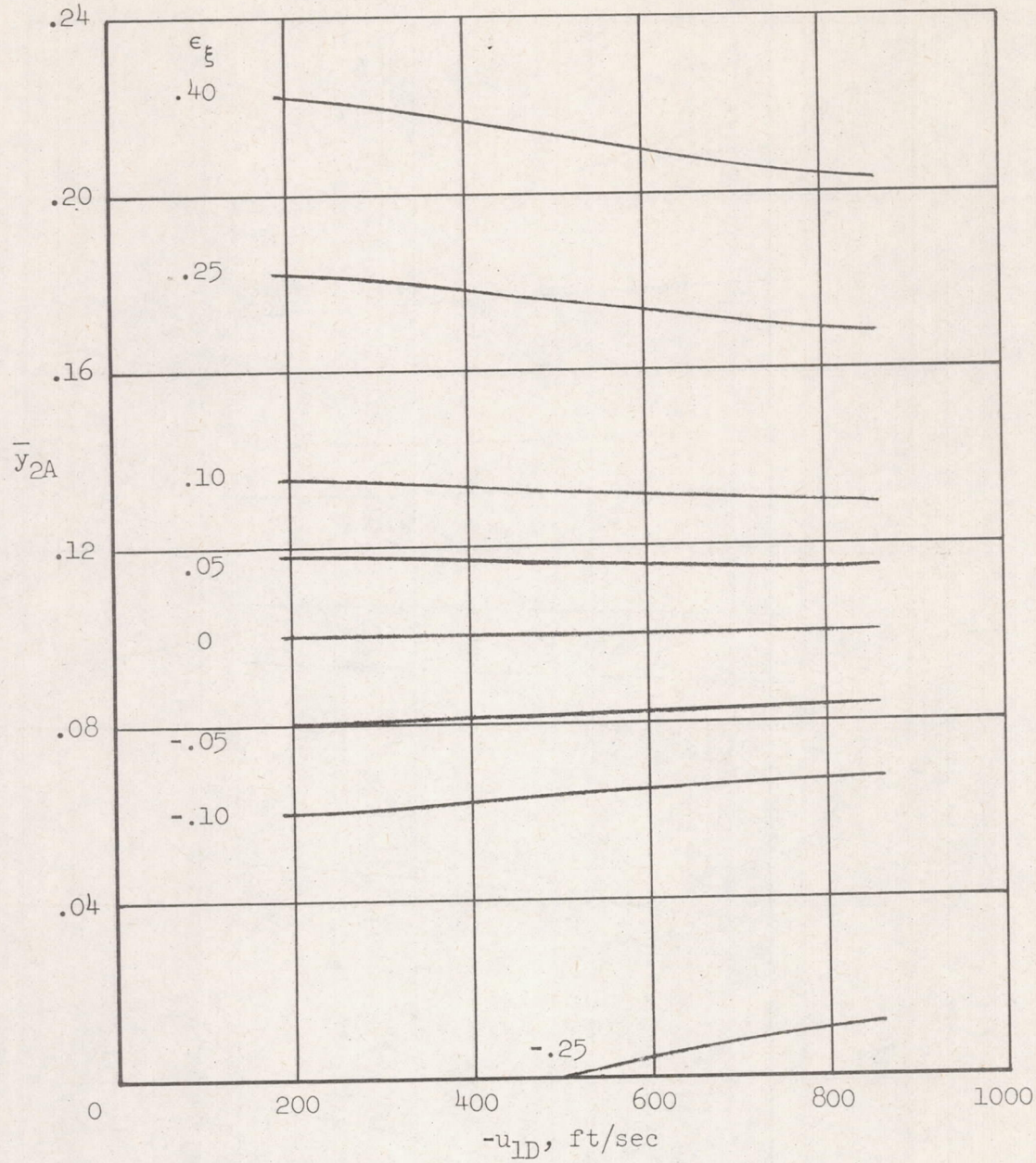

(b) $T_{1D} = 500^\circ$ R; $\mu_2(\sigma_{c2}/\rho_c) = 1.6 \times 10^6$ ft^2/sec^2; $\bar{y}_{2D} = 0.10$

Figure 12.- Continued.

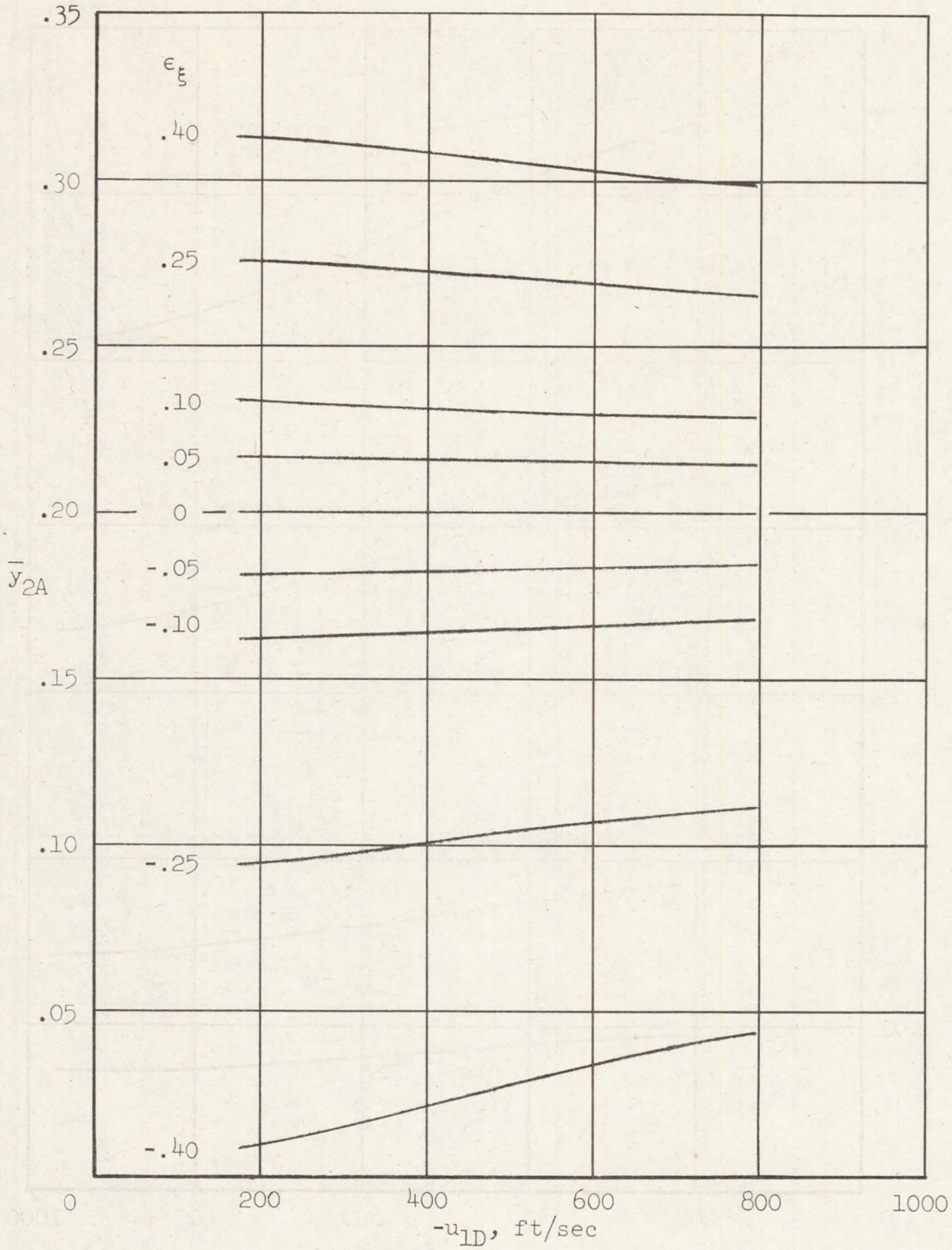

(c) $T_{1D} = 500^{\circ}$ R; $\mu_2(\sigma_{c2}/\rho_c) = 1.6 \times 10^6$ ft^2/sec^2; $\bar{y}_{2D} = 0.20$

Figure 12.- Continued.

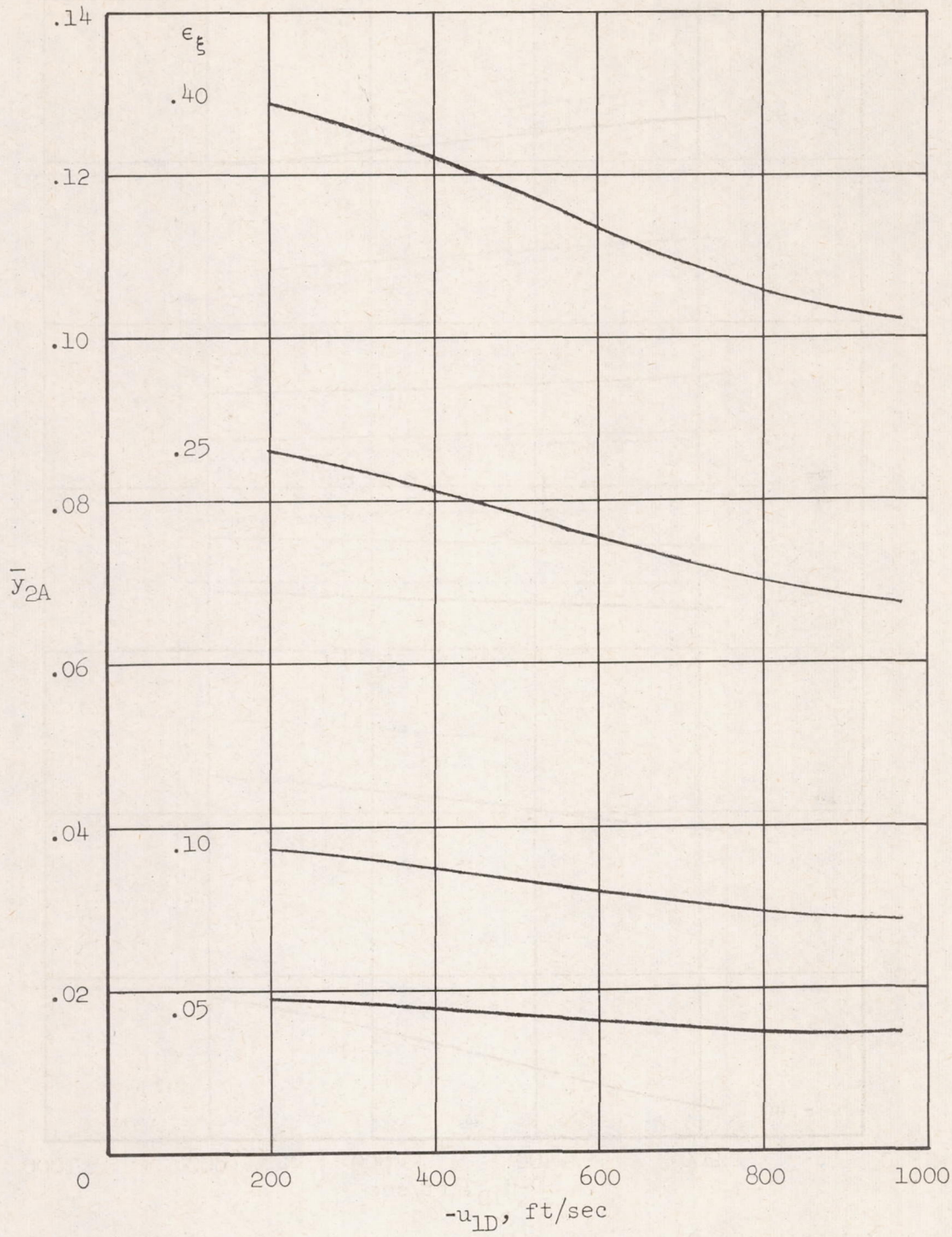

(d) $T_{1D} = 200^\circ$ R; $\mu_2(\sigma_{c2}/\rho_c) = 1.6 \times 10^6$ ft^2/sec^2; $\bar{y}_{2D} = 0$

Figure 12.- Continued.

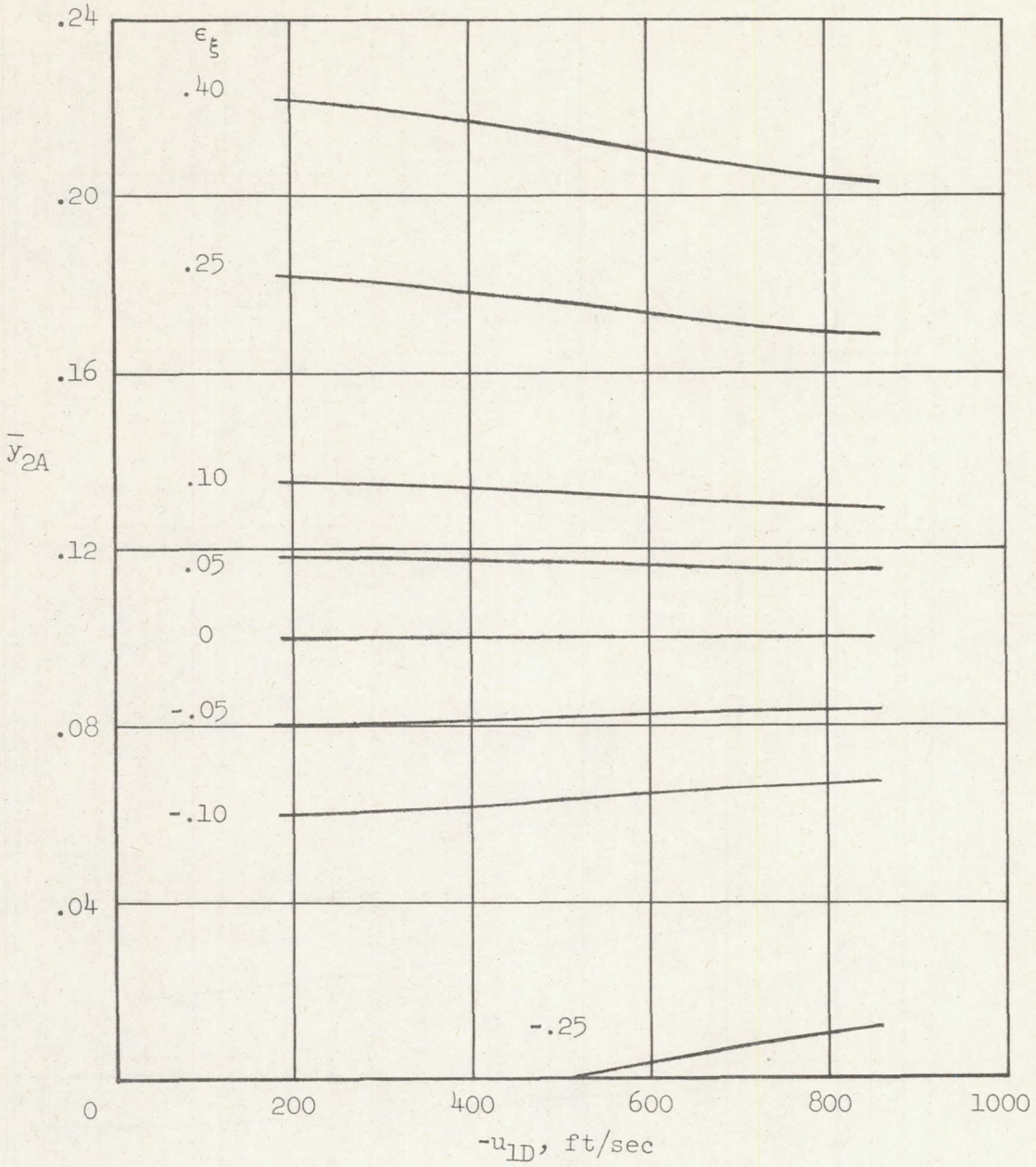

(e) $T_{1D} = 200^\circ$ R; $\mu_2(\sigma_{c2}/\rho_c) = 1.6 \times 10^6$ ft^2/sec^2; $\bar{y}_{2D} = 0.10$

Figure 12.- Continued.

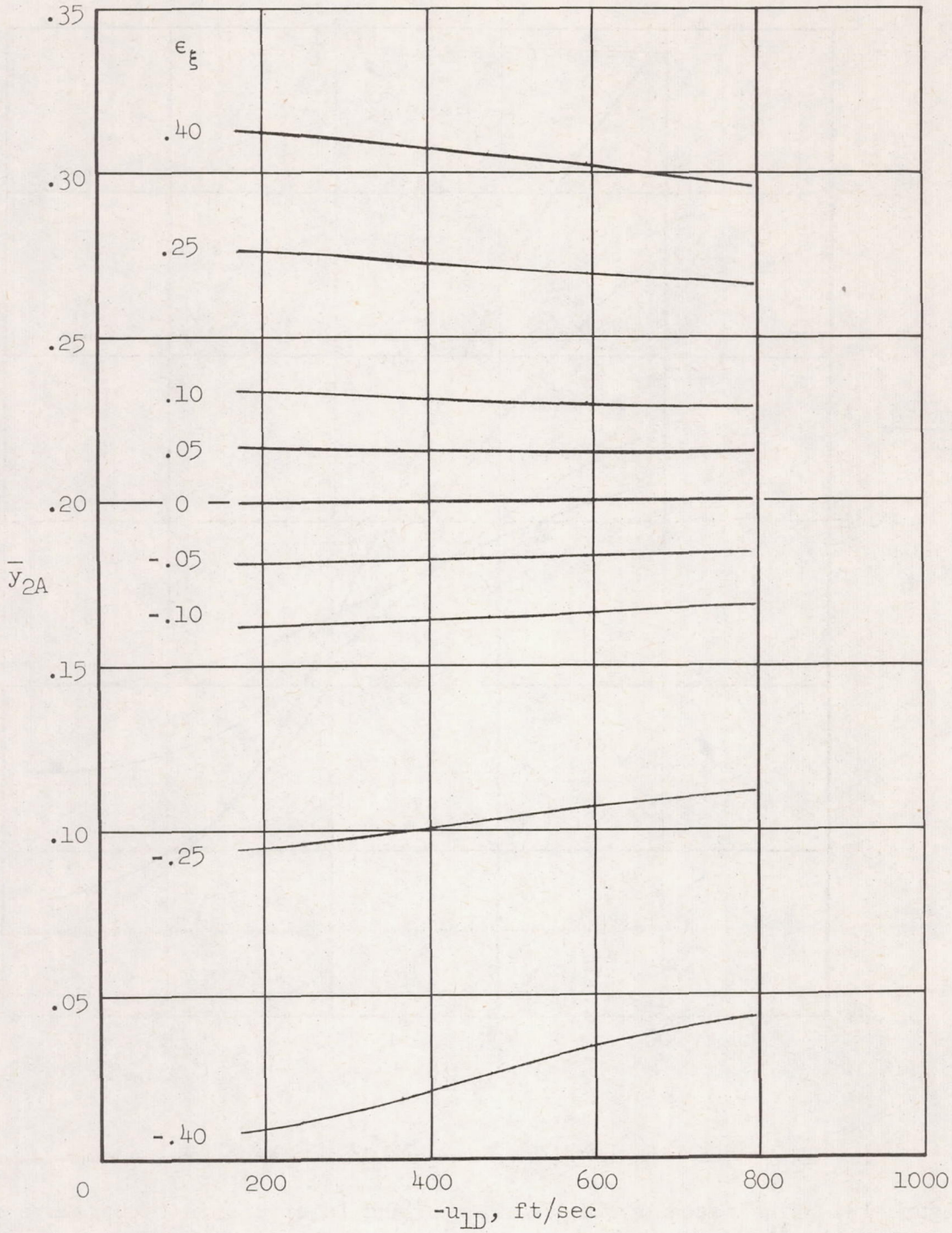

(f) $T_{1D} = 200^\circ$ R; $\mu_2(\sigma_{c2}/\rho_c) = 1.6 \times 10^6$ ft^2/sec^2; $\bar{y}_{2D} = 0.20$

Figure 12.- Concluded.

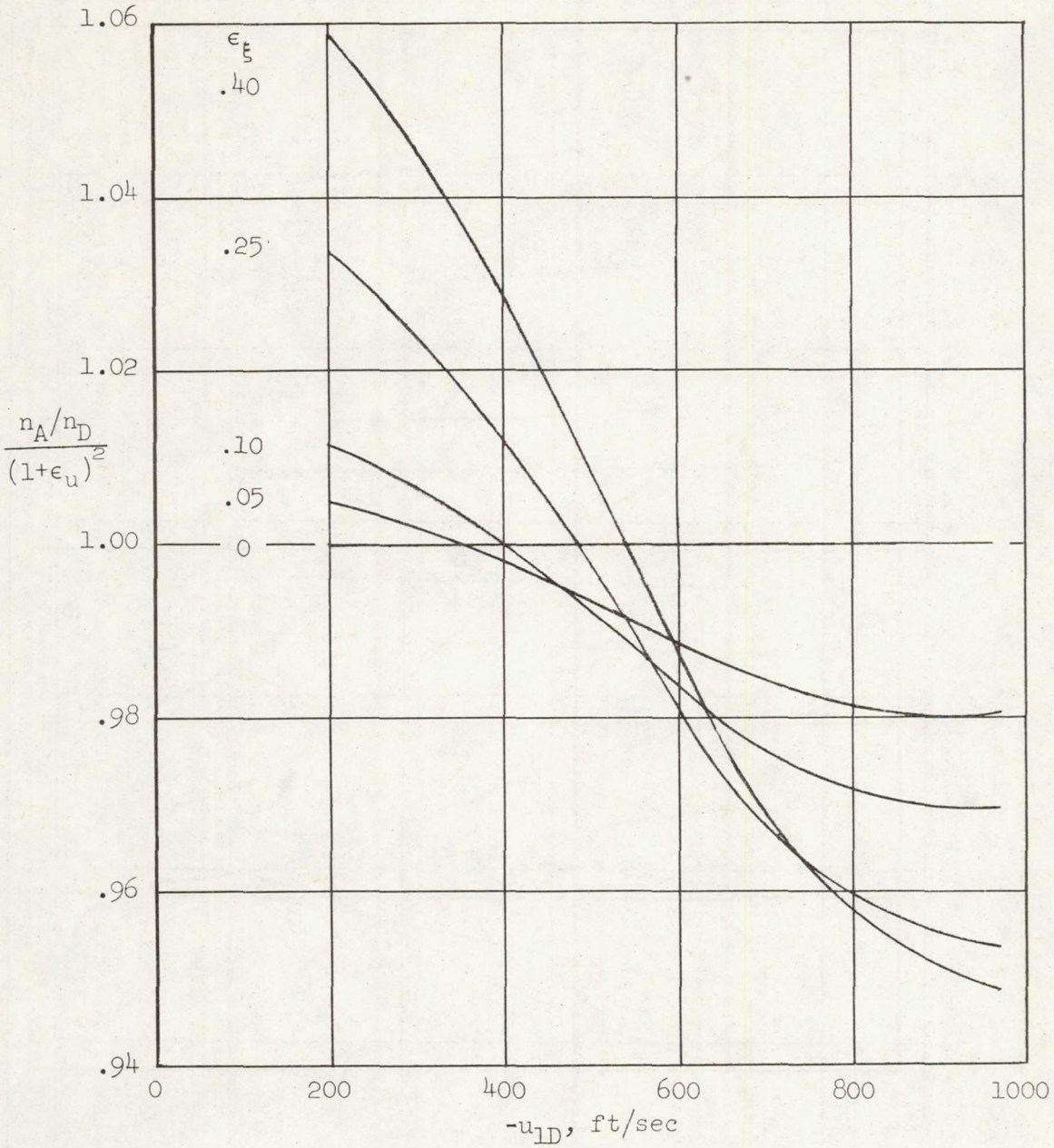

(a) $T_{1D} = 500^\circ$ R; $\mu_2(\sigma_{c2}/\rho_c) = 1.6\times10^6$ ft^2/sec^2; $\overline{v}_{2D} = 0$

Figure 13.- Final acceleration corresponding to errors in temperature or velocity (hydrogen inflating gas; $\overline{p}_a = 0$; $\sigma_{s1}/\rho_s = 10^6$ ft^2/sec^2).

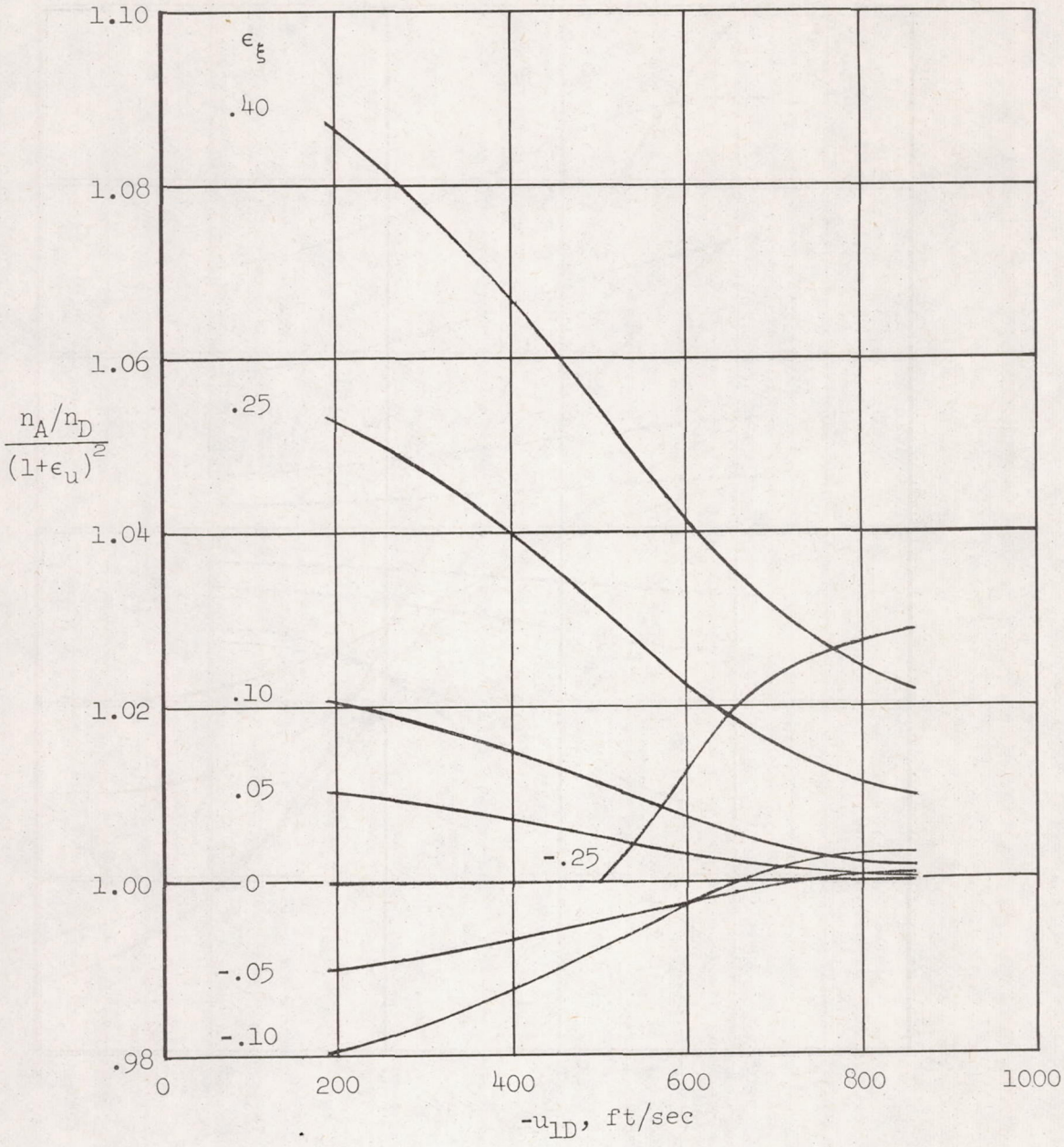

(b) $T_{1D} = 500^\circ$ R; $\mu_2(\sigma_{c2}/\rho_c) = 1.6\times10^6$ ft^2/sec^2; $\bar{y}_{2D} = 0.10$

Figure 13.- Continued.

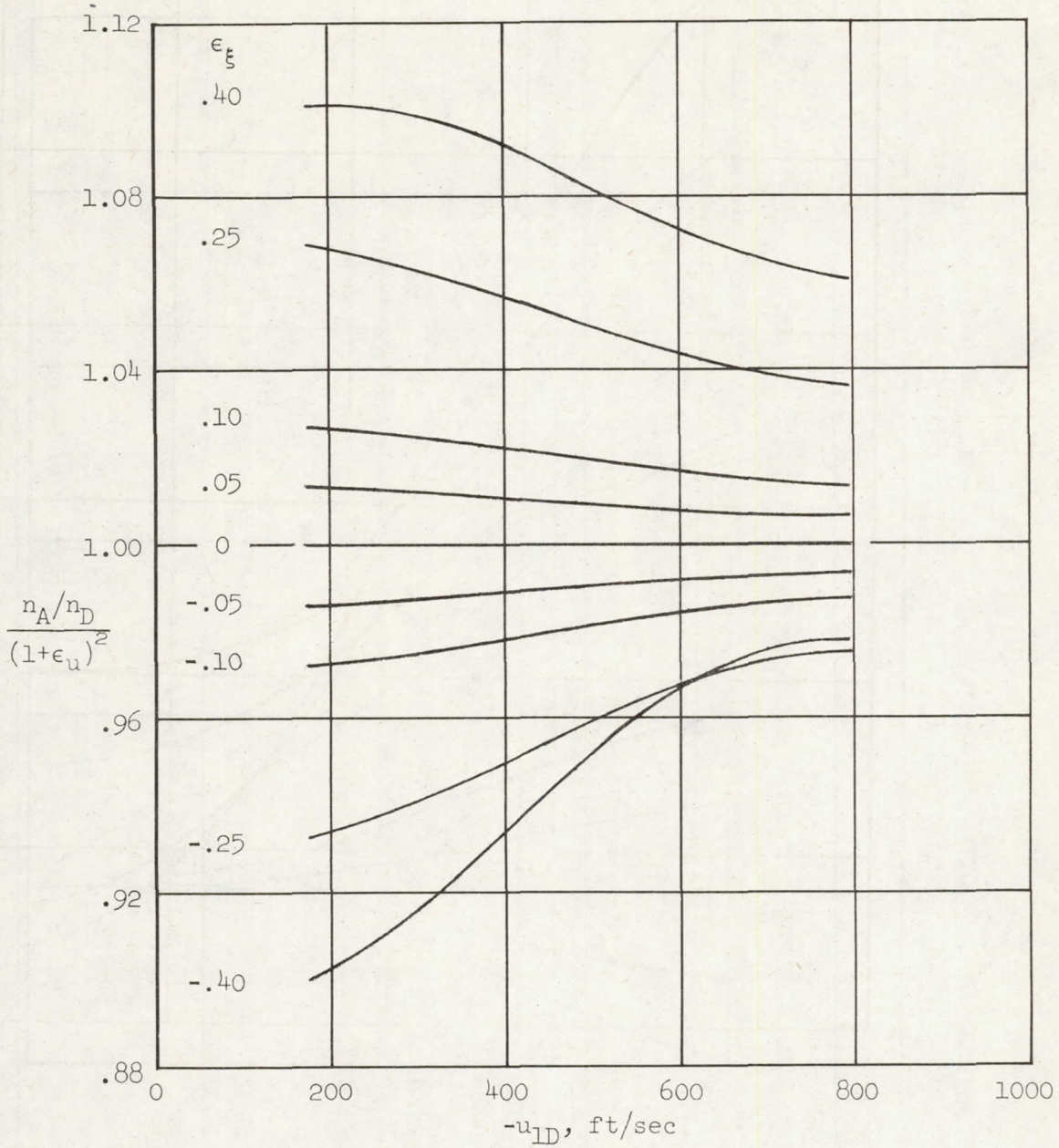

(c) T_{1D} = 500° R; $\mu_2(\sigma_{c2}/\rho_c)$ = 1.6×10⁶ ft²/sec²; $\bar{y}_{2D}$ = 0.20

Figure 13.- Continued.

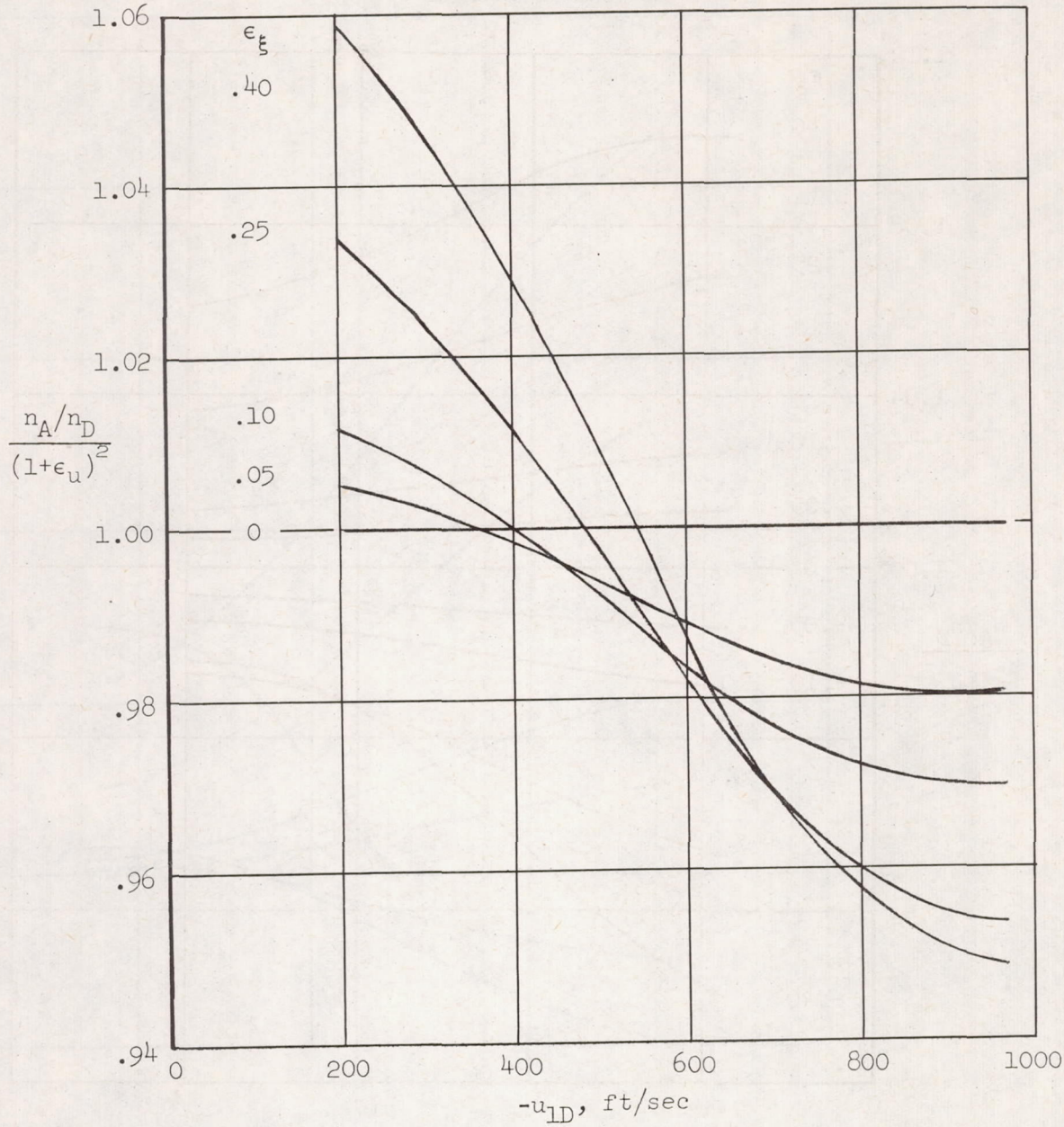

(d) $T_{1D} = 200^\circ$ R; $\mu_2(\sigma_{c2}/\rho_c) = 1.6 \times 10^6$ ft^2/sec^2; $\bar{y}_{2D} = 0$

Figure 13.- Continued.

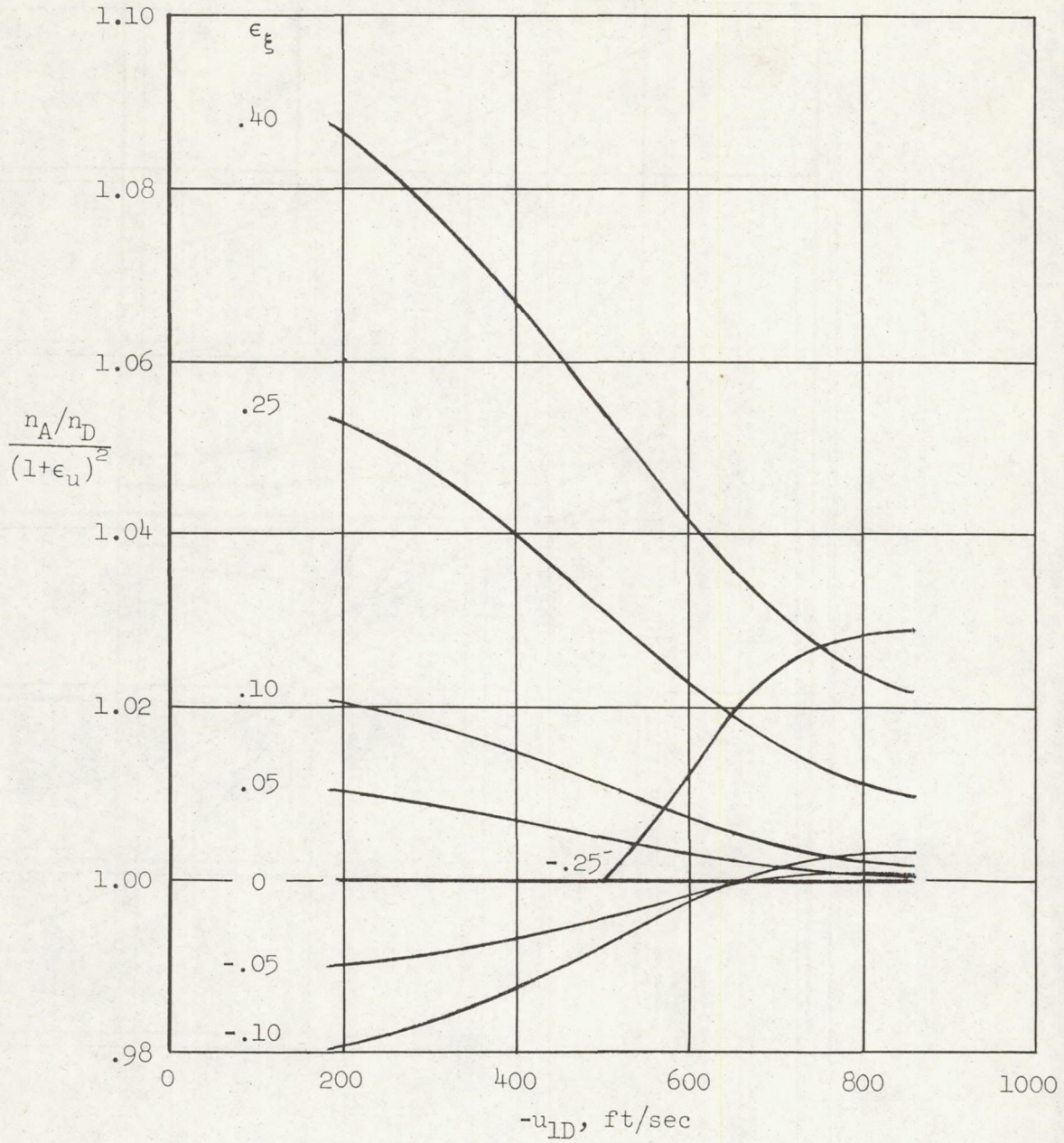

(e) $T_{1D} = 200^\circ$ R; $\mu_2(\sigma_{c2}/\rho_c) = 1.6\times10^6$ ft^2/sec^2; $\overline{y}_{2D} = 0.10$

Figure 13.- Continued.

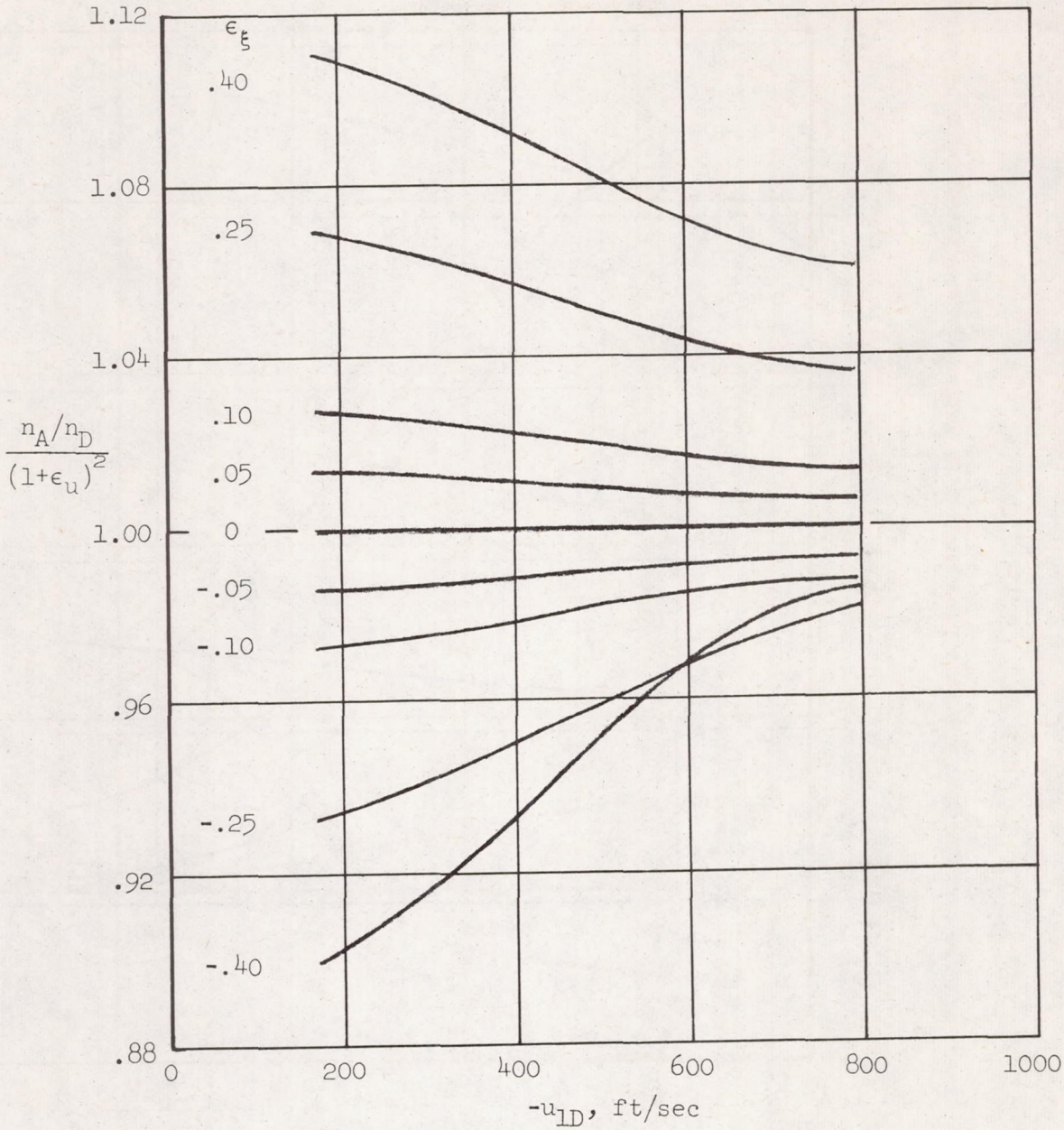

(f) $T_{1D} = 200^\circ$ R; $\mu_2(\sigma_{c2}/\rho_c) = 1.6 \times 10^6$ ft^2/sec^2; $\bar{y}_{2D} = 0.20$

Figure 13.- Concluded.

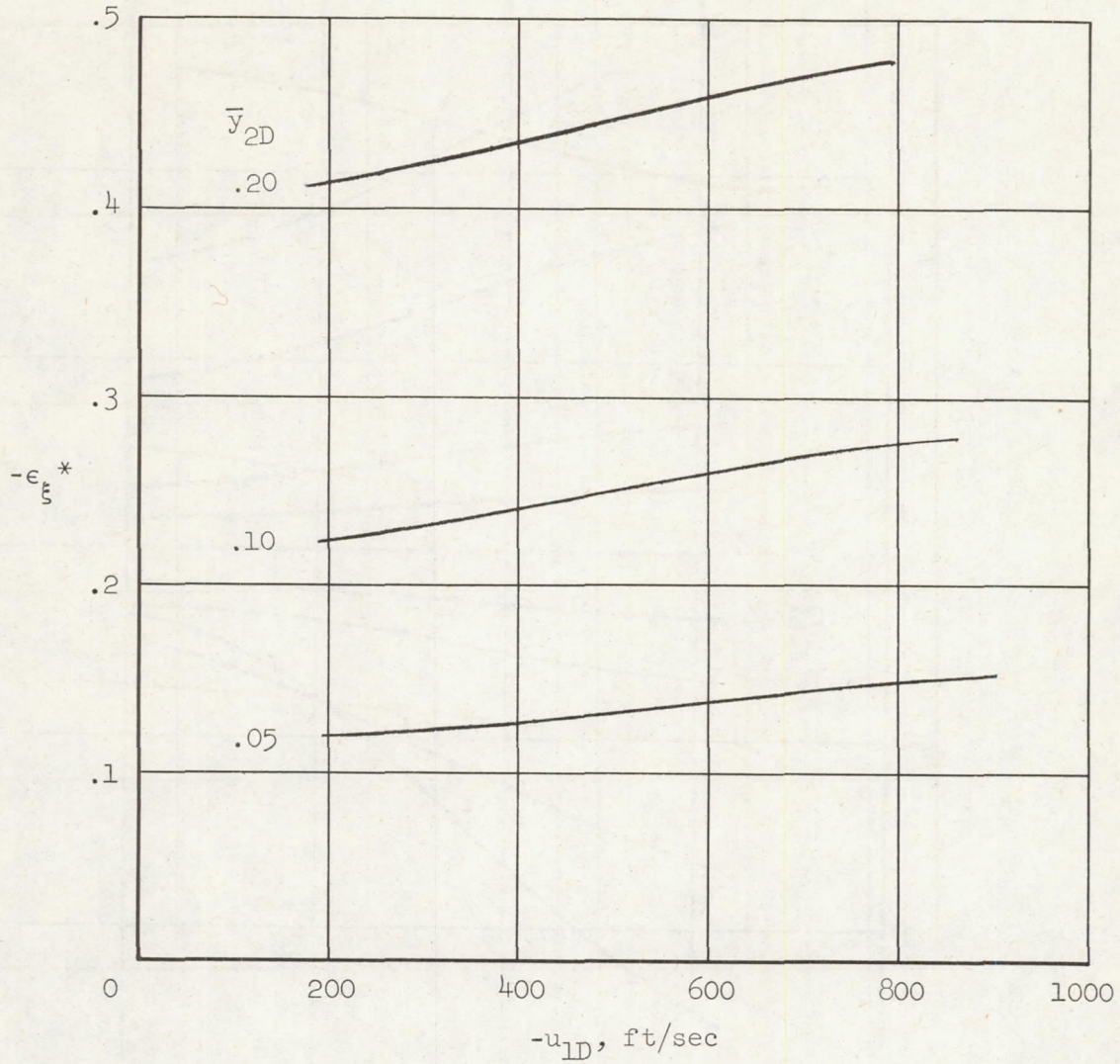

(a) $T_{1D} = 500^\circ$ R; $\mu_2(\sigma_{c2}/\rho_c) = 1.6 \times 10^6$ ft^2/sec^2

Figure 14.- Critical deviation in ξ (hydrogen inflating gas; $\bar{p}_a = 0$; $\sigma_{s1}/\rho_s = 10^6$ ft^2/sec^2).

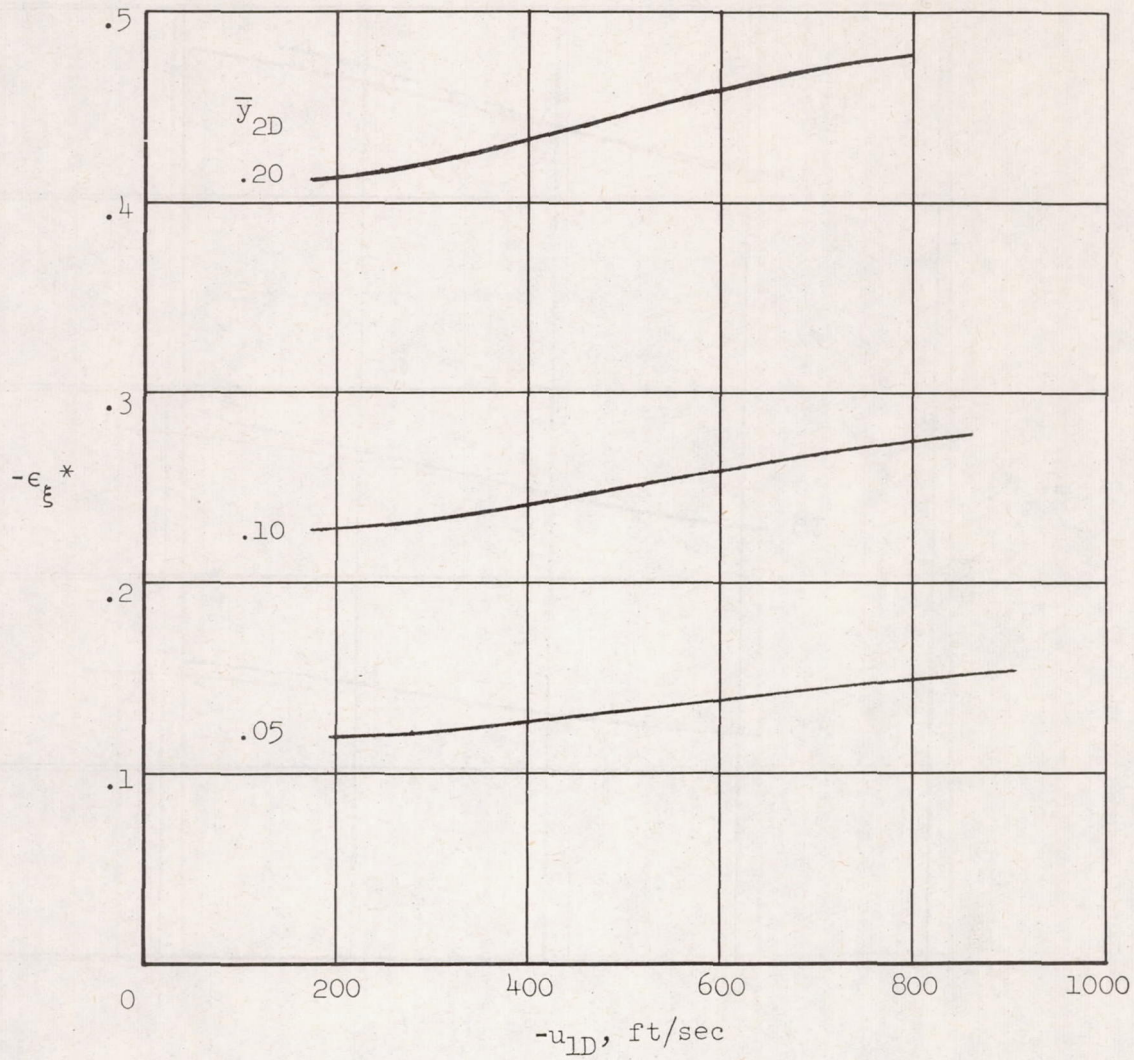

(b) $T_{1D} = 200^\circ$ R; $\mu_2(\sigma_{c2}/\rho_c) = 1.6 \times 10^6$ ft^2/sec^2

Figure 14.- Continued.

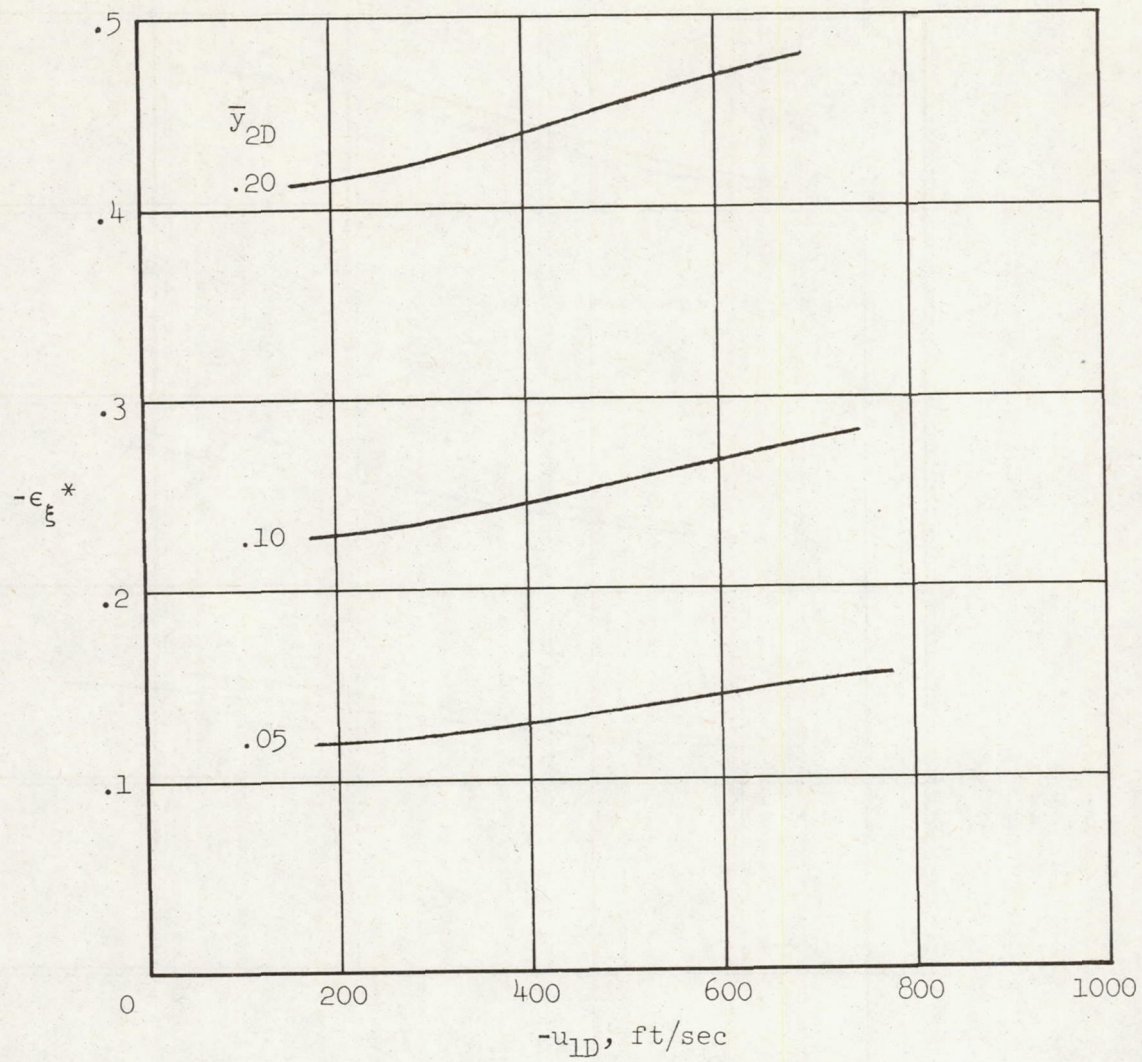

(c) $T_{1D} = 500^\circ$ R; $\mu_2(\sigma_{c2}/\rho_c) = 1.2 \times 10^6$ ft^2/sec^2

Figure 14.- Continued.

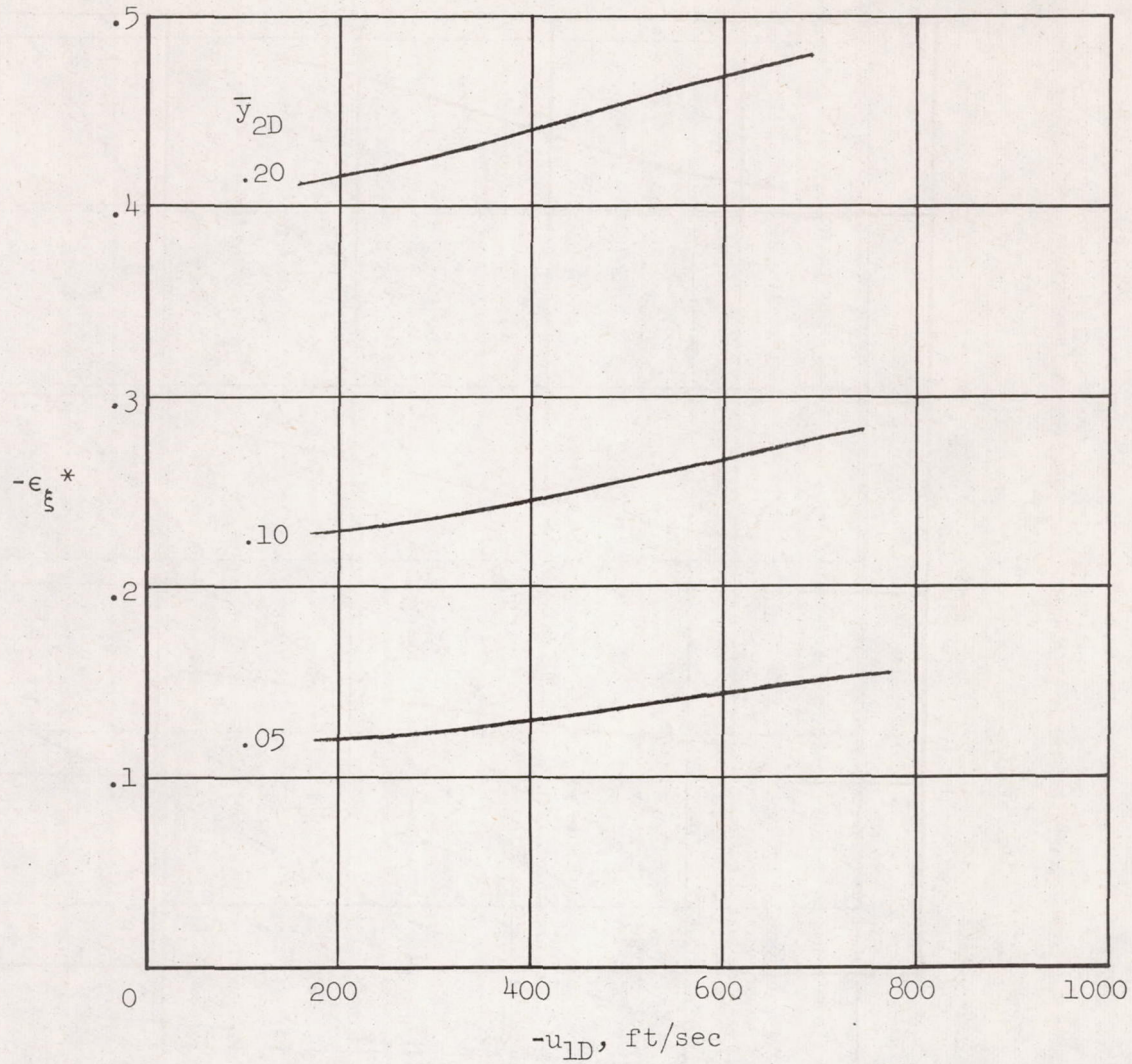

(d) $T_{1D} = 200^\circ$ R; $\mu_2(\sigma_{c2}/\rho_c) = 1.2 \times 10^6$ ft^2/sec^2

Figure 14.- Concluded.

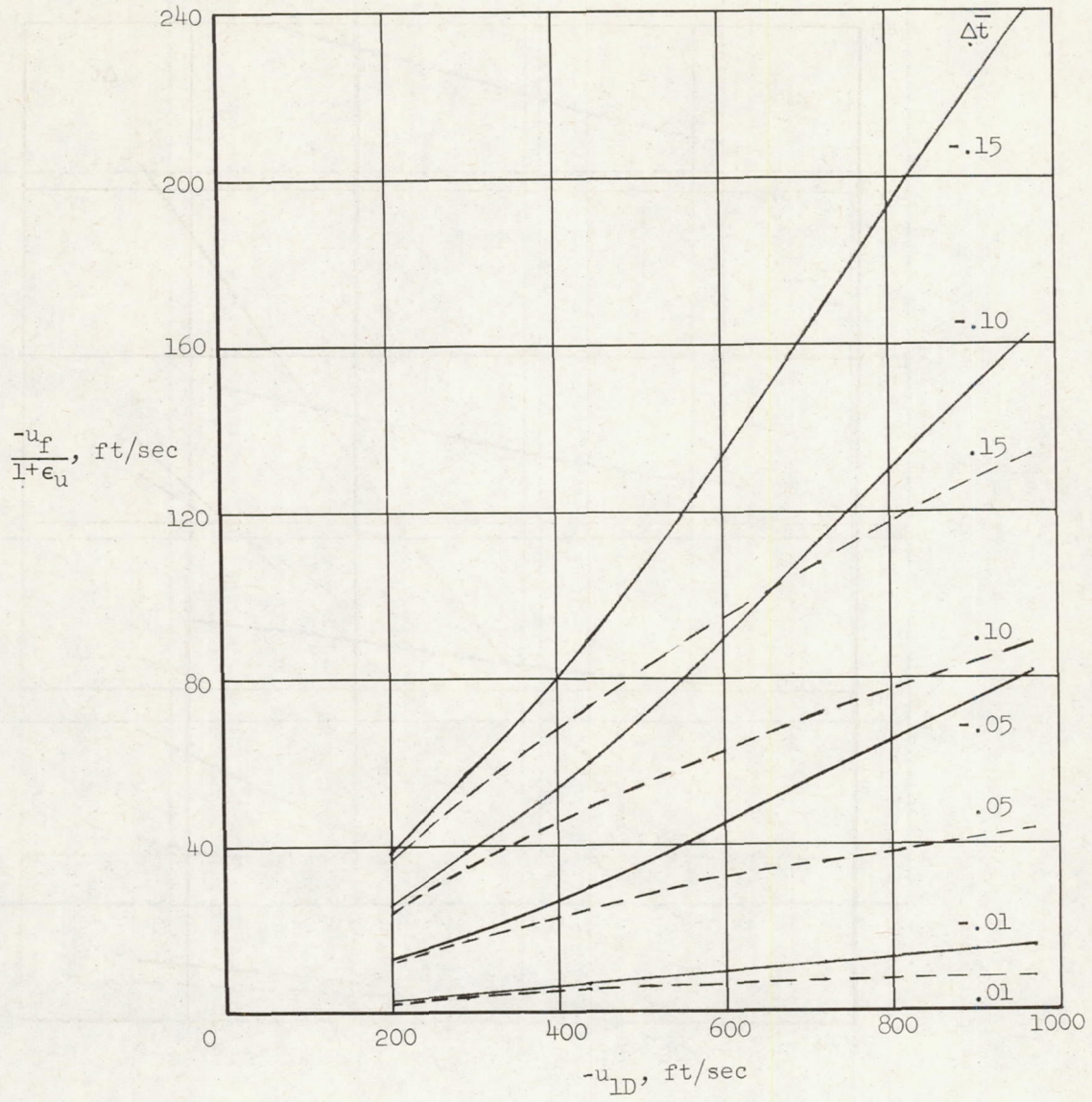

(a) $T_{1D} = 500^{\circ}$ R; $\bar{y}_{2D} = 0$

Figure 15.- Final impact velocity for errors in time at which skin is ruptured (hydrogen inflating gas; $\bar{p}_a = 0$; $\sigma_{s1}/\rho_s = 10^6$ ft^2/sec^2; $\mu_2(\sigma_{c2}/\rho_c) = 1.6\times10^6$ ft^2/sec^2; $\epsilon_\xi = 0$).

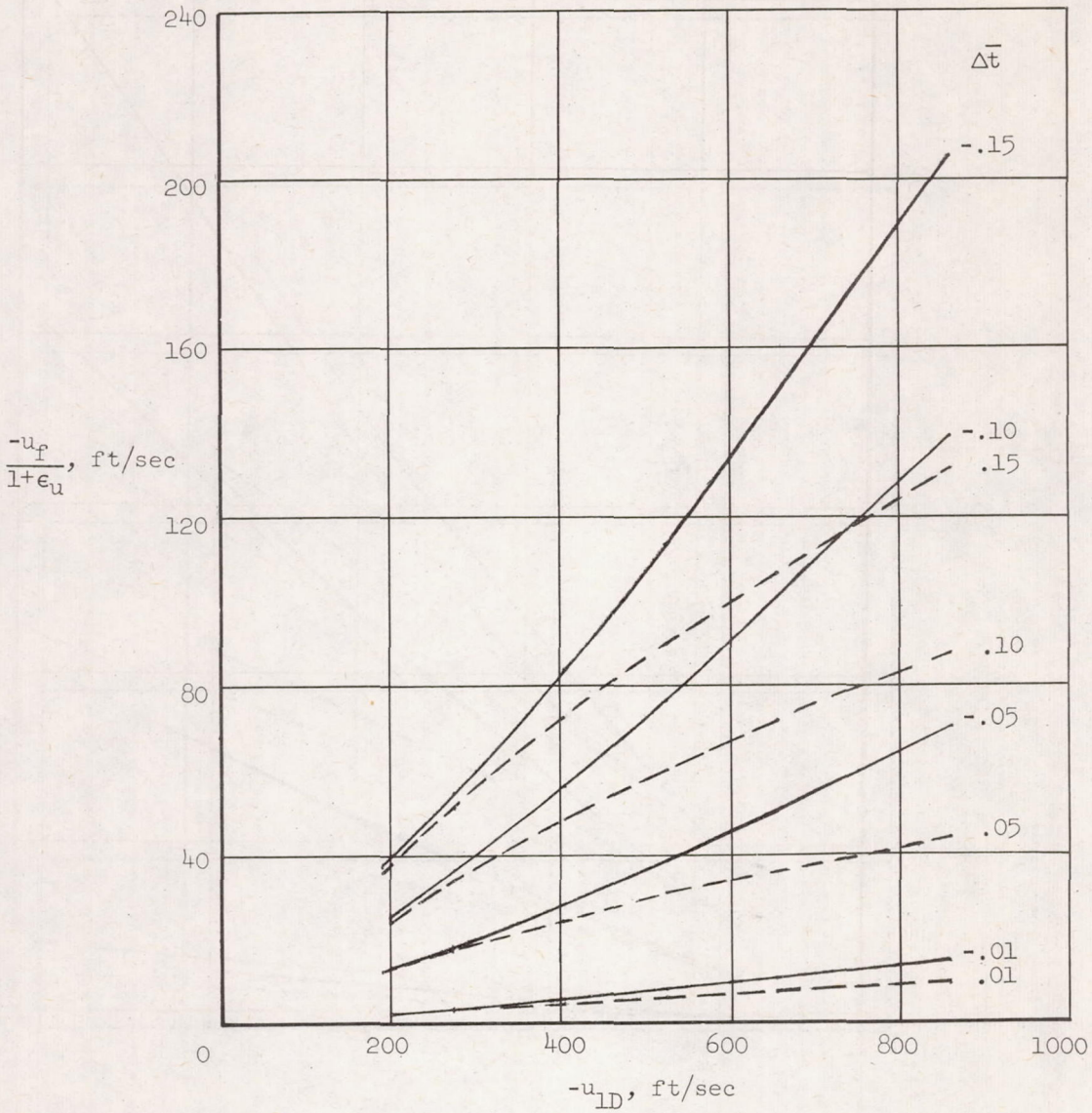

(b) $T_{1D} = 500^{\circ}$ R; $\bar{y}_{2D} = 0.10$

Figure 15.- Continued.

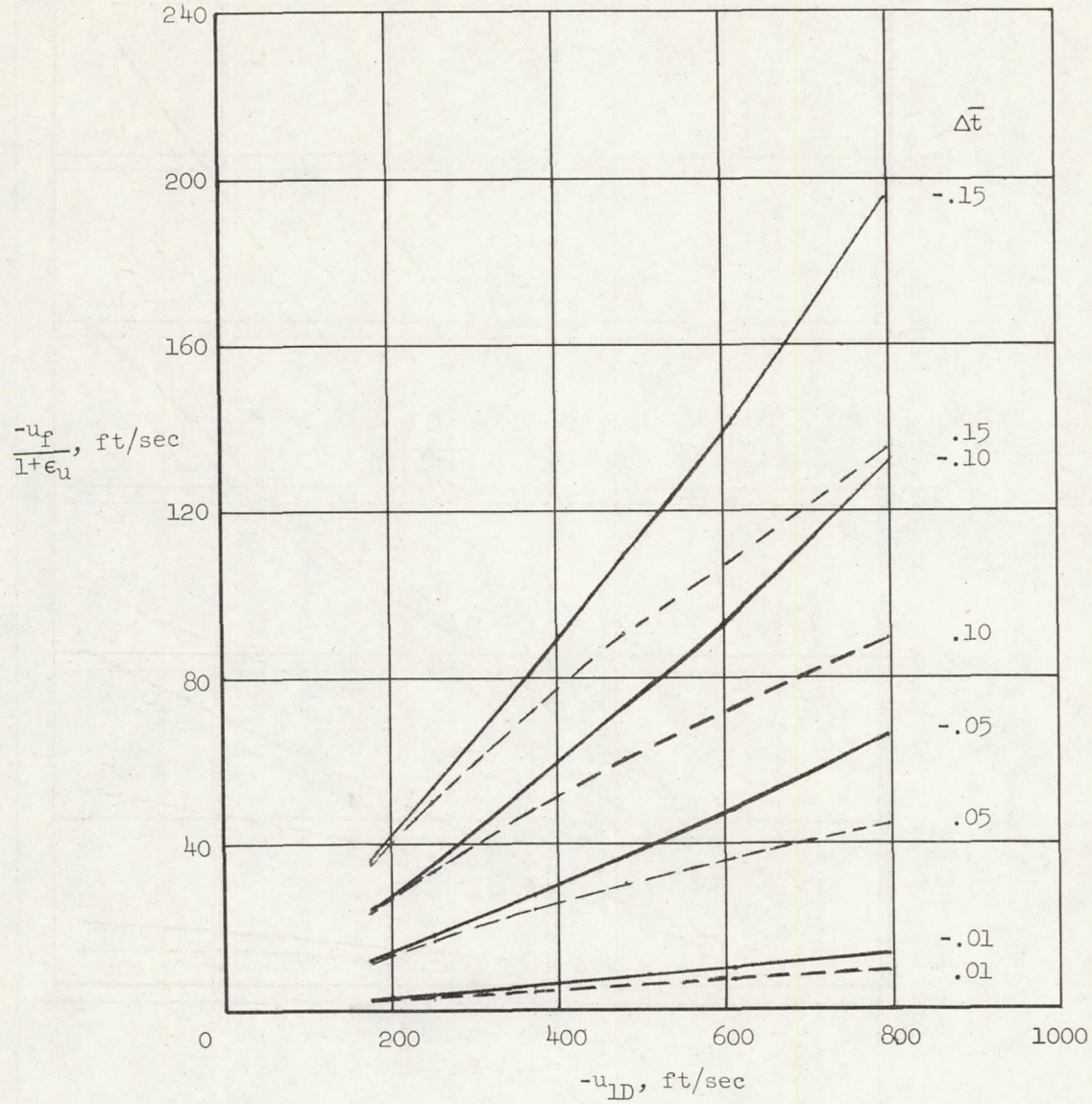

(c) $T_{1D} = 500^{\circ}$ R; $\bar{y}_{2D} = 0.20$

Figure 15.- Continued.

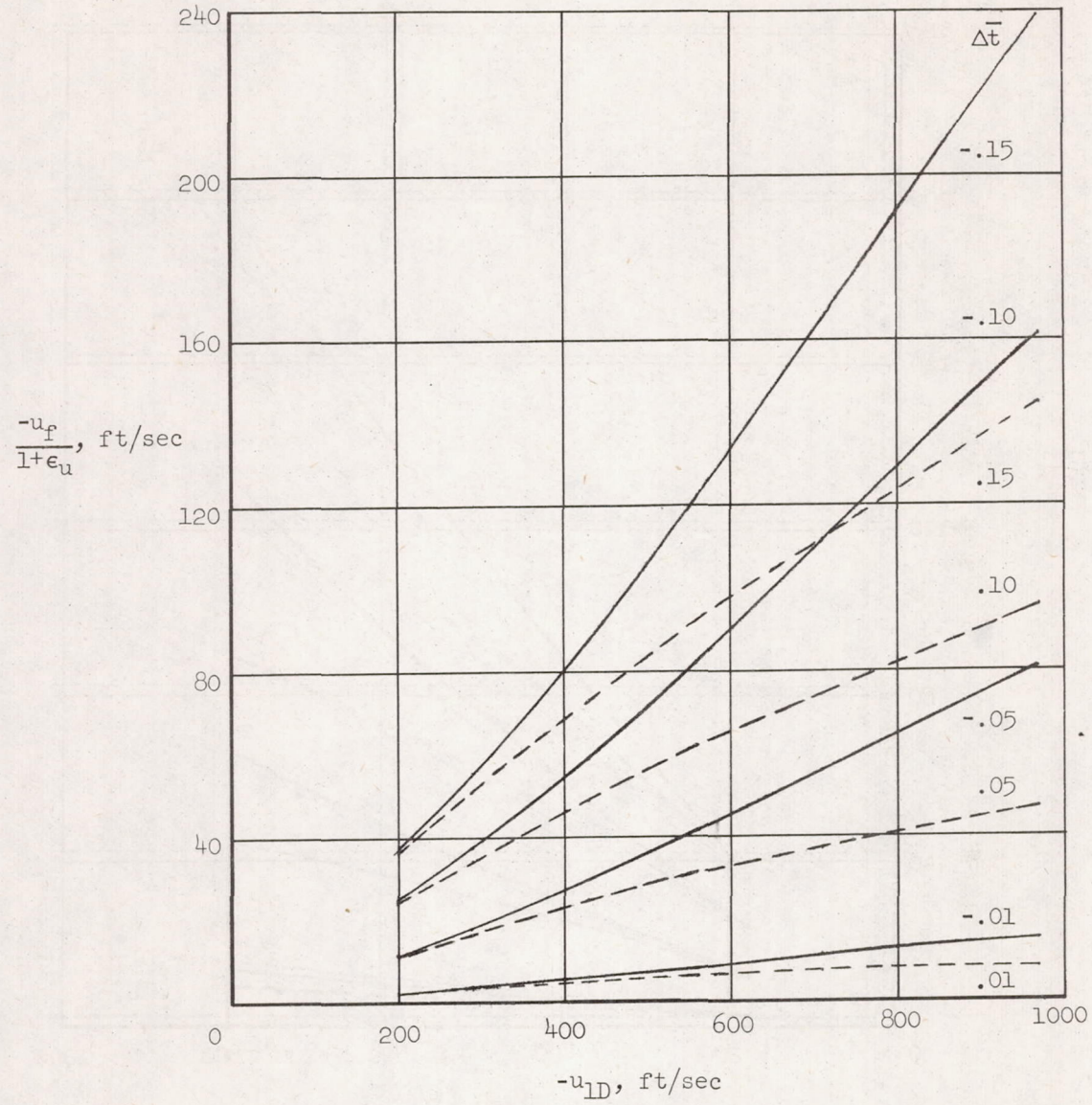

(d) $T_{1D} = 200^{\circ}$ R; $\bar{y}_{2D} = 0$

Figure 15.- Continued.

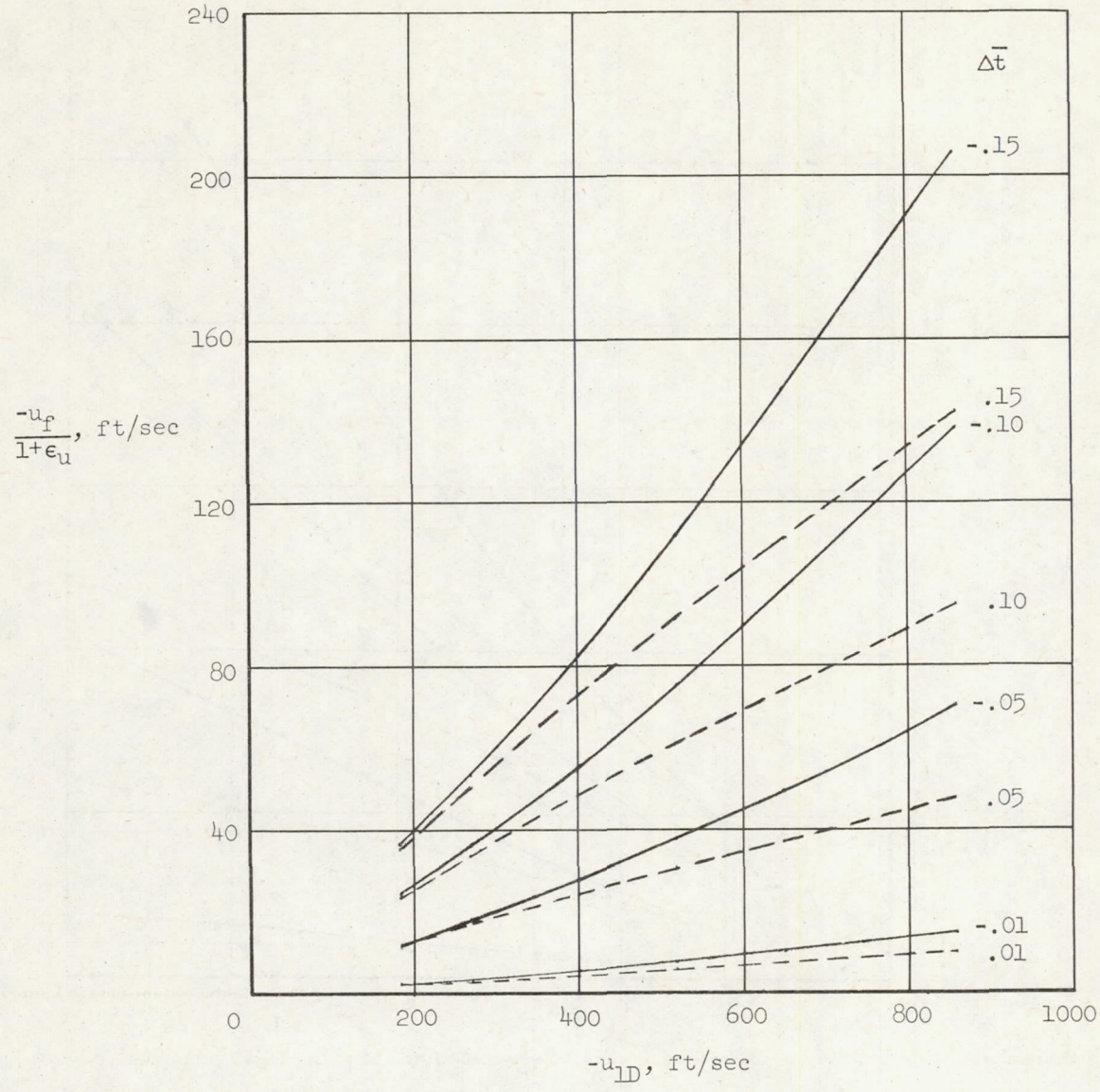

(e) $T_{1D} = 200^{\circ}$ R; $\bar{y}_{2D} = 0.10$

Figure 15.- Continued.

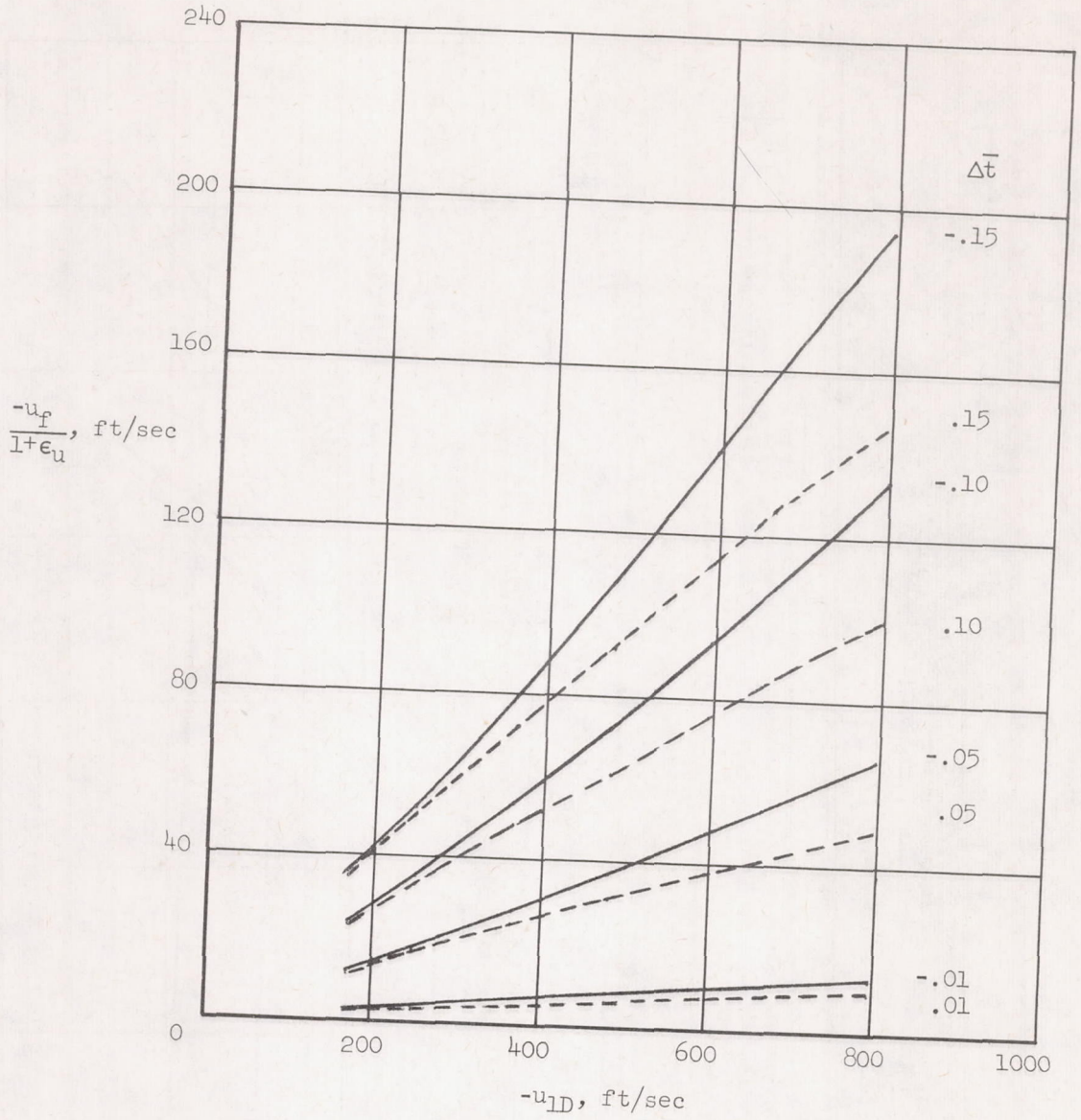

(f) T_{1D} = 200° R; $\bar{y}_{2D}$ = 0.20

Figure 15.- Concluded.

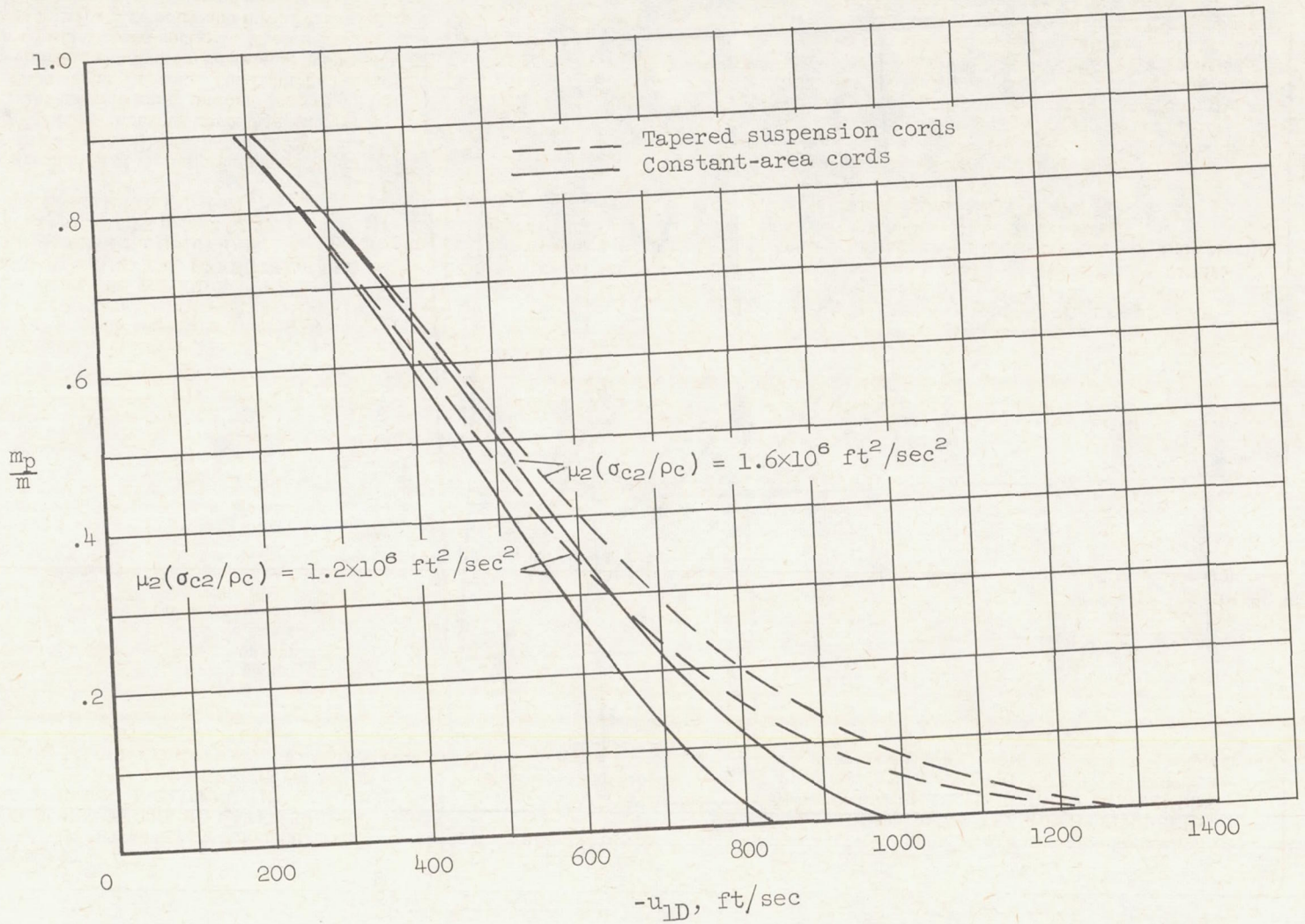

Figure 16.- Payload capability comparison with optimum system using tapered suspension cords (hydrogen inflating gas; $\bar{p}_a = 0$; $\sigma_{s1}/\rho_s = 10^6$ ft^2/sec^2; $T_1 = 500^\circ$ R; $\bar{y}_2 = 0$).

NASA - Langley Field, Va. A-4441